Extracelullar proteins enhance *Cupriavidus pauculus* 1490 and *Vibrio gazogenes* DSM 21264 Ni^{2+} resistance and cell aggregate

Dissertation

For achieving the degree of
Doctor rerum naturalium (Dr. rer. nat.)
at the Department of Microbiology and Biotechnology
Subdivision at the Faculty of Mathematics, Informatics and Natural Science
of the University of Hamburg

Submitted by
Mingwei Wang

Hamburg 2025

1st evaluator: Prof. Dr. Wolfgang R. Streit
2nd evaluator: PD Dr. Ines Krohn

Date of oral defense: 06.03.2026

Contribution to the quoted articles

The following airticles are considered with this thesis:

Mingwei Wang, Christel Vollstedt, Bente Siebels, Huang Yu, Xueling Wu, Li Shen, Jiaokun Li, Yuandong Liu, Runlan Yu, Wolfgang R. Streit, Weimin Zeng, Extracellular proteins enhance Cupriavidus pauculus nickel tolerance and cell aggregate formation, Bioresource Technology, Volume 393, 2024,130133, DOI: https://doi.org/10.1016/j.biortech.2023.130133

This is the main body of my research. I planned perfomed and evaluated all the experimental lab work. Further I evaluated and interpreted the proteomics data and wrote the main parts of the manuscript.

Prof. Dr. Wolfgang R. Streit (Supervisor)

Hamburg, 10.10. 2025,_____

Mingwei Wang

Hamburg, 10.10. 2025,_____

In addition, during the time course of this dissertation, I contributed to the following publications:

Xiao S, **Wang M**, Amanze C, et al. Mechanisms of adaptive resistance in Phytobacter sp. X4 to antimony stress under anaerobic conditions[J]. Journal of Hazardous Materials, 2024: 479. DOI: 10.1016/j.jhazmat.2024.135628.

I Contributed to this research paper by lab work, writing, editing and revising.

Prof. Dr. Wolfgang R. Streit (Supervisor)

Hamburg, 10.10. 2025,_____

Mingwei Wang

Hamburg, 10.10. 2025,_____

Wang, M.; Zeng, W.; Yan, Z.; Shen, L.; Yu, R.; Wu, X.; Li, J.; Qiu, G.; Streit, W.; Liu, Y. The Bio-Desulfurization of Cassiterite–Polymetallic Sulfide Ores Enhanced by a Consortium of Moderately Thermophilic Bacteria. Separations 2025, 12, 61. DOI: 10.3390/separations12030061

I planned perfomed and evaluated all the experimental lab work. Further I evaluated and interpreted the proteomics data and wrote the main parts of the manuscript.

Prof. Dr. Wolfgang R. Streit (Supervisor)

Hamburg, 10.10. 2025,_____

Mingwei Wang

Hamburg, 10.10. 2025,_____

Eidesstattliche Versicherung:

Hiermit versichere ich an Eides statt, die vorliegende Dissertationsschrift selbst verfasst und keine anderen als die angegebenen Hilfsmittel und Quellen benutzt zu haben. Sofern im Zuge der Erstellung der vorliegenden Dissertationsschrift generative Künstliche Intelligenz (gKI) basierte elektronische Hilfsmittel verwendet wurden, versichere ich, dass meine eigene Leistung im Vordergrund stand und dass eine vollständige Dokumentation aller verwendeten Hilfsmittel gemäß der guten wissenschaftlichen Praxis vorliegt. Ich trage die Verantwortung für eventuell durch die gKI generierte fehlerhafte oder verzerrte Inhalte, fehlerhafte Referenzen, Verstöße gegen das Datenschutz- und Urheberrecht oder Plagiate.

Affidavit:

I hereby declare and affirm that this doctoral dissertation is my own work and that I have not used any aids and sources other than those indicated.

If electronic resources based on generative artificial intelligence (gAI) were used in the course of writing this dissertation, I confirm that my own work was the main and value-adding contribution and that complete documentation of all resources used is available in accordance with good scientific practice. I am responsible for any erroneous or distorted content, incorrect references, violations of data protection and copyright law or plagiarism that may have been generated by the gAI.

Hamburg, 20.05.2025

(Mingwei Wang)

Table of Contents

List of Figures

Abstract

Microbial adsorption represents an efficient, eco-friendly, and non-secondary-pollution approach to remediating heavy metals in water bodies. However, when treating wastewater with high concentrations of Ni^{2+}, the limited heavy metal tolerance of microbes usually compromises their remediation efficiency. At the genomic level, the genes related to extracellular proteins are recognized as integral to microbial tolerance to Ni^{2+}; nonetheless, the precise response mechanisms of extracellular proteins at protein levels under Ni^{2+} stress remain largely unexplored, thereby hindering the application of microbial adsorption in treating high-Ni^{2+} wastewater. Therefore, for enhancing the capability of bacteria in remediating high concentration Ni^{2+} wastewater, it is crucial to investigate into the mechanisms of extracellular proteins to varying concentrations of Ni^{2+}. This study focuses on *Cupriavidus pauculus* 1490 (*C. pauculus*) and *Vibrio gazogenes* DSM21264 (*V. gazogenes*) as model organisms to identify Ni^{2+}-resistance genes, predict secretomic Ni^{2+}-resistant proteins, identify key Ni^{2+}-resistance proteins, elucidate the behaviors of critical extracellular proteins in response to Ni^{2+}, clarify the mechanistic roles of extracellular proteins under varying nickel stress levels, and construct a conceptual model of nickel resistance mechanisms. The primary findings are as follows:

(1) A comprehensive study integrating whole-genome and secretomic analyses has elucidated the potential molecular mechanisms underlying nickel resistance in *C. pauculus* and confirmed its resistance capacity. Whole-genome analysis identified nine cobalt/nickel (Co/Ni) resistance genes, while secretomic analysis revealed one nickel resistance protein containing a signal peptide. Fourier-transform infrared (FTIR) spectroscopy indicated that N-H, C-N, and C=O functional groups are critical for Ni^{2+} adsorption and tolerance. Three-dimensional excitation-emission matrix fluorescence spectroscopy (3D-EEM)

showed that the main fluorescent substances in extracellular polymeric substances (EPS) were aromatic proteins, such as tryptophan-like compounds, whose concentrations initially increased and subsequently decreased with rising Ni^{2+} levels. Confocal laser scanning microscopy (CLSM) revealed enhanced extracellular protein fluorescence intensity and bacterial aggregation under Ni^{2+} exposure. Quantitative real-time PCR (qPCR) demonstrated that the expression of resistance genes was upregulated within the initial 4 hours of exposure, indicating an immediate bacterial response to nickel stress. Liquid chromatography-tandem mass spectrometry (LC-MS/MS) analysis identified one protein with over a two-fold down-regulation and 43 proteins with over a two-fold up-regulation under Ni^{2+} stress. These upregulated proteins are involved in critical processes such as cell division, electron transport, lipopolysaccharide (LPS) synthesis, and reactive oxygen species (ROS) detoxification. Moreover, multidrug efflux pumps were found to be key membrane proteins regulating intracellular Ni^{2+} homeostasis in *C. pauculus*.

(2) The strain *V. gazogenes* was analyzed for heavy metal resistance based on whole genome and secretome, and its heavy metal resistance was also verified. Genome-wide sequence comparison revealed 34 heavy metal resistance genes, including 21 Co/Ni transporter protein genes, 7 arsenic resistance genes and 3 Other heavy metal resistance genes. The results of secretomics analysis showed that there were 393 extracellular proteins, including 5 signal peptide-containing metal-resistant proteins, and the amino acid residues in the metal-binding sites of Ni^{2+} transporter proteins were mainly His, Glu, and Asp. Heavy-metal resistance experiments revealed that *V. gazogenes* was resistant to Ni^{2+} and Cu^{2+}, with the maximum tolerant concentrations of 250 mg/L and 150 mg/L, respectively. Functional analyses of extracellular proteins under Ni^{2+} stimulation were carried out on *V. gazogenes*, and a preliminary model of Ni^{2+} tolerance mechanism of extracellular proteins was constructed. The quantitative analysis of extracellular polymers showed

that extracellular proteins were the main components of extracellular polymers, and their contents increased firstly and then decreased with the increase of Ni^{2+} concentration. 3D-EEM results showed that aromatic proteins such as tryptophan, humic acid, and fulvic acid were the main components of Ni^{2+}stimulated, among which, proteins and humic acid were increased and then decreased with Ni^{2+} concentration, and the fluorescence intensity of fulvic acid did not decrease with Ni^{2+} stimulation, while the fluorescence intensity of proteins was not decreased with Ni^{2+} stimulation. The fluorescence intensity of fulvic acids was not affected by Ni^{2+} concentration. CLSM results showed that Ni^{2+} promoted bacterial aggregation and biofilm formation, and the structural composition of EPS was changed. LC-MS/MS results showed that 25 proteins were significantly up-regulated more than 2-fold, and 26 proteins were significantly down-regulated more than 2-fold under Ni^{2+} stress. Among them, ROS defense proteins were the most significantly up-regulated, while cell membrane protein channel expression was the most significantly down-regulated. Extracellular protein function analysis revealed that *V. gazogenes* detoxified Ni^{2+} mainly by down-regulating membrane pore channel proteins (especially Ni^{2+} transporter), and up-regulating ABC transporter proteins, iron/manganese transport system substrate-binding proteins (PsaA), and ROS defense proteins, etc., of which PsaA may play a key role in Ni^{2+} transport.

In conclusion, this study elucidated the Ni^{2+} resistance mechanism of *C. pauculus* and *V. gazogenes* based on extracellular proteins, revealed the behaviors of the key Ni^{2+} resistance proteins, and can provide abundant theoretical basis and methodological reference for the basic theoretical research and industrial application of microbial treatment of heavy metal wastewater.

Zusammenfassung

Die mikrobielle Adsorption stellt einen effizienten, umweltfreundlichen und sekundärverschmutzungsfreien Ansatz zur Sanierung von Schwermetallen in Gewässern dar. Bei der Behandlung von Abwasser mit hohen Ni^{2+}-Konzentrationen beeinträchtigt jedoch die begrenzte Schwermetalltoleranz der Mikroben in der Regel ihre Sanierungseffizienz. Auf genomischer Ebene werden die Gene, die mit extrazellulären Proteinen in Verbindung stehen, als wesentlich für die Toleranz von Mikroorganismen gegenüber Ni^{2+} angesehen. Dennoch sind die genauen Reaktionsmechanismen extrazellulärer Proteine auf Proteinebene unter Ni^{2+}-Stress weitgehend unerforscht, was die Anwendung der mikrobiellen Adsorption bei der Behandlung von Abwasser mit hohem Ni^{2+}-Gehalt behindert. Um die Fähigkeit von Bakterien zur Sanierung von Abwässern mit hoher Ni^{2+}-Konzentration zu verbessern, ist es daher von entscheidender Bedeutung, die Mechanismen extrazellulärer Proteine bei unterschiedlichen Ni^{2+}-Konzentrationen zu untersuchen. Diese Studie konzentriert sich auf *Cupriavidus pauculus* 1490 (*C. pauculus*) und *Vibrio gazogenes* DSM21264 (*V. gazogenes*) als Modellorganismen, um Ni^{2+}-Resistenzgene zu identifizieren, sekretomische Ni^{2+}-resistente Proteine vorherzusagen, wichtige Ni^{2+}-Resistenzproteine zu identifizieren, das Verhalten kritischer extrazellulärer Proteine als Reaktion auf Ni^{2+} aufzuklären, die mechanistischen Rollen extrazellulärer Proteine unter unterschiedlichen Nickelstressniveaus zu klären und ein konzeptionelles Modell der Nickelresistenzmechanismen zu erstellen. Die wichtigsten Ergebnisse sind wie folgt:

(1) Eine umfassende Studie, die Ganzgenom- und Sekretom-Analysen integriert, hat die potenziellen molekularen Mechanismen der Nickelresistenz in *C. pauculus* aufgeklärt und dessen Resistenzfähigkeit bestätigt. Die Ganzgenomanalyse identifizierte neun Kobalt/Nickel (Co/Ni)-Resistenz-Gene,

während die Sekretom-Analyse ein Nickelresistenzprotein mit einem Signalpeptid aufdeckte. Die Fourier-Transform-Infrarot (FTIR)-Spektroskopie zeigte, dass N-H-, C-N- und C=O-Funktionsgruppen für die Ni^{2+}-Adsorption und -Toleranz entscheidend sind. Die dreidimensionale Anregungs-Emissions-Matrix-Fluoreszenzspektroskopie (3D-EEM) zeigte, dass die wichtigsten fluoreszierenden Substanzen in extrazellulären polymeren Substanzen (EPS) aromatische Proteine wie Tryptophan-ähnliche Verbindungen waren, deren Konzentrationen zunächst mit steigenden Ni^{2+}-Konzentrationen anstiegen und anschließend abnahmen. Die konfokale Laserscanning-Mikroskopie (CLSM) zeigte eine erhöhte extrazelluläre Proteinfluoreszenzintensität und bakterielle Aggregation unter Ni^{2+}-Exposition. Die quantitative Echtzeit-PCR (qPCR) zeigte, dass die Expression von Resistenzgenen innerhalb der ersten 4 Stunden der Exposition hochreguliert war, was auf eine sofortige bakterielle Reaktion auf Nickelstress hindeutet. Die Flüssigchromatographie-Tandem-Massenspektrometrie (LC-MS/MS)-Analyse identifizierte ein Protein mit einer mehr als zweifachen Herunterregulierung und 43 Proteine mit einer mehr als zweifachen Hochregulierung unter Ni^{2+}-Stress. Diese hochregulierten Proteine sind an kritischen Prozessen wie Zellteilung, Elektronentransport, Lipopolysaccharid (LPS)-Synthese und Entgiftung reaktiver Sauerstoffspezies (ROS) beteiligt. Darüber hinaus wurde festgestellt, dass Multidrug-Effluxpumpen wichtige Membranproteine sind, die die intrazelluläre Ni^{2+}-Homöostase in C. pauculus regulieren.

(2) Der Stamm *V. gazogenes* wurde anhand des gesamten Genoms und des Sekretoms auf Schwermetallresistenz untersucht, und seine Schwermetallresistenz wurde ebenfalls bestätigt. Der genomweite Sequenzvergleich ergab 34 Schwermetallresistenzgene, darunter 21 Co/Ni-Transporterproteingene, 7 Arsenresistenzgene und 3 weitere Schwermetallresistenzgene. Die Ergebnisse der Sekretomik-Analyse zeigten, dass es 393 extrazelluläre Proteine gab, darunter 5 signalpeptidhaltige

metallresistente Proteine, und dass die Aminosäurereste in den Metallbindungsstellen der Ni^{2+}-Transporterproteine hauptsächlich His, Glu und Asp waren. Schwermetallresistenzversuche ergaben, dass *V. gazogenes* gegen Ni^{2+} und Cu^{2+} resistent war, mit maximalen Toleranzkonzentrationen von 250 mg/l bzw. 150 mg/l. Es wurden Funktionsanalysen von extrazellulären Proteinen unter Ni^{2+}-Stimulation an *V. gazogenes* durchgeführt und ein vorläufiges Modell des Ni^{2+}-Toleranzmechanismus extrazellulärer Proteine erstellt. Die quantitative Analyse extrazellulärer Polymere zeigte, dass extrazelluläre Proteine die Hauptkomponenten extrazellulärer Polymere waren und ihr Gehalt mit steigender Ni^{2+}-Konzentration zunächst anstieg und dann abnahm. Die 3D-EEM-Ergebnisse zeigten, dass aromatische Proteine wie Tryptophan, Huminsäure und Fulvosäure die Hauptkomponenten der Ni^{2+}-Stimulation waren, wobei Proteine und Huminsäure mit steigender Ni^{2+}-Konzentration zunächst anstiegen und dann abnahmen, während die Fluoreszenzintensität von Fulvosäure mit Ni^{2+}-Stimulation nicht abnahm und die Fluoreszenzintensität von Proteinen mit Ni^{2+}-Stimulation ebenfalls nicht abnahm. Die Fluoreszenzintensität von Fulvosäuren wurde durch die Ni^{2+}-Konzentration nicht beeinflusst. CLSM-Ergebnisse zeigten, dass Ni^{2+} die bakterielle Aggregation und Biofilmbildung förderte und die strukturelle Zusammensetzung von EPS verändert wurde. LC-MS/MS-Ergebnisse zeigten, dass 25 Proteine unter Ni^{2+}-Stress um mehr als das Zweifache signifikant hochreguliert und 26 Proteine um mehr als das Zweifache signifikant herunterreguliert waren. Unter diesen waren ROS-Abwehrproteine am stärksten hochreguliert, während die Expression von Zellmembranprotein-Kanälen am stärksten herunterreguliert war. Die Analyse der extrazellulären Proteinfunktion ergab, dass *V. gazogenes* Ni^{2+} hauptsächlich durch Herunterregulierung von Membranporenkanalproteinen (insbesondere Ni^{2+}-Transporter) und Hochregulierung von ABC-Transporterproteinen, Eisen/Mangan-Transportsystem-Substratbindungsproteinen (*Psa*A) und ROS-

Abwehrproteinen usw. entgiftete, wobei *Psa*A möglicherweise eine Schlüsselrolle beim Ni^{2+}-Transport spielt.

Zusammenfassend lässt sich sagen, dass diese Studie den Ni^{2+}-Resistenzmechanismus von *C. pauculus* und *V. gazogenes* auf der Grundlage extrazellulärer Proteine aufgeklärt, das Verhalten der wichtigsten Ni^{2+}-Resistenzproteine aufgezeigt und eine reichhaltige theoretische Grundlage und methodische Referenz für die grundlegende theoretische Forschung und industrielle Anwendung der mikrobiellen Behandlung von Schwermetallabwässern liefern kann.

1 Introduction

Due to the rapid development of industrialization, urbanization, and reckless exploitation of natural resources, heavy metal pollution in the water body becomes a severe problem and receives widespread research attention (Wang et al., 2022). It's reported that approximately 40% of the population is struggling with water scarcity (Calzadilla et al., 2011). Heavy metals easily accumulate in organisms and directly or indirectly impact all kinds of life due to their non-biodegradable, toxic, and persistent (Shah, 2021). The overdose of heavy metals could cause Reactive Oxygen Species (ROS), proteins DNA damage, etc. (Agarwal & Khan, 2020). Therefore, the bioremediation of heavy metals pollution has attracted widespread attention globally due to its sustainability, low cost, and high efficiency (Singh et al., 2022).

1.1 Ni^{2+} pollution in waterbody

1.1.1 The source of nickel water pollution

Nickel (Ni) is an essential element for organisms, participating in the activity of enzymes (Kumar et al., 2023). However, the overdose of Ni (>25 mg/L) can be toxic to living beings, including leading to cancer, and allergy for humans (Genchi et al., 2020). The elevated entry of Ni into the food chain through plant adsorption poses substantial health risks to residents and threatens the environmental stability of the entire system (Amit et al., 2021). Interestingly, vegetables usually contain more Ni than Other food items; at the same time, legumes, spinach, and nuts also have high levels of Ni (Das et al., 2019).

It's stated that approximately 30000 tons/year of Ni are released into the

air from natural sources, including windblown sand, volcanic activity, wild forests, marine environments, and continental volatiles (Amit et al., 2023). The content of Ni from the soil was transferred into the groundwater due to acid rain (Qi et al., 2022). Ni is found in air, food, tobacco products, and water (Qi et al., 2022). It's reported that one common cigarette discharges about 0.04-0.58 g of Ni (Poonkothai & Vijayavathi, 2012). In addition, Ni was also found in incompetent vehicle engines through conveyance (Kumar et al., 2023). Moreover, the production and processing of nickel compounds and their derivatives, Ni-waste disposal, and the recycling of Ni-waste products (Kumar et al., 2019).

Nickel polluted areas in the European Union are primarily concentrated in industrial zones in Figure 1. Reports indicate that nickel pollution from industrial waste in Greece has resulted in nickel concentrations in the Asopos River Basin being 2.5 times higher than those in soil and groundwater, posing a threat to the river ecosystem (Muhammad et al., 2020; Panagopoulos et al., 2015). Other industrial areas are mainly located in the Mediterranean region (excluding most of Spain and southern Italy), where nickel concentrations in numerous samples have exceeded the standard threshold (Vischetti et al., 2022). The Arctic region also faces nickel pollution, largely due to large industrial companies in the Russian Arctic, such as Norilsk Nickel. In 2022, its wastewater discharge reached 168 million tons, and a leakage incident occurred in 2020 (Hønneland, 2003). In Indonesia, excessive nickel concentrations are attributed to smelting and extraction of nickel ore. The increasing nickel production has detrimental effects on forests and the environment, leading to deforestation, habitat degradation, and air and soil pollution (Nasution et al., 2024).

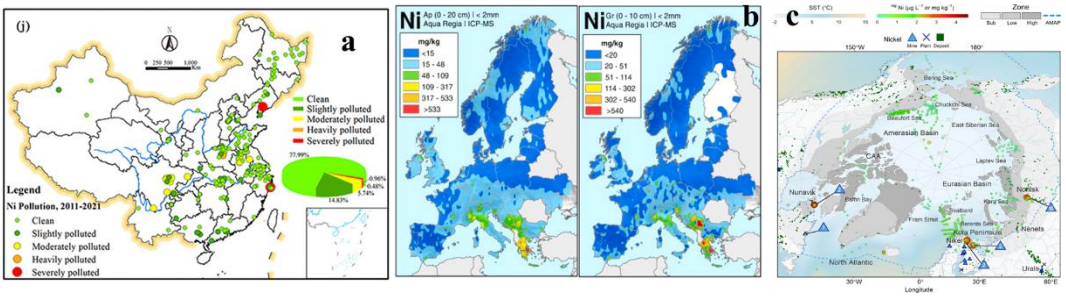

Figure 1: Global nickel pollution in China, Europe, and Arctic region. a, red circle represented severely polluted region, caused by industrial activities, orange circle represented heavy polluted region, yellow circle means moderately polluted region, and green means no pollution or slight pollution; b, nickel pollution distributed in Europe, mainly in Italy, Spain and Greece etc. c, nickel pollution in Arctic region, caused by mining and smelting

1.1.2 The toxic of Ni

Numerous negative health consequences result from coming into contact with both soluble and insoluble nickel compounds. Ni may enter a human's body through food, drink, or air. Employees in the industries that produce and process Ni are susceptible to inhalation and, to a lesser extent, skin contact (Soares et al., 2003). Nickel exposure will cause human health problems, such as allergies, lung and nasal cancer, and even DNA damage (Aleksandra Duda-Chodak, 2008).

When Ni^{2+} enter water bodies, Ni^{2+} can acculturate in the organism through the food chain. Then Ni^{2+} circulates within the ecosystem through the decomposition action of microorganisms. If the short-term accumulation of Ni^{2+} exceeds the self-purification capacity of the ecosystem, the biological communities in aquatic environments can suffer severe harm. Numerous studies indicated that Ni^{2+} can accumulate in animals, thereby affecting normal growth (Soares et al., 2003). The same effect was found on plants. Excessive Ni also harmed plant growth through reduced vegetative growth such as plant

height, biomass production, ultrastructure of leaves, thickness of mesophyll cells, etc. (Shahzad et al., 2018). In addition, Ni^{2+} will affect the biological membranes and integrity. Excessive Ni^{2+} will induce much of reactive oxygen species (ROS) that have damaging effects on cell membranes, proteins, lipids, and DNA through lipid peroxidation, which causes harm to not only plants but also bacteria and other organism (Shahzad et al., 2018).

1.2 Current progress in nickel resistance in microorganisms

Bacteria have a variety of mechanisms to resist metal stress. These diverse methods include efflux excessive metals out of cells, reducing metals uptake, extracellular interaction, metal binding proteins complexation, ion change, converting metals into less toxic forms, extracellular sequestration, etc (Figure 2)(Thai et al., 2023). The methods of Ni defense were emphasized, however, it's important to note that there is extensive overlap with cobalt (Co) resistance.

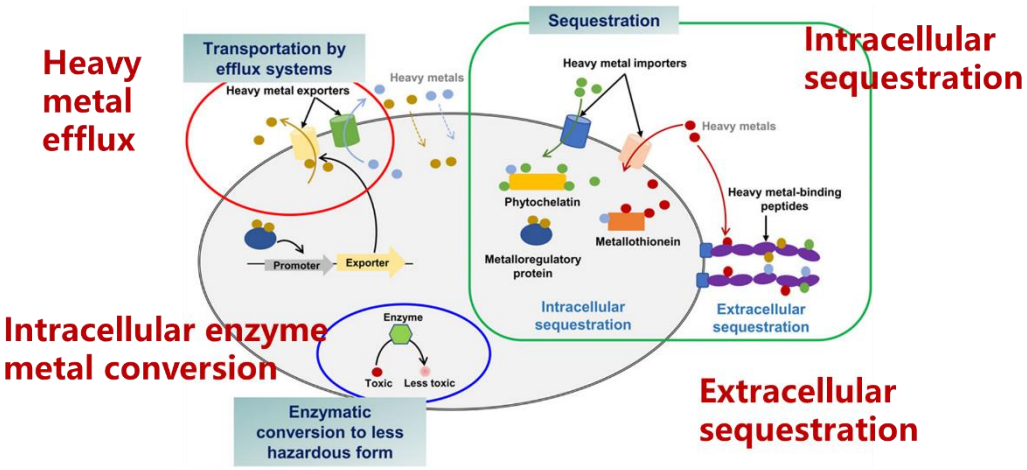

Figure 2: Heavy metal resistance mechanisms in bacteria (Thai et al., 2023). Bacteria detoxify heavy metals by heavy metal efflux pumps, intracellular sequestration, extracellular sequestration, and intracellular enzyme metal conversion

1.2.1 Nickel efflux system

The primary mechanism of nickel resistance in most bacteria is mediated by efflux transport proteins (Hausinger, 2016).

1.2.1.1 The resistance nodulation and cell division family

The resistance nodulation and cell division (RND) family comprises a variety of metal efflux proteins, including inner membrane pumps, outer membrane channels, and periplasmic adaptor proteins (Hussain et al., 2022). Heavy metals were transported to extracellular through these systems through proton motive force (Hausinger, 2016). Moreover, the RND family for Ni resistance has been discovered in numerous organisms, such as *Cupriavidus* (Große et al., 2022), *Achromobacte* (Chaintreuil et al., 2007), *Bradyrhizobium* (Chaintreuil et al., 2007) and *Helicobacter* (Kumar et al., 2022). For instance, the chromosomal *cznCBA*, in conjunction with the plasmid-borne gene clusters *cnrCBA* and *nccCBA*, collectively play a role in Ni resistance. It's reported that *MrdH* in *pseudomonas putida* encompasses an *RncA*-like domain and an RND-like domain, which can be expressed under stimulation of Cd^{2+}, Ni^{2+}, Zn^{2+}, and Co^{2+} (Haritha et al., 2009). Deletion of *mrdH* in *Pseudomonas putida* leads to increased sensitivity and accumulation of Cd^{2+}, Ni^{2+}, and Zn^{2+} compared to the wild-type cells (Haritha et al., 2009).

1.2.1.2 The Major Facilitator Superfamily Family

The major facilitator superfamily (MFS) of efflux proteins is characterized by the presence of 12 transmembrane helices distributed across two domains. For instance, *NreB* has been shown to confer Ni resistance by transporting cytoplasmic Ni into the periplasm. The MFS proteins, responsible for Ni transport, are thought to utilize the proton gradient to actively transport Ni against its concentration gradient. They are commonly located in operons along with Other transporters and/or regulatory proteins (Hausinger, 2022).

1.2.1.3 Cation diffusion facilitators family

The cation diffusion facilitators (CDF) are a widely distributed family of

cation proton antiporters that are characterized by six transmembrane domains. *CzcD*, the first defined member of the CDF family of transporters, was demonstrated to have a role in heavy metal resistance in *Cupriavidus metallidurans* (Olga et al., 2015). Moreover, *DmeF* in *Cupriavidus metallidurans* (Munkelt et al., 2004) and *NepA* from *Rhizobium etli* (Cubillas et al., 2013) conferred Ni resistance.

1.2.1.4 P-type ATPase efflux systems

P-type ATPase efflux systems transfer metal ions across the plasma membrane and into the periplasm and have a high affinity for sulfhydryl groups (Cu^{+}/Ag^{+}, $Zn^{2+}/Cd^{2+}/Pb^{2+}$) (Joshi et al., 2023). *NmtA* and *CtpD* can help *Mycobacterium* resist Ni, while *CtpD* showed a preference for Co^{2+} (Musiani et al., 2015). Although lacking characterization of structure, these proteins likely resemble copper-transporting ATPase *CopB* (Hausinger, 2022). Initial studies identified these two p-types ATPases in *Mycobacterium*, while the subsequent research showed conflicting results. Knock out *cptD* in *Mycobacterium smegmatics* increased sensitivity to Ni. However, there was no difference observed in *Mycobacterium tuberculosis* (Hausinger, 2016).

1.2.1.5 Extracellular compartmentalization and sequestration

Microbes tolerate Ni also through reduction, sequestration, compartmentalization, and Other mechanisms (Robert, 2022).

Compartmentalization and sequestration strategies for Ni^{2+} are not commonly observed in bacteria. Nonetheless, there are some examples. The sulfate-reducing bacterium *Desulfotomaculum*, which is known for its high resistance to Ni, has been shown to precipitate Ni as both Ni sulfide and a Ni-protein complex outside of the cell (Hausinger, 2016). Ni can be precipitated in the periplasm and on the cytoplasmic membrane in *Pseudomonas aeruginosa* (Sar et al., 2001), which proved that Ni reduction with lots of electron donors is a resistance strategy for cell detoxification (Geets et al., 2006).

Bacteria defense Ni^{2+} involves in reducing its concentration through extracellular sequestration, or in the periplasm or inner cells, such as binding Ni^{2+} through extracellular polymeric substance (EPS). It's well known that the poly-γ-glutamate capsule and cell wall in *Bacillus* play a role in the adsorption of Ni^{2+} (McLean et al., 1990). It's also reported that cell-produced proteins in periplasm can bind the metals tightly with Ni^{2+} exposure. For instance, Ni sequestration in the periplasm in *Cupriavidus pauculus* KPS 201 through two proteins of 74- and 66-kDa (Pal & Paul, 2010). While there is no identification of these proteins and analysis of the proteins' interactions with Ni. Lu et al. proposed an 82-residue peptide that can sequestrate cellular Ni^{2+} in *S. coelicolor* but lacks clear evidence for its participation in Ni resistance (Mo Lu, 2014).

Instead of sequestration mechanisms, compartmentalization is the other way for Ni resistance. The metal was placed into a vacuole as a complex with the amino acid histidine in *Saccharomyces cerevisiae* which can prevent Ni^{2+} into a subcellular organelle (Pearce & Sherman, 1999). Besides, the proteins related to cell shapes and membrane composition, and the enzymes related to lipopolysaccharide or branched amino acid could also have a significant up-regulated with Ni^{2+} treatment. It seems they play an important role in Ni resistance (Hausinger, 2022). Nevertheless, there is no analysis of the precise mechanism.

In summary, numerous mechanisms beyond Ni efflux systems are involved in enabling microorganisms to defend Ni. Unfortunately, there is still lacking convincing proof and significant research on these mechanisms.

1.3 Ni and antibiotics co-resistance

Recently, antibiotics have been prevalent contaminants in water bodies, contributing to the emergence of antibiotic resistance. There is a potential for

the transfer of resistant bacteria and genes between the environment, animals, and humans, which poses health risks (Nada et al., 2023). Therefore, antibiotic resistance has been identified as one of the most serious dangers to global public health (Hu et al., 2017). Numerous studies indicate that heavy metals can induce bacterial antibiotic resistance (Sonia et al., 2023). Heavy metal defense mechanisms have been discovered to be commonly similar to antibiotic resistance pathways, so bacteria can develop antibiotic resistance in conjunction with heavy metal resistance with continuous heavy metal exposure (Pal et al., 2017a).

The mechanism of heavy metals-driven antibiotic resistance includes co-resistance, cross-resistance, and co-regulation. Co-resistance occurs when the genes that determine resistant phenotypes are located on the same genetic element, such as plasmids, transposons, or integrons. It is usually acquired under selection pressure (Craig et al., 2006). It's reported that plasmid pLKSZ04 in *Escherichia coli* E308 contains *ChrA* which is located in the heavy metal resistance gene (HMRG). *ChrA* is responsible for Cr resistance and was significantly associated with antibiotic resistance genes (ARGs), which may cause co-resistance to Cr and antibiotics (Shengzhi et al., 2020). Moreover, the mercury resistance genes are highly linked to ARGs although the mercury and arsenic resistance genes are highly related to integron-associated integrases(Pal et al., 2015). Interestingly, the cadmium (Cd) and zinc (Zn) resistance genes occasionally co-occur with macrolides and aminoglycosides resistance genes (Pal et al., 2015).

The mechanism for cross-resistance has occurred combined with antibiotic and heavy metal pollution. The same mechanism expressed antibiotic and heavy metal resistance, metals or antibiotics may interact with the same target, the same apoptotic process, or via the same route, leading to metal-induced antibiotic resistance (Zhou et al., 2022). Usually, cross-resistance mainly happens through the same efflux pump for transporting heavy metals and

antibiotics to extracellular space (Zhou et al., 2022). It's reported that Cd^{2+} and Zn^{2+} cross-resistance with sodium dodecyl sulfate, beta-lactams, kanamycin, erythromycin, novobiocin, and ofloxacin due to the DsBA-DsbB disulfide bond formation system in *Burkholderia cepacia* (Hayashi et al., 2000). Similarly, cross-resistance was observed in focal strains collected from sediments in the United Kingdom demonstrating intl1 gene contributed to Zn and cefotaxime, oxacillin, and trimethoprim resistance (Dickinson et al., 2019). Interestingly, heavy metals such as Zn, Co, and Cd were found to be expelled by the multidrug efflux pump encoded by the *MdrL* protein in *Listeria monocytogenes*. It also can pump antibiotics out, such as erythromycin, josamycin, and clindamycin, as well as biocides such as benzalkonium chloride (Mata et al., 2000).

Heavy metals have been reported to generate antibiotic resistance by triggering the co-regulation of ARGs. Metal stimulation enhancing the expression of ARGs was observed in *Enterobacteriaceae bacterium* LSJC7, leading to a promoted ability to survive antibiotic exposure. Arsenate (As) caused the overexpression of various ARGs, such as *emrD* and the tetracycline resistance gene tet34 (Chen et al., 2015). Additionally, the Co-Zn-Cd (*czc*) gene cluster in *Ralstonia metallidurans* was proved to be a prerequisite for antibiotic resistance, which promotes the cross-selection of antibiotic resistance under heavy metal exposure (Tang et al., 2021). Similarly, *CzcRS* in *Pseudomonas aeruginosa* were also found co-regulation of antibiotic and metal resistance. It can regulate not only the expression of the *czcCBA* efflux system but also decrease the expression of *OprD* porin, leading to increased resistance to carbapenems (Perron et al., 2004). Besides, the *robA* gene encoded Rob proteins which is a binding protein that regulates both heavy metal and antibiotic resistance (Nakajima et al., 1995).

The knowledge gap is that we assume the resistance genes from DNA sequences to be expressed. However, not all genes are expressed even under

the simulation of heavy metals or antibiotics. In addition, resistance genes are widespread across various environments, but many unidentified resistance genes have yet to be discovered. Moreover, there is a lot of DNA genome information and databases but still a lack of the secretome or proteomics data of the metals or antibiotics resistance proteins information. Searches based on metal-binding protein sequence motifs or domains may also be a nice try to find new resistance proteins.

1.4 Intention of this study

The insufficient study of how extracellular proteins detoxify heavy metals and help bacteria resist heavy metals. Therefore, the current study focused on two major goals. Firstly, demonstrate the mechanism of extracellular proteins on Ni resistance and adsorption in *C. pauculus* and *V. gazogenes*. The exoproteomes were qualitative and quantitatively analyzed. The extracellular proteins were extracted, characterized, and identified. The genes related to heavy metal resistance were verified by quantitative polymerase chain reaction (qPCR). Altogether the results provide a conceptual model for understanding how e-PNs in *C. pauculus* enhance heavy metal resistance and adsorption of Ni^{2+}. Secondly, *V. gazogenes* is a strain which exhibits the capability to biodegrade polyethylene terephthalate, starch and cellulose. However, recent findings have revealed its tolerance to Ni^{2+} concentrations exceeding 100 mg/L. It's the first time to report Ni^{2+} resistantce in *V. gazogenes*. While, it can resist Ni^{2+}, and owns the Ni^{2+}-transport system but can't resist higher concentration of Ni^{2+} compared to the typical heavy-metals-resistant bacteria, such as *C. pauculus*. Therefore, in order to figure out the reason, we explored the e-PNs' role in Ni^{2+} resistance and difference from the Ni^{2+} resistance mechanism in *C. pauculus and V. gazogenes*. In addition, two strains detoxification mechanisms were also explored.

The research route as follows in Figure 3:

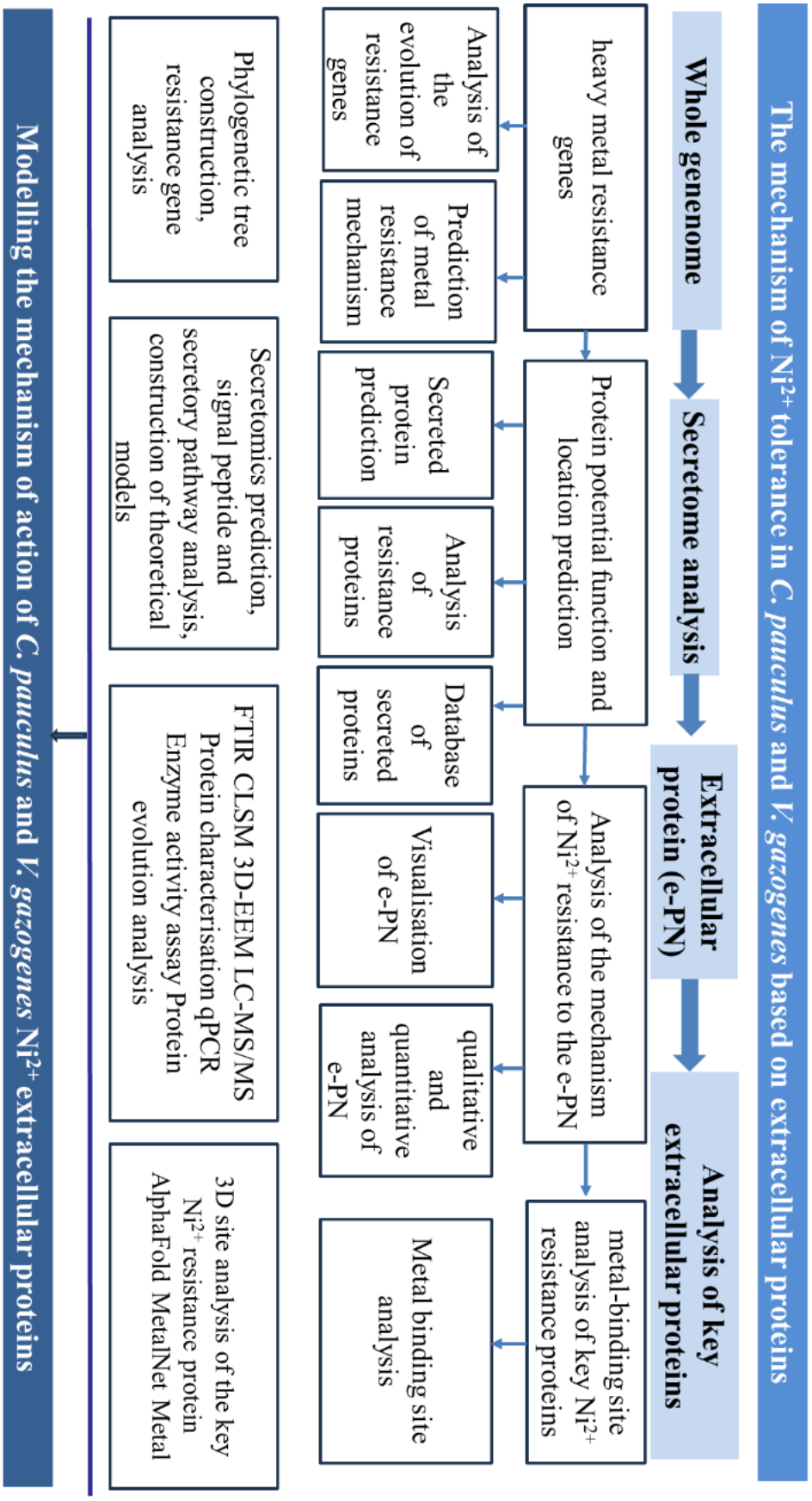

Figure 3: Research route; Through whole-genome analysis, identify genes associated with heavy metal resistance, such as Ni^{2+} resistance-related regulatory factors, efflux pump genes, and response mechanisms, while validating Ni^{2+} resistance capacity. Based on whole-genome prediction of the secretome, analyze Ni^{2+} resistance mechanisms mediated by secreted proteins. Based on the secreted proteome, construct e-PN database. Employ LC-MS/MS-based extracellular proteomics to identify differences in resistance mechanisms between typical heavy metal-resistant *C. pauculus* and non-resistant *V. gazogenes*. Elucidate both broad-spectrum Ni^{2+} resistance mechanisms and Ni^{2+} resistance-specific mechanisms based on e-PN

2 Marterial and Methods

2.1 Bacterial strains and primers

The bacteria used in this study is *Cuprividus pauculus* 1490 (*C. pauculus*) and *Vibrio gazogenes* DSM 21264 (*V. gazogenes*). *V. gazogenes* was purchased from Leibniz Institute DSMZ (Braunschweig, Germany). The primers used in this study are listed in the Table 1.

Table 1. Primers used in this study

Name	**Sequence (5'→3')**
SecY	Forward: TGTCGCGCTTTACCGTCTT
	Reverse: TGCCTGCCCTTCCTTCTTC
CnrH	Forward: GTTTGGCGCGCGTGTATTC
	Reverse: CCGCAAGGTGCTCGATTTC
WP_017510984.1	Forward: AGATGCGGGACTTGTAT
	Reverse: AATGGCCGTCAGGACTA
DmeF	Forward: TGGACCCACTCCCACAT
	Reverse: TGGACCCACTCCCACAT
SHF70550.1	Forward: GCTTCTTCCAGCCCTACC
	Reverse: TCTTCCGCCCATTTATTT
SHE59989.1	Forward: GGCCTGTTGATCGTAATG
	Reverse: GAGCCAAGCGAACCCTGT
SHF49653.1	Forward: ACCTGGAGTGGTCACGAT
	Reverse: AGACCTAACGGCTCTTCC
SHE60021.1	Forward: ATAAGTATGCCTATCGGAGTC
	Reverse: GTATTGCCTGAGCGTGAT
16s rRNA gene	27F: AGAGTTTGATCCTGGCTCAG
	1492R: TACGGYTACCTTGTTACGACTT

2.2 Growth medium and conditions

C. pauculus was cultivated in LB medium containing 10.0 g/L peptone, 5.0 g/L yeast extract, and 10.0 g/L NaCl. *C. pauculus* was incubated at 30°C until the mid-late logarithmic growth phase under aerobic conditions, then diluted 1:100 into fresh medium and incubated at 30°C, 150 rpm, in triplicate. Solutions of different metal concentrations were prepared by dissolving NiCl2 in distilled water to obtain metal concentrations of 1.7 mM (100 mg/L), 3.4 mM (200 mg/L), 5.1 mM (300 mg/L), and 6.8 mM Ni^{2+} (400 mg/L). *V. gazogenes* was purchased from Leibniz Institute DSMZ (Braunschweig, Germany). The strains were incubated with artificial seawater in a 1-L flask at 28 °C, 135 rpm until the mid-late logarithmic growth phase. Then incubation 1% to medium for cultivation and shaken at 28 °C, 135 rpm, in triplicate. The artificial seawater medium is listed in Table 2(Berges et al., 2001). Dissolving $NiCl_2$ in distilled water yielded solutions with metal concentrations of 1.7 mM (100 mg/L Ni^{2+}), 2.55 mM (150 mg/L Ni^{2+}), 3.4 mM (200 mg/L Ni^{2+}), 4.25 mM (250 mg/L Ni^{2+}).

Table 2 The artificial seawater medium

Reagent	Concentration (g/L)
Solution A	
NaCl	28.13
$CaCl_2$• $2H_2O$	1.60
KCl	0.77
$MgCl_2$• $6H_2O$	4.8
$MgSO_4$• $7H_2O$	3.5
$NaHCO_3$	0.11
ddH_2O	Until 1000 mL
Solution B (pH 7.4)	
Yeast extract	10

Trypsin	10
Tap water	Until 250 mL

2.3 EPS extraction and characterization

The protocol of EPS extraction was followed as described (Xia et al., 2019; Zeng et al., 2020b). After 1-day incubation, cell pellets were collected at 5000 g for 10 min at 4 °C, then, washed three times using phosphate-buffered saline (PBS). We used 1.5 M NaCl to resuspend cell pellets and vortexed at 300 rpm, 4 °C for 1h. Supernatants were collected at 10000 g for 1 hour at 4 °C. And filtered with a 0.2 nm filter membrane. Then we used Thermo Scientific™ SnakeSkin™ Dialysis Tubing to desalt the supernatants with MilliQ water for 48 hours at 4 °C. Changed MilliQ water every 6 hours and concentrated with PEG 8000. Samples were stored in a 4 °C fridge for the next steps of analysis. More details were listed in our previous research (Zeng et al., 2020b).

The concentration of e-PNs was measured with Bradford Assay (Thermo Fisher Scientific, Germany) (Harlow & Lane, 2006). Quantitative assessment of polysaccharide contents was conducted with phenol sulphuric acid method with glucose as the standard (Masuko et al., 2005; Yu et al., 2022a). DNA content was determined using a NanoDrop ND-1000 spectrophotometer (NanoDrop Technologies, Wilmington, USA)(Zeng et al., 2020a; Zeng et al., 2020b). The cell lysis rate was calculated according to the activity of the glucose-6-

phosphate-dehydrogenase (G6PDH) (Zeng et al., 2020b). The protocols were followed as in our previous study (Shen et al., 2018).

Cell pellets were collected and freeze-dried to characterize the groups from the cell surface using Fourier transform infrared transmission spectroscopy (FTIR, 8400, Japan). We used tree-dimensional excitation-emission matrix (3D-EEM) fluorescence quenching technology (Cary Eclipse, Varian, USA) to characterize the difference of EPS under stimulation of nickel (Zhu L, 2012).

2.4 Visual observation of extracellular polymeric substance

EPS was observed using a laser scanning confocal microscope (CLSM). E-PNs were stained with FITC (1 mg/mL in dimethyl sulfoxide (DMSO), and extracellular polysaccharide was stained with A-tetramethylrhodamine conjugate solution (0.25 mg/mL in DMSO) and calcofluor white (30 mg/mL in DMSO) (Zhang et al., 2020). All samples were collected in 1.5 ml tubes at 5000 g, 10 min, and 4^{o}C, and washed three times with PBS buffer. Then added FITC into the tube and suspended the cells, incubating them in the dark for 1 hour. Centrifuged the samples and washed the pellets three times. Then A-tetramethylrhodamine conjugate solution and calcofluor white, separately. During this process, the pellets were washed three times by PBS and the incubate for 30 min, separately (Wang et al., 2024) Table 3 outlines the information for the dyes' excitation and emission wavelengths.

Table 3 Excitation and emission wavelengths for dyes and corresponding

targets

Dye	Targets	Excitation (nm)	Emission (nm)
Fluorescein Isothiocyanate (FITC)	Proteins	488	500-550
Concanavalin A	α-D-glucopyranose polysaccharides	561	570-590
Calcofluor white	β-D-glucopyranose polysaccharides	400	410-480

2.5 LC-MS/MS-based proteomics

In-gel digestion of triplicate samples was performed following Shevchenko et al.(Shevchenko et al., 2006). Chromatographic separation of peptides was achieved with a two-buffer system (buffer A: 0.1% FA in H_2O, buffer B: 0.1% FA in ACN) on a nano-UPLC (Dionex Ultimate 3000 UPLC system, Thermo Fisher). Attached to the UHPLC was a peptide trap (100 µm x 20 mm, 100 Å pore size, 5 µm particle size, C18, Nano Viper, Thermo Fisher) for online desalting and purification, followed by a 25 cm C18 reversed-phase column (75 µm x 250 mm, 130 Å pore size, 1.7 µm particle size, peptide BEH C18, nanoEase, Waters). Peptides were separated using an 80 min method with linearly increasing ACN concentration from 2% to 30% ACN over 60 minutes. MS/MS measurements

were performed on a quadrupole-orbitrap hybrid mass spectrometer (QExactive, Thermo Fisher Scientific). Eluting peptides were ionized using a nano-electrospray ionization source (nano-ESI) with a spray voltage of 1,800 and analyzed in data dependent acquisition (DDA) mode. For each MS1 scan, ions were accumulated for a maximum of 240 milliseconds or until a charge density of 1 x 10^6 ions (AGC Target) was reached. Fourier-transformation based mass analysis of the data from the orbitrap mass analyzer was performed covering a mass range of 400 – 1,200 m/z with a resolution of 70,000 at m/z = 200. Peptides being responsible for the 15 highest signal intensities per precursor scan with a minimum AGC target of 5 x 10^3 and charge state from +2 to +5 were isolated within a 2 m/z isolation window and fragmented with a normalized collision energy of 25% using higher energy collisional dissociation (HCD). MS2 scanning was performed, covering a mass range starting at 100 m/z and accumulated for 50 ms or to an AGC target of 1 x 10^5 at a resolution of 17,500 at m/z = 200. Already fragmented peptides were excluded for 20 s.

LC-MS/MS was searched with the Sequest algorithm integrated in the Proteome Discoverer software (v 2.4.1.15), Thermo Fisher Scientific) against the secretome of DSM 21264 or *C. pauculus* and *V. gazogenes*. Prediction of N-terminal signal peptides was performed with SignalP v.6.0 in fast mode (Teufel et al., 2022). The genome accession number is GCA_900129185.1. Carbamidomethylation was set as a fixed modification for cysteine residues and the oxidation of methionine, and pyro-glutamate formation at glutamine

residues at the peptide N-terminus, as well as acetylation of the protein N-terminus, were allowed as variable modifications. A maximum number of 2 missing tryptic cleavages was set. Peptides between 6 and 144 amino acids were considered. A strict cutoff (FDR<0.01) was set for peptide and protein identification. Quantification was performed using the Minora Algorithm, implemented in Proteome Discoverer.

Statistical analysis was performed in Perseus (https://maxquant.net/perseus/). Obtained protein abundances were log_2-transformed and normalized by column-median normalization. Values were reduced to >2 valid value per group resulting in 154 proteins used for Student's t-testing. As significance cut-off an adjusted p-value < 0.05 (permutation-based FDR) was set, as well as a fold change > 2. Visualizations were performed with an in-house script in R Studio.

2.6 Reactive oxygen species assay and electron transport system activity assay with Ni^{2+} treatment

Reactive oxygen species (ROS) levels were determined using ROS assay kit (Solarbio, Beijing). *C. pauculus* was incubated at 30 ^{o}C in LB medium for 24 hours. Cells with/without Ni^{2+} were collected at 4^{o}C, 5000 g, 5 min. dichlorodihydrofluorescein diacetate (DCFH-DA) staining were diluted from 10 mM to 10 μM with Phosphate-Buffered Saline (PBS). Cell pellets were diluted in DCFH-DA to a final cell density of 10^7 cells/mL. And incubated at 30^{o}C for 30

min in the dark. Every 5 min, the solution was inverted and gently mixed to ensure DCFH-DA-cells thorough contact with DCFH-DA. The cells were then washed three times with PBS and finally resuspended in 1 mL PBS. The fluorescence intensity of samples was performed at the excitation wavelength 488 nm and emission wavenumber 525 nm by fluorescence spectrophotometer (Hitachi, Japan). All the experiments were repeat for 3 times.

Electron transport system activity (ETSA) was measured using (2-(p-iodophenyl)-3-(p-nitrophenyl)-5-phenyltetrazolium chloride (INT) (Cheng et al., 2011; He et al., 2021). 0.01g cells collected (after incubation for 24 hours) were incubated with 1 mL 0.2% INT in 10 mL falcon tubes at 150 rpm, 30^{o}C for 30 min. Then 1 mL 37% methanol was added, and the cell pellets were collected at 8000 g for 5 min. Cell pellets were resuspended in 5 mL methanol and incubated at 30^{o}C, 150 rpm for 10 min. The supernatant was collected at 8000 g for 5 min and the absorbance was measured at 485 nm by UV-vis spectrophotometer. ESTA were calculated as follows (Li et al., 2011):

$$ESTA=D_{485}V/(kWt)$$

D_{485} is the absorbance read at 485 nm; V is the volume of extractant, mL; k is the slope of standard curve, mLμg^{-1}; W is the weight of cells, mg; and t is the incubation time, h.

2.7 Real-time quantitative Polymerase Chain Reaction analysis

The extraction method followed the manufacturer's protocol. Total RNA

was extracted at different time points of *C. pauculus* growth, including the first hour, second hour, third hour and fourth hour, using TRIzol reagent. 3.4 mM Ni^{2+} was added into the medium when the OD_{600} reached 0.2. The primers listed in Table 1 were designed using Primer Premier 5 software. And they were synthesized by Tsingke (Changsha) Co.Ltd., the sequence of genes was downloaded from NCBI. The gene expression value was calculated as follows (TG: target gene, CG: control gene):

$$2^{-\Delta\Delta CT}=2^{-[(C_{T,TG}-C_{T,CG})treated-(C_{T,TG}-C_{T,CG})tested]}$$

2.8 Removal of part of extracellular proteins

Experiments were performed in triplicates. Solutions of different metal concentrations were prepared by dissolving $NiCl_2$ in distilled water to obtain metal concentrations of 1.7 mM (100 mg/L), 3.4 mM (200 mg/L), 5.1 mM (300 mg/L), and 6.8 mM Ni^{2+} (400 mg/L). The culture conditions were the same as in 2.2. The optical density (OD_{600}) was determined daily using an ultraviolet (UV) spectrophotometer (Shimadzu UV-2550, Japan). According to the growth curve of Ni^{2+} resistance, the experiments were divided into Ni^{2+} (1.7 mM, 3.4 mM) and control. Proteinase K was proved that it was accessible to the outer cell membrane (Bae et al., 2000). Therefore, the two groups consisted of no proteinase K and 10 mg/mL proteinase K. 10 mg/mL proteinase K was added to the initial medium.

2.9 Constructing a Phylogenetic Tree

Blast the sequences on NCBI (https://www.ncbi.nlm.nih.gov/) and download the similar proteins sequences (Query cover > 90%, Percent Identity > 70%). Use MEGA software to construct the phylogenetic tree. Then, beautify the tree using the iTOL online tool, available at: https://itol.embl.de/.

2.10 Predicting Ni^{2+} Binding Sites Using Metal 3D, AlphaFold 3, and MetalNet

The prediction of metal sites is based on Metal 3D, a universal deep learning model that accurately predicts the positions of metal ions in proteins. The code link is as follows: https://github.com/lcbc-epfl/metal-site-prediction [Dürr, 2023 #1006]. This model primarily identifies Zn^{2+} but also recognizes other transition metals such as Cu^{2+}, Ni^{2+}, Mn^{2+}, Zn^{2+}, Fe^{2+}, and Fe^{3+} [Dürr, 2023 #1006]. AlphaFold 3 link: https://alphafoldserver.com/. Select the Protein-Glycan-Ion: PDB 7BBV model for prediction. MetalNet link: http://152.136.132.42:8080/ [Cheng, 2023 #1008].

3 Extracellular proteins enhance *Cupriavidus pauculus* nickel tolerance and cell aggregate formation

In the first part of this thesis, this study focused on firstly investigating the role of e-PNs in heavy metal resistance using proteinase K to remove part of e-PNs. EPS was quantified and chemically characterized with Ni^{2+} treatment by three-dimension excitation emission matrix fluorescence spectroscopy (3D-EEM), fourier transform infrared spectroscopy (FTIR) and confocal laser scanning microscopy (CLSM). Specifically, e-PNs were identified using liquid chromatography with mass spectrometry (LC-MS/MS) and analyzed base on secretome to exclude interference from intracellular proteins. Meanwhile, the genes related to heavy metal resistance, the involved electron transfer system activity (ETSA) and reactive oxygen species stress (ROS) were evaluated which also supported the proteomic data. Together, the experiments and conceptual model reveal the e-PNs' function on resistance and adsorption of Ni^{2+}. The objective of this study was to advance the understanding of Ni^{2+} tolerance and adsorption of *C. pauculus* and underlying mechanism mediated by e-PNs (Mingwei et al., published in Bioresource Technology, Wang M, Vollstedt C, Siebels B, et al. Extracellular proteins enhance *Cupriavidus pauculus* nickel tolerance and cell aggregate formation[J]. Bioresource Technology, 2023: 130133.

https://doi.org/10.1016/j.biortech.2023.130133).

3.1 Results

C. pauculus is a highly metal-resistant gram-negative bacterium. The strain was isolated from the mineral water, and in general it is an ubiquitous non-pathogenic organisms found in soil and water samples (Zeng et al., 2020b). The precise molecular mechanisms of heavy metal resistance in bacteria are yet poorly understood. The knowledge gap is caused by the inability to extract EPS, identify e-PNs, and demonstrate the interaction of e-PNs during Ni^{2+} treatment. In this study, the impact of Ni^{2+} treatment was analyzed on *C. pauculus* on a molecular level.

3.1.1 Nickel resistance Gene from *C. pauculus* whole genome

As shown in Table 4, nine genes associated with nickel resistance in *C. pauculus* were identified, encompassing both bacterial nickel response and tolerance mechanisms. The nickel resistance systems were shown in Figure 4. The nickel response mechanisms include three extracytoplasmic function sigma factors (ECF): *CnrH*, *CnrY*, and *CnrX*; one Ni^{2+} response regulator, NikR; and three genes involved in specific nickel tolerance mechanisms. These tolerance mechanisms include a nickel efflux system composed of the RND family proteins (subunits *CnrA*, *CnrB*, and *CnrC*) and one CDF family protein, *DmeF*. The RND family proteins are involved in metal efflux, consisting of an

inner membrane pump, an outer membrane channel, and a periplasmic adaptor protein, which use proton motive force to export metals. The CDF family is a widely distributed family of cation/proton antiporters characterized by six transmembrane domains.

Table 4 Prediction of Ni resistance proteins and secretion systems

Accession number	Prediction
WP_011239970.1 periplasmic nickel sensor *CnrX*	Other
WP_011239971.1 cobalt_nickel resistance anti-sigma factor *CnrY*	Other
WP_017510981.1 nickel efflux RND transporter permease subunit *CnrA*	Other
WP_017510983.1 nickel efflux RND transporter outer membrane subunit *CnrC*	SP
WP_017510984.1 nickel resistance ECF sigma factor *CnrH*	Other
WP_029306711.1 nickel diffusion facilitator *CnrT*	Other
WP_029306712.1 nickel efflux RND transporter periplasmic adaptor subunit *CnrB*	Other
WP_150980960.1 nickel-responsive transcriptional regulator *NikR*	Other
WP_244786576.1 CDF family Co/Ni efflux transporter *DmeF*	Other

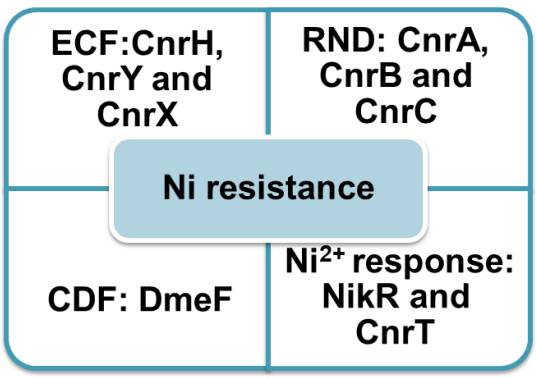

Figure 4: Prediction of Ni resistance proteins

For phylogenetic analysis, we selected the RND family protein CnrC as a representative protein. Proteins with over 70% similarity were analyzed, revealing high homology between the CnrC protein in *C. pauculus* and those in Other species. Notably, the similarity with the model strain *Cupriavidus metallidurans* within the same genus was 84.45%. The similarity to a protein from *Burkholderiaceae* (WP_024570395.1) was 89.95%. Since *Cupriavidus* belongs to the *Burkholderiaceae* family, the protein is related to the TolC family, which also enhances copper resistance as mentioned in the introduction. The similarity to *Achromobacter xylosoxidans* was 74.4%, and the RND family outer membrane subunit NccC from *Burkholderiaceae* also showed a similarity of 74.4%, indicating close homology with *Achromobacter xylosoxidans*. The similarity to *Ralstonia* sp. was 72.31%, as illustrated in Figure 5, with homologous proteins being more distantly related but still over 70% similarity. All these homologous proteins belong to the TolC family. Studies have shown that TolC family proteins can influence protein secretion, polysaccharide synthesis, heavy metal resistance, and antibiotic resistance.

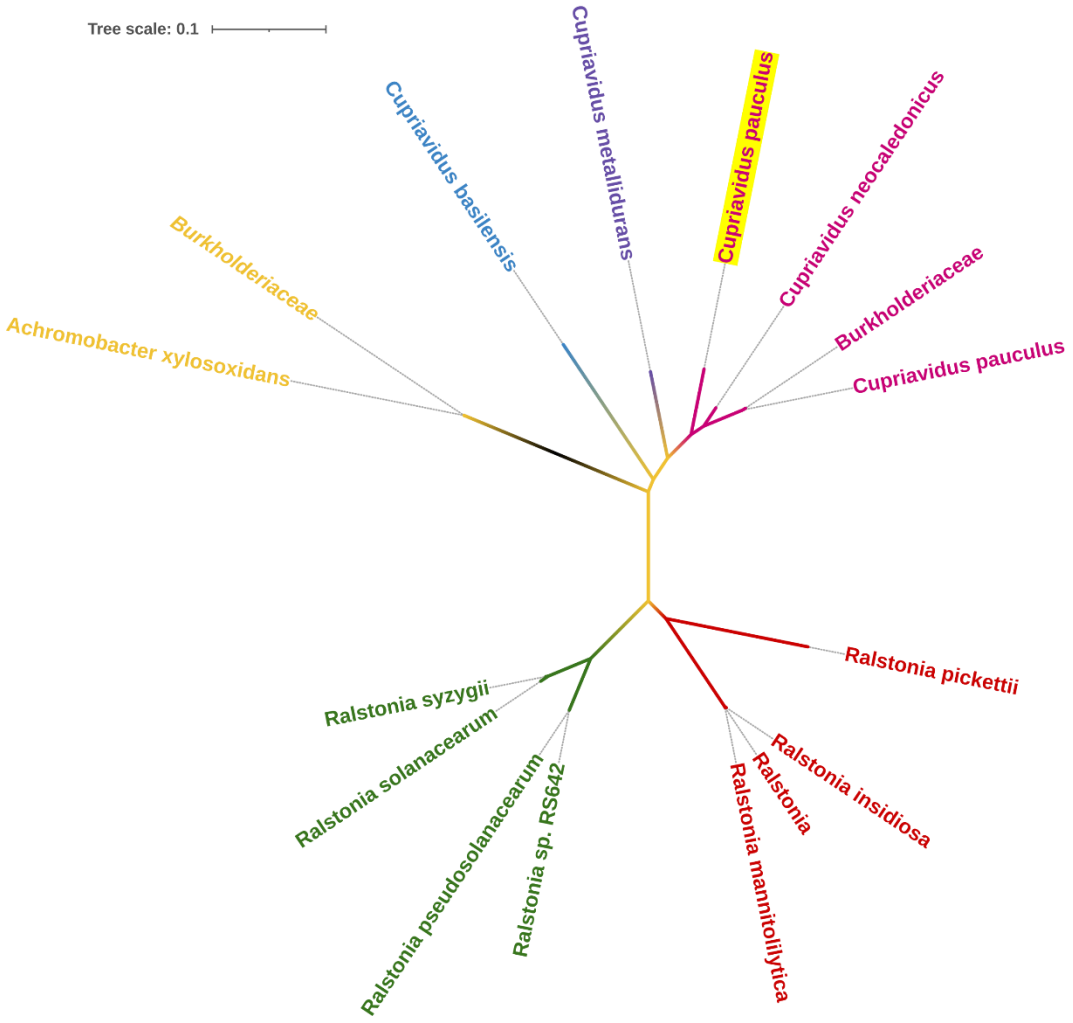

Figure 5 Phylogenetic tree of RND family protein CnrC. *Burkholderiaceae* (WP_051385297.1)，*Achromobacter xylosoxidans* (Q44584.1)，*Ralstonia* (WP_024542618.1)，*Ralstonia mannitolilytica* (AJW47711.1)，*Ralstonia insidiosa* (MBA9871483.1)，*Ralstonia pickettii* (WP_154205965.1)，*Ralstonia pseudosolanacearum* (WP_269438489.1)，*Ralstonia sp.* RS642 (UZF26717.1)，*Ralstonia syzygii* (WP_211904536.1)，*Ralstonia solanacearum* (WP_118869201.1), *Cupriavidus basilensis* (WP_059414357.1)，Cupriavidus metallidurans (WP_186426155.1), *Cupriavidus pauculus* (WP_341249119.1)，*Burkholderiaceae* (WP_024570395.1), *Cupriavidus neocaledonicus* (SPD46685.1)

3.1.2 Nickel resistance mechanism in *C. pauculus* according to the whole genome

As shown in Figure 6, the nickel resistance mechanism in *C. pauculus* is remarkably similar to that of the model organism *Cupriavidus metallidurans*. One key player in this mechanism is *CnrH* (ECF20), a member of the ECF sigma factor family, which regulates cobalt and nickel resistance in *Cupriavidus*. As illustrated in Figure 6, *CnrH* is regulated by a complex composed of two transmembrane proteins, the metal sensor *CnrX* and the anti-sigma factor *CnrY*. In the absence of Ni^{2+} stimulation, *CnrH* is sequestered on the membrane by *CnrY*. Upon exposure to Co^{2+} or Ni^{2+}, these ions bind to *CnrX*, leading to the release of *CnrH* from *CnrY*. This release promotes the expression of genes involved in metal efflux into the periplasmic space or extracellular environment. *CnrX* is a membrane-anchored dimeric protein with a C-terminal periplasmic metal-sensing domain, specifically binding Co^{2+} or Ni^{2+} over other transition metal cations. It has been reported that *CnrX* has a 10 to 100-fold higher affinity for Ni^{2+} compared to Co^{2+}. Upon metal sensing in the periplasmic space, signal transduction occurs through the interaction between *CnrX* and *CnrY*. In the inner membrane near the periplasmic side, the C-terminus of the anti-sigma factor *CnrY* docks into the hydrophobic cavity of the *CnrX* dimer. *CnrY* is a single-pass transmembrane protein with a 45-amino acid cytoplasmic domain containing two helices, which enclose the σ2 and σ4 domains of CnrH(Antoine et al., 2014).

The genes regulated by the *CnrYXH* complex are part of the cobalt-nickel resistance (cnr) determinant cluster, *CnrYXH-CBAT*, in the *C. pauculus* genome. This cluster consists of two operons: *cnrCBAT* and cn*rYXH*. Under the control of the *cnrCp* promoter, the *cnrCBAT* operon encodes the transmembrane heavy metal efflux pump complex *CnrCBA* and the inner membrane transport protein *CnrT*. In high concentration of Ni^{2+} environments, Ni^{2+} is transported from the cytoplasm to the periplasmic space by *CnrT* and subsequently expelled out of the cell by *CnrCBA*. Additionally, the *cnrYXH* operon, regulated by the *cnrYp* promoter, encodes the signal transduction system that regulates the expression of *cnrCBAT*(Antoine et al., 2014).

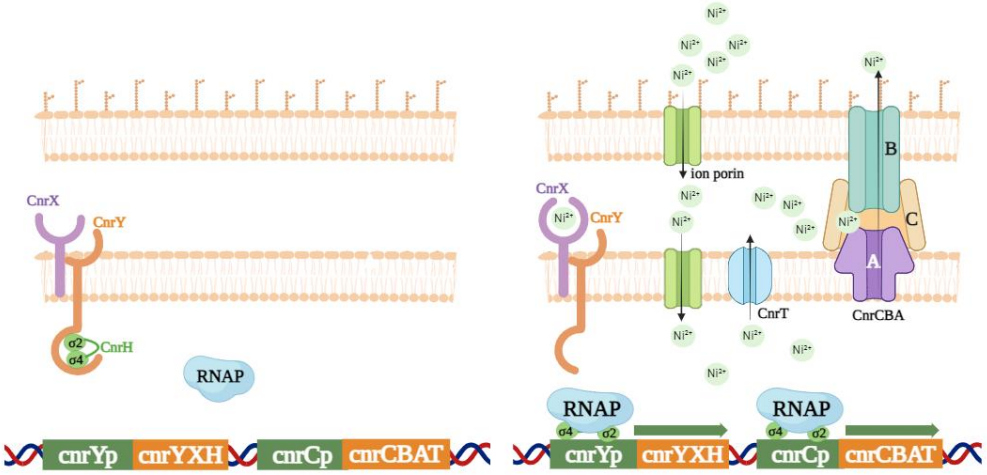

Figure 6: Mechanism of action of the *C. pauculus CnrH* sigma factor; When nickel is transported to the periplasm, Ni^{2+} binds to *CnrX*. This binding triggers the release of the σ2 and σ4 domains of *CnrH* by *CnrY*. The released σ2 and σ4 domains then associate with RNA polymerase and the *CnrY* promoter, initiating the expression of the *CnrCBA* nickel transporter genes.

3.1.3 The effect of Ni^{2+} on *C. pauculus* growth

Treatment of *C. pauculus* with elevated Ni^{2+} resulted in increased growth. Doubling times were increased slightly (up to 0.8-fold) and the optical densities were up to 2-fold increased (Figure 7) in the presence of 1.7 mM Ni^{2+}. However, cell density was inhibited slightly under 3.4 mM Ni^{2+}. And, its growth was severely suppressed when the Ni^{2+} concentration exceeded 5.1 mM Ni^{2+}. In addition, the lag phase of bacterial growth also increased. Moreover, the cell density decreased under 3.4 mM Ni^{2+} with proteinase K treatment. It indicated that e-PNs is crucial for Ni^{2+} resistance.

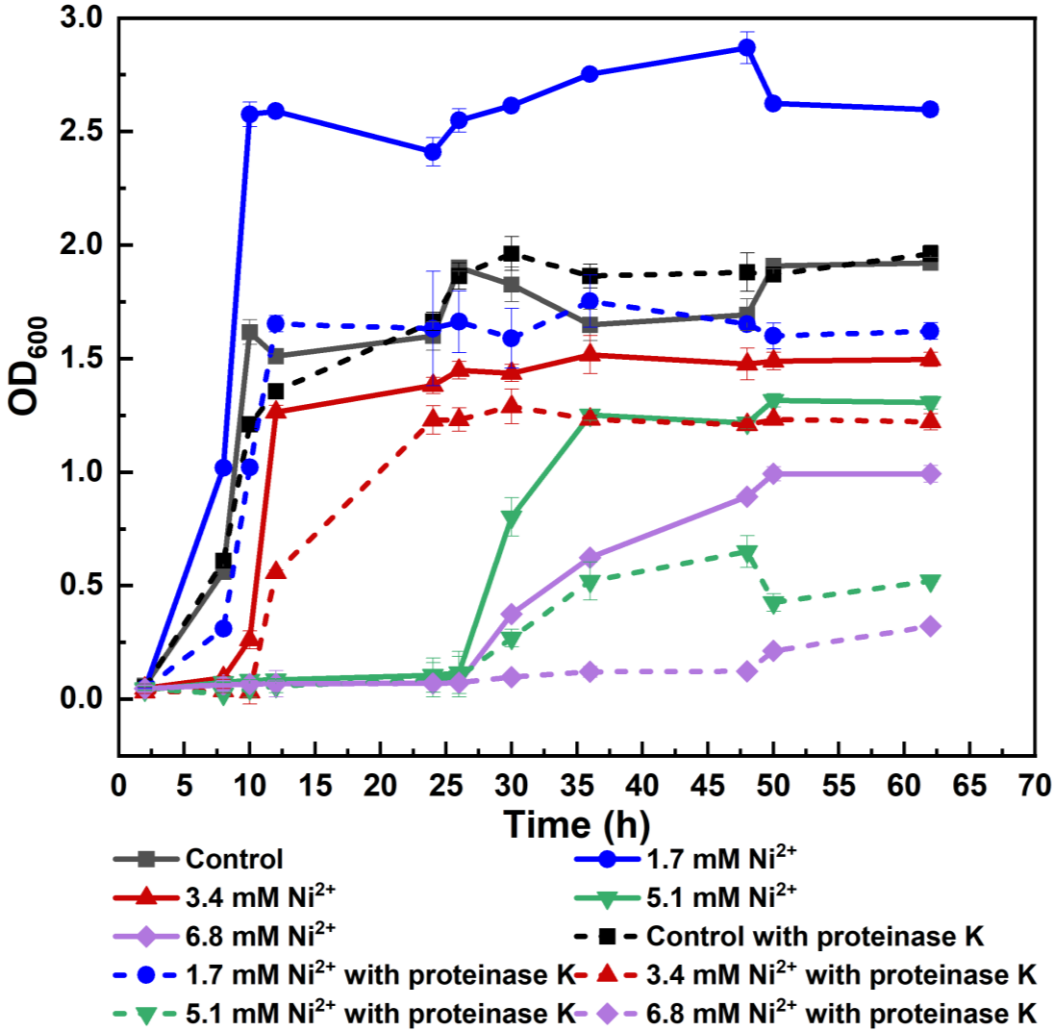

Figure 7: Growth of *C. pauculus* supplemented with Ni^{2+}. *C. pauculus* was cultivated in LB medium at 30 °C under aerobic conditions with concentration of 1.7 mM Ni^{2+}, 3.4 mM Ni^{2+}, 5.1 mM Ni^{2+} and 6.8 mM Ni^{2+} treatments. bars indicate standard deviation and data are mean values of three independent measurements. Proteinase K was used to remove or break part of e-PNs at the initial of the experiments

3.1.4 Spectroscopic analyses of e-PNs

Fourier Transform infrared spectroscopy (FTIR) analyses showed changes in functional group occurrence as wavenumber changes. To demonstrate the microbial adsorption of heavy metals, the crucial functional groups of e-PN were shown in Figure 8. Functional groups of *C. pauculus* were detected under different concentrations of Ni^{2+}. The spectra were shorter after proteinase K was added to the medium, especially under stimulation of heavy metals. It indicated that the proteinase K reduced the number of surface groups of the cells. Spectra were stretched down under 1.7 mM Ni^{2+} stimulation compared to the control. However, the spectra under 3.4 mM Ni^{2+} stimulation showed the opposite result. The possibility of peak attenuation lies in the complexation of heavy metals with the functional group. The increased intensity of peaks with Ni^{2+} treatment indicated that e-PNs play a vital role in Ni^{2+} adsorption and adoption in *C. pauculus*.

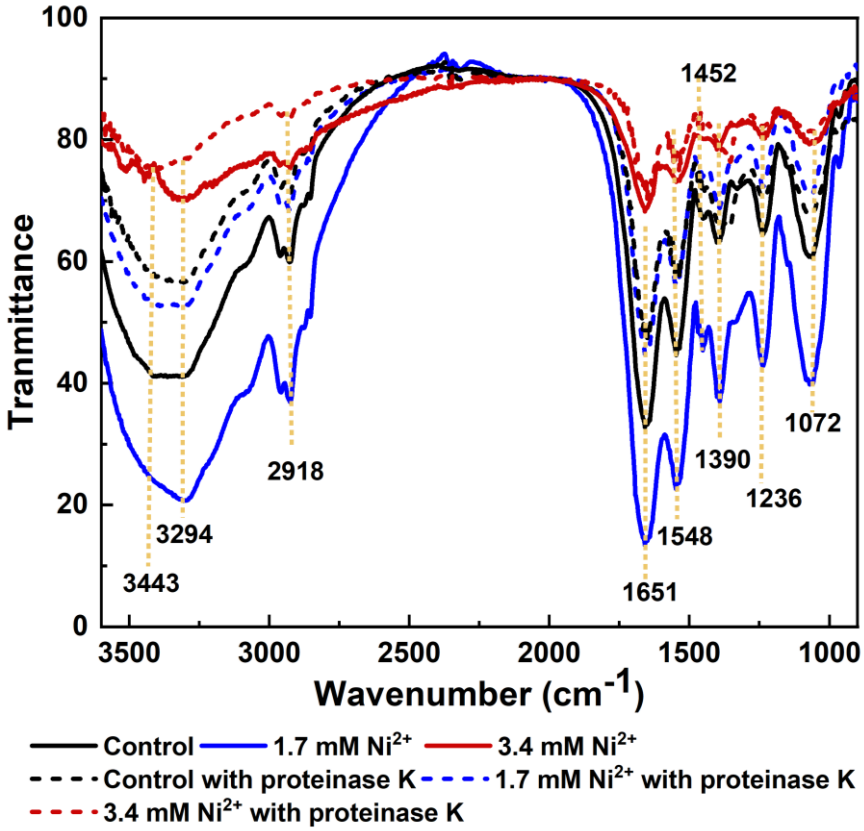

Figure 8: FTIR of *C. pauculus* 1490 under stimulation of Ni^{2+} with proteinase K and control. 2922, asymmetric stretching vibration of CH_2; 1658, C—O and N-H stretching in the amide group (peptidic bond); 1546, N–H bending and C–N stretching in the amide group (peptidic bond); 1402, C–O symmetric stretching of carboxyl groups (Carboxylates); 1240, P–O stretching of phosphate (Carboxylic acids); 1089, P–O stretching of phosphate groups (Carboxylic acids)

3.1.5 The impact of Ni^{2+} treatment on concentration of EPS

The major components of EPS in *C. pauculus* were extracellular polysaccharides (e-PS) and e-PNs. The total amount of e-PNs with Ni^{2+} treatment was significantly increased compared to the controls (Figure 9). The contents of e-PS with Ni^{2+} treatment and control almost had no difference.

However, the contents of e-PNs under Ni^{2+} stimulation were increased compared to control. In addition, e-PNs reduced as the increased Ni^{2+} concentration. With 1.7 mM Ni^{2+} treatment, the content of e-PNs was 103.67 mg/g-DW while the content of e-PNs under 3.4 mM Ni^{2+} stimulation was 39.23 mg/g-DW.

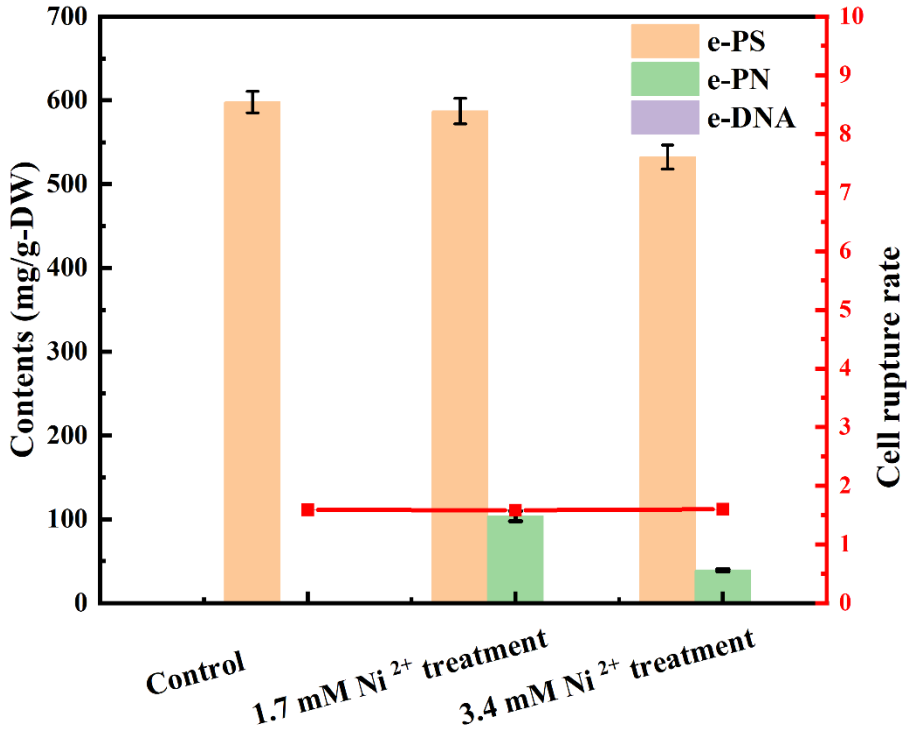

Figure 9: The impact of Ni^{2+} treatment on concentration of EPS. The concentration of e-PS was determined by the phenol sulphuric acid method with glucose as the standard. Protein contents were measured using the Bradford protein assay kit with bovine serum albumin as the standard. DNA content was determined using a NanoDrop ND-1000 spectrophotometer (NanoDrop Technologies, Wilmington, USA). Bars indicate standard deviation and data are mean values of three independent measurements. Cells rupture rate (the red line) was calculated by G6PDH. To evaluate the extent of cell lysis, the activity of G6PDH in the EPS extract was measured using a G6PDH kit (Beijing Solarbio Technologies Ltd, Beijing, China) in accordance with the product's

instructions

3.1.6 Chemical composition and quantitative analysis of extracellular polymeric substances

Tryptophan protein-like (peak A) and aromatic protein-like substances (peak B) increased after 24h incubation in response to Ni^{2+} stimulation using 3D-EEM analysis (Figure 10 a, b, c). And in the 1.7 mM Ni^{2+} treatments (Figure 10 b), the levels of these two types of substances were higher than 3.4 mM Ni^{2+} treatments (Figure 10 c). Confirmation of this observation was obtained by determining the concentration of EPS (Figure 10). With 3.4 mM Ni^{2+} treatments (Figure 10c), tryptophan protein-like substances (peak A) increased compared to control. Notably, Other aromatic-rich proteins had not such an effect (peak B) and decreased in comparison to the control (Figure 10 a).

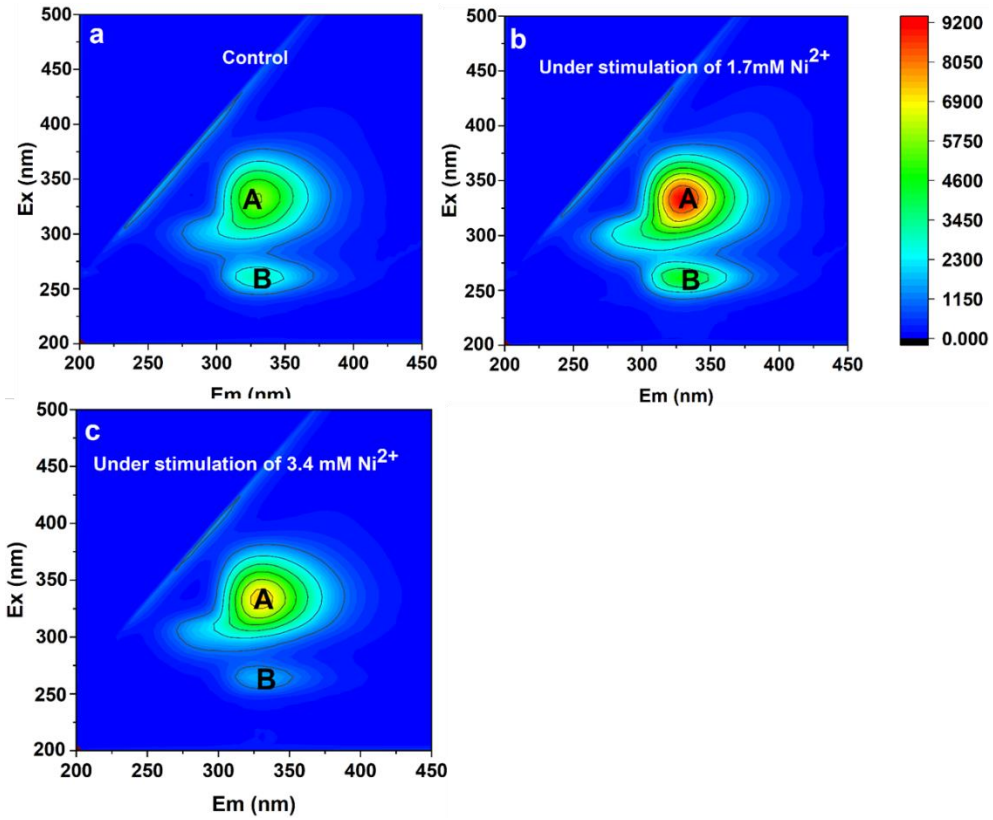

Figure 10: 3D-EEM fluorescence quenching of EPS fractions of 24 h culture extracts. The fluorescence characteristics of EPS were determined using 3D-EEM fluorescence quenching technology. (a,b,c) 3D-EEM fluorescence spectra of EPS extracted from *C. pauculus* 1490 with Ni^{2+} treatment and control. Peak A and B represent different tryptophan and aromatic protein-like substances respectively

3.1.7 Confocal laser microcopy for visualization of extracellular polymeric substances

Under Ni^{2+} stimulation, the overall structure and composition of the EPS and the e-PNs changed. At the first 3 hours of Ni^{2+} treatment, cells were more likely to clump together and formed aggregates (Figure 11 a2-3). But after incubation for hours, the opposite phenomenon was observed (Figure 11 c3). When staining EPS of *C. pauculus* cells after 3 (Figure 11 a1-b3) and 24 hours

(Figure 11 c1-d3), clear differences between treated with and without Ni^{2+} were observed. α-D-glucopyranose polysaccharides (α-PS) as part of the EPS was stained using concanavalin A, β-D-glucopyranose polysaccharides (β-PS) using calcofluor white, and e-PNs using fluorescein isothiocyanate (FITC), as described in Material and Methods. Main colors observed were green indicating e-PNs; purple stained cells are resulting from different ratios of α- and β-PS stained; blue stained cells show higher levels of β-PS. In the presence of 3.4 mM Ni^{2+} (Figure 11 a3, b3) in general more e-PNs were observed and compared to the 1.7 mM Ni^{2+} treatments (Figure 11 a2, b2) in the first 3 hours. At the same time a change in color indicated a change in the structure of e-PS (α-PS and β-PS) (Figure 11 a). However, after 24 hours, the fluorescence intensity of e-PNs in 1.7 mM Ni^{2+} treatments (Figure 11 c2, d2) were higher than in 3.4 mM Ni^{2+} treatments (Figure 11 c3, d3).

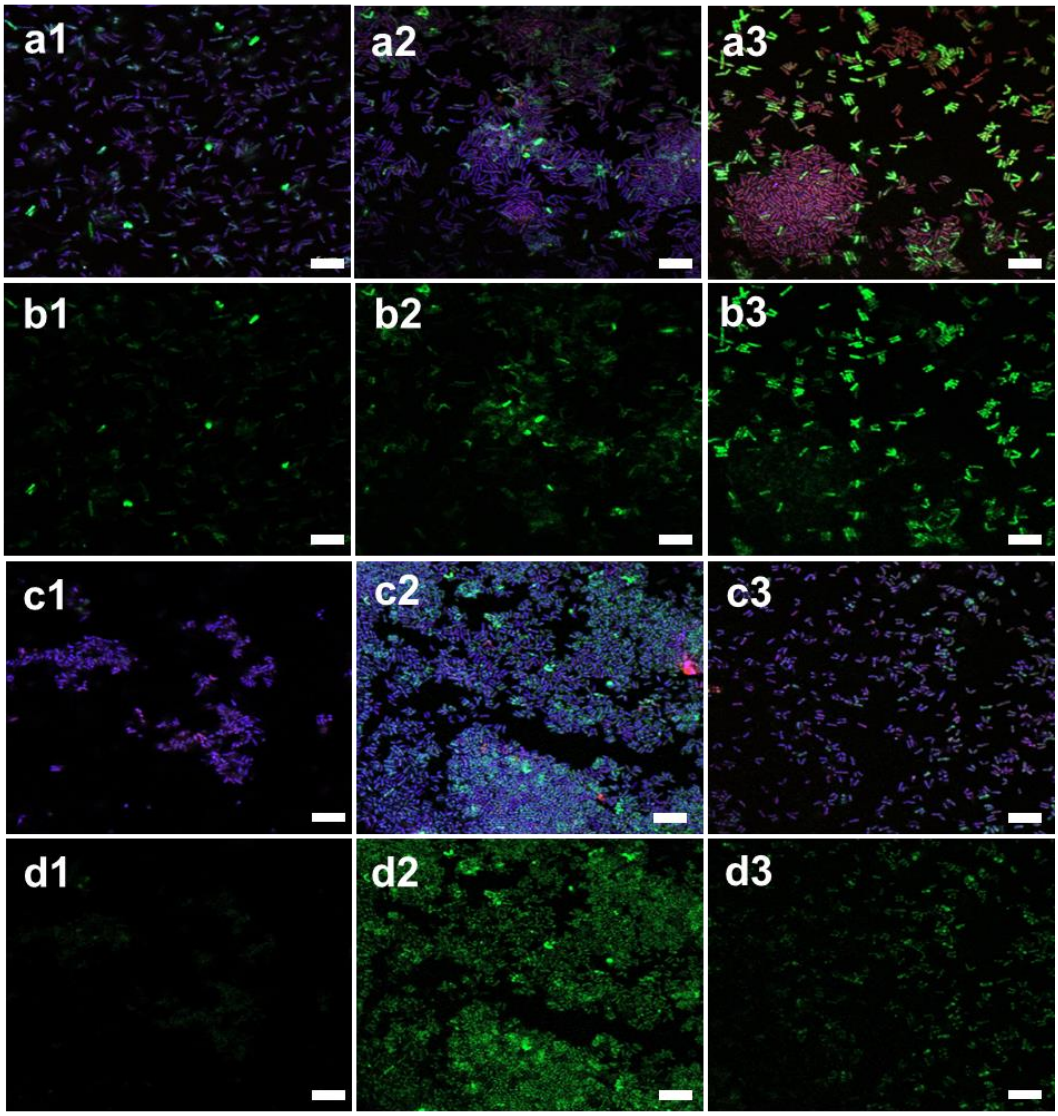

Figure 11: EPS staining of *C. pauculus* 1490 cells after 3 (a1-b3) and 24 hours (c1-d3) in LB medium treated with/or without Ni^{2+}. White box indicates scale bar (5 ㎛). α-D-glucopyranose polysaccharides (α-PS) was stained by concanavalin A, β-D-glucopyranose polysaccharides (β-PS) was stained using calcofluor white, and e-PNs were stained using fluorescein isothiocyanate (FITC). Main colors observed were green indicating e-PNs; purple stained cells are resulting from different ratios of α- and β-PS stained; blue stained cells show higher levels of β-PS as they are mainly stained with calcofluor white

3.1.8 Functional potential and localization of extracellular proteins

In a next step, how the extend the pattern of e-PNs changes was investigated in response to Ni^{2+} treatment. For this LC-MS/MS analyses were performed on samples incubated with and without Ni^{2+}, and the obtained protein masses were analyzed. Proteins related to different environmental resistance, nickel efflux, electron transfer, and EPS synthesis, as well as response to Ni^{2+} resistance and adsorption, showed a significant upregulation. They were located at the cell membrane or periplasm, including the inner and outer membranes. 8,429 peptides and 1,229 proteins were identified, of which 920 were identified across all samples. Fifty-two proteins significantly changed in their occurrence, including 43 up- and 9 down-regulated proteins (Figure 12). Among these only one protein was more than 2-fold down-regulated (response regulator containing an atypical phosphorylation pocket, WP_061955464.1) whereas 27 proteins were upregulated over 2-fold change. Most intriguingly, the lipopolysaccharide synthesis protein LpxC (WP_061958371.1) related to nickel adsorption was upregulated over a 2-fold with Ni^{2+} treatment. Furthermore, the (WP_061955464.1, CysM) was also significantly overexpressed in response to Ni^{2+} treatment. CysM participates in cysteine biosynthesis, which can enhance Ni^{2+} adsorption. Interestingly, *C. pauculus* codes for 10 potential and predicted heavy metal efflux proteins, including 4 nickel efflux proteins and 6 heavy metal efflux proteins from predicted secretome data listed in Table 4. With the exception of a single multidrug efflux

protein (WP_244787460.1), none of the heavy metal efflux proteins was significantly altered in its expression level on a protein level.

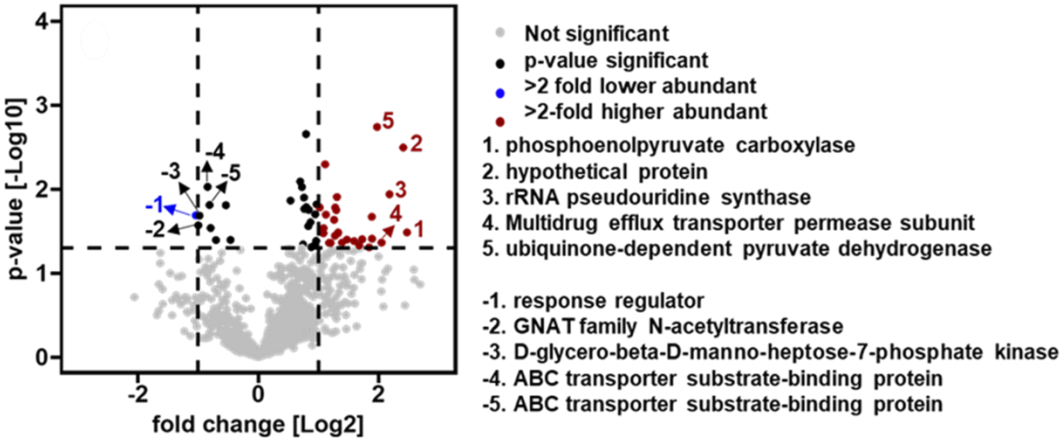

Figure 12: Volcano plot visualization of t-testing results between the phenotypes and proteome analysis of e-PNs. Proteins were considered significantly differential abundant if they exceeded a p-value cutoff <0.05 and> 2-fold difference. Red and blue dots represent significantly up-regulated and down-regulated proteins over 2-fold, respectively. Black dots mean significant changes <2-fold difference. Grey dots indicate no significant changes

In order to figure out the expression of the Ni^{2+} transporter and efflux pump from whole genome, RT-PCR was carried out. The results showed that few genes related to nickel resistance and efflux (WP_061957565.1, CnrH, SecY, and DmeF) were upregulated (12-300-fold) (Figure 13 a, b, c, d) at first 4 hours. It indicated that Ni^{2+} transporters expression were immediately response to Ni^{2+}

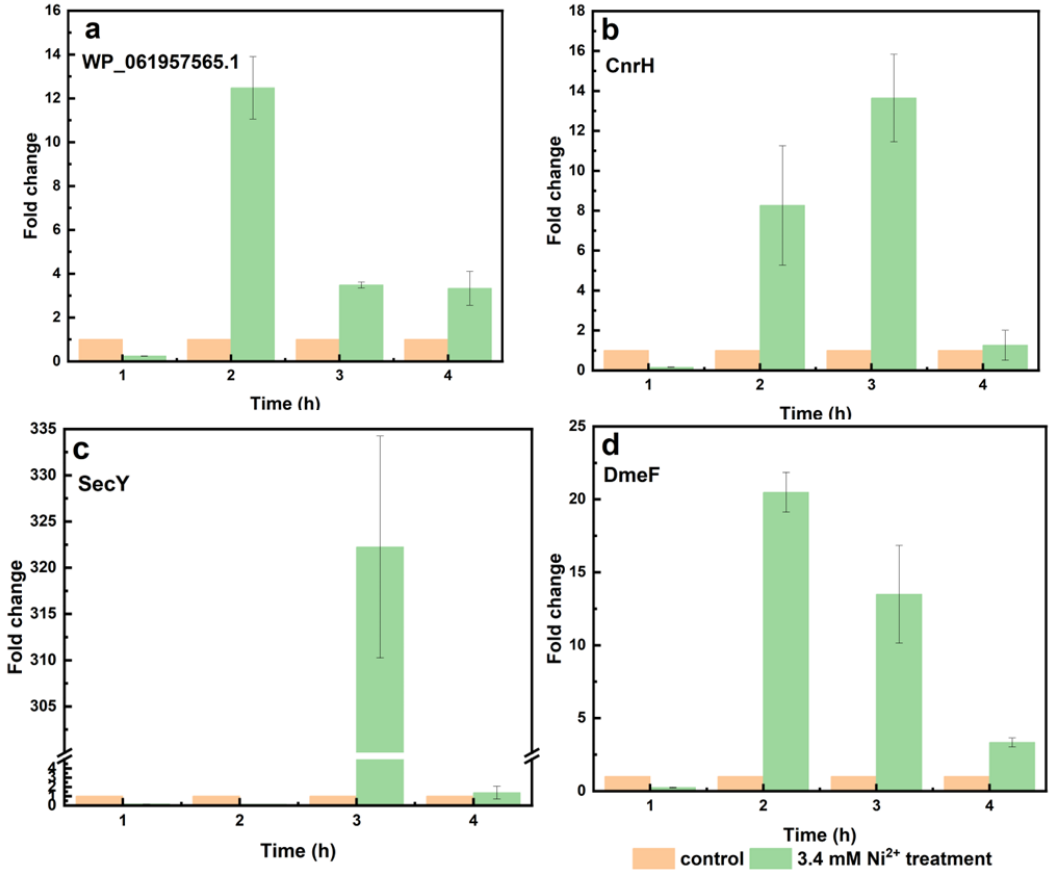

Figure 13: Gene expression levels of selected ORFs linked to Ni resistance in LB cultures at different time points. The orange bars represent the control group, while the green bars represent the group under 200 mg/L Ni^{2+} stress. Data were generated using qRT-PCR protocols as outlined in Material and Methods. The ORFs analyzed were WP_061957565.1, *secY* (WP_061956538.1), *cnrH* (WP_017510984.1) and *dmeF* (WP_244786576.1). Data are results of three independent measurements and cultures. Error bars indicate the standard deviations. Data were normalized against the 16S rRNA gene. WP_061957565.1 is involved in amino acid ABC transport substrate-binding protein. *SecY* is an outer membrane protein. *CnrH* is a nickel resistance ECF sigma factor and *DmeF* is involved in nickel efflux transporter

3.1.9 Analysis of ROS level and ETSA with nickel treatment

As shown in Figure 14 a, ROS levels increased siginificantly followed the increased concentrations of Ni^{2+}. With 3.4 mM Ni^{2+} treatment, the ROS levels is almost two-fold-change compared with control. The florescence intensity is 30,880 under 3.4 mM Ni^{2+} treatment while that of control is 16,297. In addition, ETSA increased two-fold-change with 1.7 mM Ni^{2+} treatment compared to control (Figure 14 b); however, it decreased as the increased concentration of 3.4 mM Ni^{2+} treatment. But it was still higher than that of control.

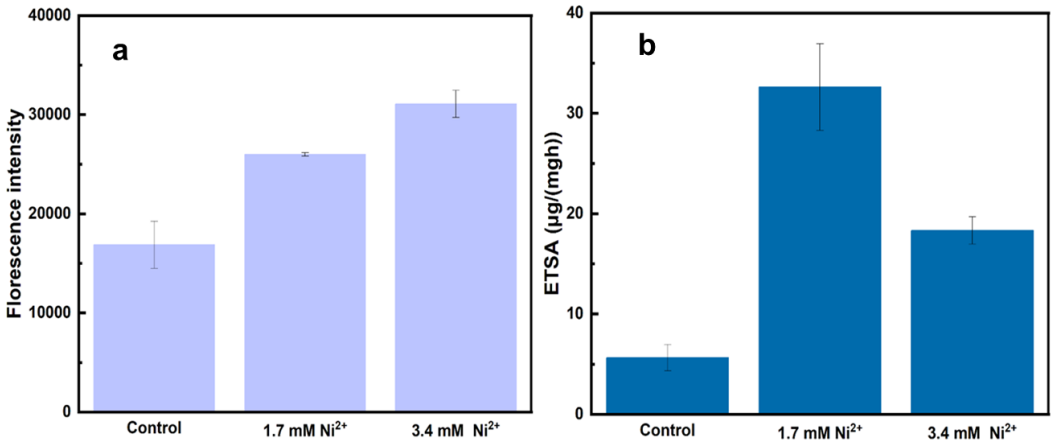

Figure 14 ROS and ESTA detection. (a), ROS levels detection under Ni^{2+} stimulation; (b) ESTA measurement with Ni^{2+} treatment. Data are results of three independent measurements and cultures. Error bars indicate the standard deviations.

3.2 Discussion

According to the assumed function of e-PNs, a hypothetical model of essential proteins involved in Ni^{2+} resistance and adsorption was constructed (Figure 15). The bacterial strategy from the findings for heavy metal resistance has three

parts related to EPS: extracellular barrier, active transport of metal ions (efflux) and extracellular sequestration.

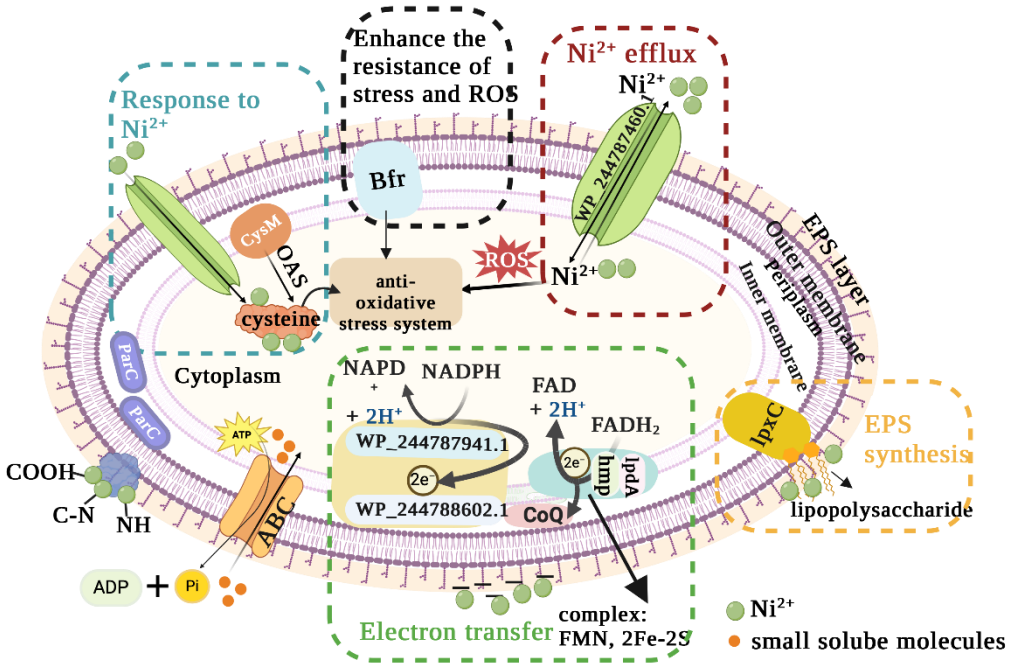

Figure 15: Conceptual Model of key proteins involved in Ni^{2+} resistance and adsorption in *C. pauculus* 1490. The e-PNs were classified into six types, including ROS response to Ni^{2+}, EPS synthesis, ABC transporters, electron transfer and Ni^{2+} efflux. They are at the outer cell membrane, inner membrane and periplasm. Proteins in the cyan box were related to the response to Ni^{2+}, WP_06195546.1, response regulator, was the only one protein downregulated over 2-fold change. CysM is a protein involved in cysteine synthesis. WP_244787450.1 in the red box was a Ni^{2+} efflux protein that also has multidrug resistance. Bfr in the black box is a bacterioferritin-comigratory protein involved in iron storage, responding to environmental stress and detoxifying ROS. LpxC was associated with lipopolysaccharide synthesis. WP_244787941.1 and WP_244788602.1 were combined to a complex involved to NAPD synthesis, hmp and lpdA were flavoproteins combined to the Other complex. They all belong to the electron transfer chain in the green box. ParC is a protein related to cell division. ABC transporters were related to amino

acids and Other small soluble molecules transmembrane

3.2.1 Chemical composition and quantitative analysis of extracellular polymeric substances

As Figure 8 shown, the optical densities were up 2-fold increased under 1.7 mM Ni^{2+} stimulation compared to control. This seems counterintuitive since heavy metals are toxic to organisms. While, one strategy of bacteria to detoxify heavy metals is by cell division (Efaq et al., 2022). As shown in LC-MS analysis, ParC related to cell division up-regulated over 2-fold change, can support this result. It's also reported that *Cupriavidus necator* has a much shorter lag and logarithmic period under a specific copper ion concentration stimulation than the control (Makkar & Casida Jr, 1987). Moreover, bacteria may produce more energy for growth and reproduction, leading to biomass increased. The proteins related to carbon metabolism were consistent with listed in LC-MS data. However, higher concentration of Ni^{2+} has a negative effect on bacterial growth. Toxicity and bioavailability of metals lead to a decrease in the cells' growth rate (Guo et al., 2010).

3D-EEM results indicated that tryptophan protein-like substances were major contributor to Ni^{2+} adsorption and resistance. Other research also showed the same phenomenon, tryptophan protein-like substances were gradually quenched with increased metal cations concentrations (Ferreira dos Santos et al., 2022; Lu et al., 2021; Luo et al., 2022), because binding of metal ions to

tryptophan was shown to decrease the florescence of the amino acids. E-PNs can improve heavy metal resistance, and metal-binding proteins provide resistance against metal and Other environmental stresses. Two theoretical bidentate tryptophan-metal complex structures were predicted: (a) the nitrogen of the amine (NH_2) and the oxygen of the carbonyl group (C=O) bind with metal ions and (b) carboxylic acid (-COOH, the most favored structure) bind with heavy metals (Bellmaine et al., 2020). All the groups were detected in FTIR results (Figure 9). Tryptophan residues are concentrated on the membrane's periplasmic side and form hydrogen bonds with carbonyl oxygens, contributing to protein and membrane stabilization. However, when heavy metals' concentration increased, tryptophan-rich proteins adsorbed metal ions and were consumed (Lu et al., 2021). It may demonstrate that tryptophan-rich proteins decreased caused cell density decrease of 3.4 mM Ni^{2+} as shown in Figure 10. Moreover, tryptophan involved in protein-ligand interactions and can participate in the formation of hydrophobic cores which is the major driving force of cell adhesion. It may also explain why cells form aggregates under Ni^{2+} stress (Figure 11 c1, c2, c3).

3.2.2 The hypothetical model of essential proteins involved in Ni^{2+} resistance and adsorption

According to the assumed function of e-PNs, a hypothetical model of essential proteins involved in Ni^{2+} resistance and adsorption was constructed

(Figure 15). The bacterial strategy from the findings for heavy metal resistance has three parts related to EPS: extracellular barrier, active transport of metal ions (efflux) and extracellular sequestration. LxpC involved in LPS synthesis belongs to the extracellular barrier and contributes to cell adhesion (Huang & Puma, 2022). Cells can form metal ion complexes and protect themselves from environmental stress through cell wall LPS. LPS is well known to be a common mechanism of resistance. Metals bound most likely to phosphoryl groups in the core-lipid A of LPS, and the negatively charged side chains influenced binding to Gram-negative bacteria by affecting cell hydrophobicity. However, the tolerance conferred by LPS is insufficient to support tolerance to the higher levels of stress imposed. In addition, the homologous protein structure has evolved into conductive substances (especially increasing the contents of redox enzymes and humic-like substances) and thus contributed to the successful establishment of EET conditions (Huang & Puma, 2022). The increased amount of cysteine (Cys) positioned at the cell surface can enhance the bioaccumulation of heavy metals, which belongs to extracellular sequestration. It was previously reported that the cysteine-rich amino acid sequence, Gly-Cys-Gly-Cys-Pro-Cys-Gly-Cys-Gly bound metals. Usually, metallothioneins are a group of cysteine-rich proteins and its primary function is to detoxify heavy metals by storage, binding of metals and transportation (Liancheng et al., 2022). It's reported that bacteria exhibited significantly enhanced heavy metal binding capacities and tolerance through increasing binding more metal ions after site-

directed mutagenesis from lysine residues to cysteine residues (Li et al., 2021). Moreover, cysteine synthesis and metabolism promote bioaccumulation of Cd^{2+} in *Cupriavidus nantongensis* X1 (Liancheng et al., 2022). Cysteine involved in Fe-S protein synthesis and glutathione. Fe-S proteins were oxidized to $[2Fe\text{-}2S]^{3+}$ and $[4Fe\text{-}4S]^{3+}$ by ROS (reactive oxygen species). Then GPx, superoxide dismutase (SOD) and catalase (CAT) were active expression, which can reduce ROS (Liancheng et al., 2022). Thus, the observation that CysM expression was upregulated fits well within this concept.

Furthermore, bacteria detoxify heavy metals through efflux of the overdose of heavy metals from inner cells or periplasm. *C. pauculus* has specific nickel efflux pumps that were active at the first 4 hours after Ni^{2+}challenge (Figure 13 a, b, d). Hence, it is speculated that during the onset of growth, nickel efflux pumps were the primary way to transport Ni^{2+} out of the cell, while later on multidrug efflux pumps would take over this part. It seems cells exposed to higher nickel concentrations would negatively affect the nickel-specific efflux pump. The multidrug efflux pumps (WP_460) were activated at a later stage (Figure 13). Multidrug efflux is well known for expelling a wide range of toxic compounds from bacterial cells (Yang & Zhang, 2020b). Growing evidence shows that metal-antibiotic resistance is co-selected through resistance mechanisms (Nguyen et al., 2023b). Heavy metal resistance is resembling antibiotic resistance because they adapt to various external threats. The heavy metals and antibiotics resistance could be co-selected by cross-resistance (the

presence of the same genetic determinant confers resistance to both antibiotics and metals) and co-regulation (the metal or antibiotics acts as an inducer of a common regulatory system that is responsible for the expression of diverse metal an antibiotic resistance determinants) (Sincak et al., 2023). *Burkholderia cepacian*, *Salmonellaa typhimurium* and *Listeria monocytogenes* could resist both heavy metals and antibiotics through same efflux pumps system (Pal et al., 2017b). It seems that heavy metals generated genes in bacteria involved in multidrug efflux pump and outer membrane porin permeability (Sumei et al., 2022). Exposure heavy metals, upregulation of multidrug efflux pump and downregulation of outer membrane porin promoted antibiotics resistance (Sincak et al., 2023; Xu et al., 2022; Yu et al., 2022b). It reported that heavy metals can induce antibiotic resistance that were not previously available in *E. coli* (Xu et al., 2022). The previous reported that heavy metals can induce ROS formation, which was formed by external stimulation to cause mutagenesis, leading to the emergence of bacterial resistance to multidrug (Xu et al., 2022). Therefore, it seems that high concentration of heavy metals destroyed the nickel efflux pump (specific efflux pump) and induced multidrug efflux pump emergency at the later growth period. Thus, the results advance understanding on the interplay of heavy metal and antibiotic resistance.

Using Metal 3D models based on machine deep learning, the metal-binding sites of WP_460 were analyzed, as shown in Figures 16. Metal 3D predicted multiple metal-binding sites for WP_460, with the top two candidates having

probabilities of 49.05% and 48.41%, respectively. The amino acid residues for the top-ranked binding site are His336 and Glu339 (Figure 16), while those for the second-ranked site are His580 and His598 (Figure 16). Due to the low probability and the model's primary focus on Zn^{2+} prediction, simulations were additionally performed using MetalNet and AlphaFold 3.

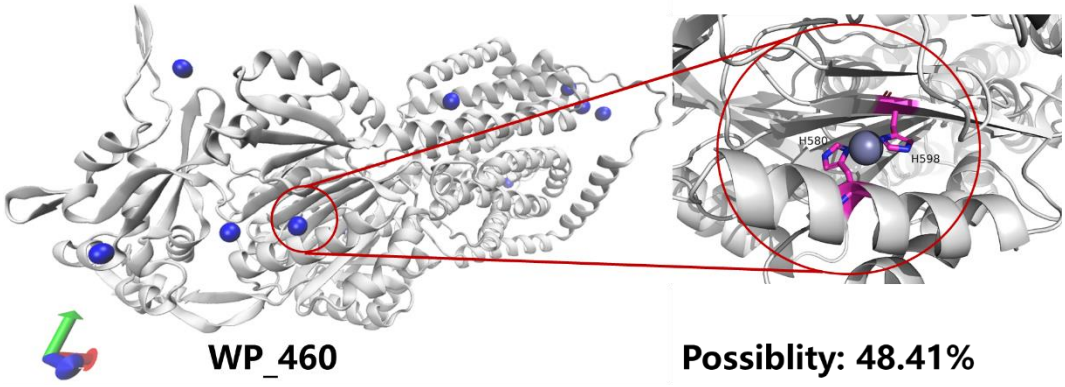

Figure 16: Metal binding sites predicted based on Metal 3D; blue and grey balls: metal ions; possible binding metal ions include metal ion Cu^{2+}, Ni^{2+}, Mn^{2+}, Zn^{2+}, Fe^{2+}, and Fe^{3+} binding sites; H: His

Based on AlphaFold 3 and MetalNet, there is a 54.58% probability that the amino acid residues H149 and E332 of WP_460 are metal binding sites (Figure 17). In addition, the possible binding metal ions include metal ion Cu^{2+}, Ni^{2+}, Mn^{2+}, Zn^{2+}, Fe^{2+}, and Fe^{3+}.

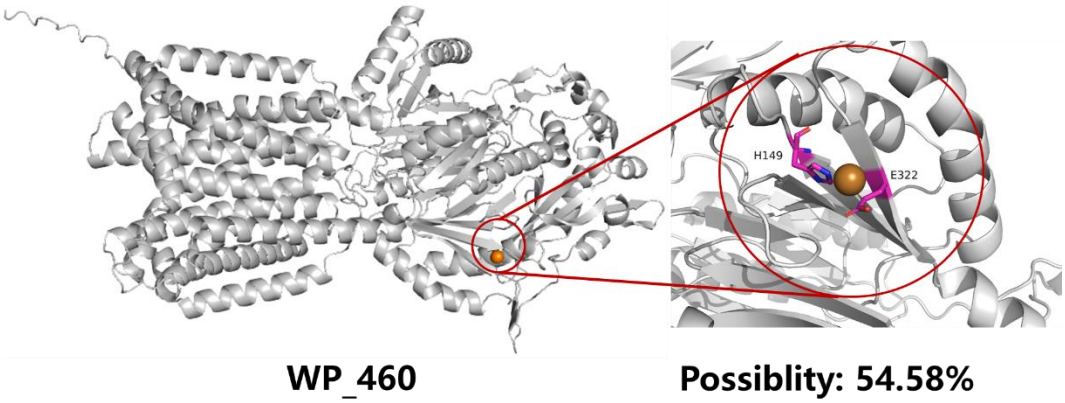

Figure 17: Metal binding sites predicted based on AlphaFold 3 and metal Net; orange balls: metal ions; H, His; E, Glu

Heavy metal treatment further results in an increased occurrence of reactive oxygen species (ROS) (Figure 14 a). ROS were increased as the concentration of Ni^{2+}. Nickel can catalyze the production of ROS by Fenton and Haber Weis reaction, producing superoxide radical, caused DNA, lipids, and proteins as well as cytoplasmic molecules damage (Fashola et al., 2023; Figueiredo et al., 2012). Bacterioferritins (Bfr) have capacity to detoxify damaging action of ROS by attenuating the production of -OH. Moreover, Bfr could regulate the intracellular level of iron and antioxidant proteins to detoxify ROS (Figueiredo et al., 2012). Increasing researches showed that extracellular electron transfer (EET) involved in biomineralization, reduction, bioleaching and microbial electrochemical systems (Yu et al., 2022a). But few researches reported the association of electron transfer chain, flavoproteins and flavin adenine dinucleotide (FAD) with heavy metals resistance. WP_244787941.1 is a FAD-containing oxidoreductase, electron carrier, associated with organic matters or carbon source degradation, heavy metals redox reactions and amino acid metabolism through electron transfer. This type of protein seemed to be related to environmental responses, such as heavy metals, antibiotics, and toxic inorganic and organic pollutants. WP_061957596.1, WP_244787941.1 and WP_061957347.1 were involved in electron transfer. As reported, heavy metals could inhibit enzymes, bind electron acceptors, destroy receptors in

membrane and ion porin, and disrupt proteins synthesis involved in electron transfer, which lead to negatively impact the function of electron transfer (Pal et al., 2022). Moreover, metal chelation and surface binding may act together to enhance respiration in environment with a high metal content. Bacteria respond Ni^{2+} stress with higher metabolic activities. Electron transport system activity (ETSA) was measured with Ni^{2+} exposure (Figure 14 b). The concentration of ETSA with Ni^{2+} exposure was higher compared to control, which is consistent with the results of LC-MS/MS (Figure 12). The activity of key enzymes in the electron transport system is highly correlated with ETSA. Therefore, it is frequently evaluated to access electron transfer process. Cells consume more carbon and produce more enzymes to generate more energy (protein related to carbon degradation and amino acid product). As reported, energy metabolism pathways adjustments were the central strategy to response stress (Chen et al., 2016). The results provide evidence against the widely held assumption in metabolic processes were inhibited in *Enterobacter sp*. with exposure Cd^{2+}, but consistent with the finding in *E. coli* (Chen et al., 2016). In addition, to pump the excess intracellular Ni^{2+} to out of the cells, more ATP was consumed. Moreover, it is well known that the cell partition locus ParC can contribute to survival in the presence of high levels of toxic pollutants like antibiotics. It seems to be a site for pollutant binding or contribution to evolution.

4 Extracellular proteins mediated Ni^{2+} resistance and biofilm formation of *Vibrio gazogenes* DSM 21264

Vibrios are widely distributed in aquatic environments (Wang et al., 2020). *V. gazogenes* is a strain that can produce several extracellular enzymes such as amylase, proteases, and ligases (Catherine Ratcliffe). The previous studies demonstrated that *V. parahaemolyticus* can resist Co^{3+}, Cd^{2+} Cu^{2+} etc.(Chang-Ho et al., 2018). However, the precise molecular mechanisms of heavy metal resistance in *V. gazogenes* and the difference with other strains remain unknown. Therefore, we analyzed the extracellular proteins (e-PN) with Ni^{2+} treatment on Ni^{2+} resistance in this study. *C. pauculus* is a typical heavy metal resistance bacterium (Wang et al., 2024) while *V. gazogenes* is polyethylene terephthalate (PET)-degrading bacterium (Weigert et al., 2022) which was found to have Ni^{2+} resistance in this study. Therefore, we are interested in the difference of the mechanism on Ni^{2+} resistance in these two bacteria. In this study, the impact of Ni^{2+} treatment on *C. pauculus* and *V. gazogenes* was demonstrated on a molecular level. The mechanisms of heavy metal resistance in these two bacteria were analyzed.

4.1 Results

4.1.1 Nickel resistance Gene from *V. gazogenes* whole genome

As shown in Table 5, there are a total of 21 nickel-specific transport proteins involved in Ni^{2+} transport, including 5 proteins that belong to the Sec secretion system and 17 Other non-secretory proteins. Within the complete genome of *V. gazogenes*, there are 16 peptide/nickel transport system permease proteins. These proteins form channels in the *V. gazogenes* cell membrane, facilitating the transmembrane transport of Ni^{2+}. They play a crucial role in the peptide/nickel transport system by assisting bacteria in maintaining internal Ni^{2+} balance and ensuring its proper distribution within the cell. Through a series of complex cellular processes, they participate in the absorption, transport, and allocation of nickel, influencing bacterial growth, metabolism, and Other vital physiological functions.

As shown in Table 5, the genome of *V. gazogenes* also contains 3 Co^{2+}/Ni^{2+} transport proteins, which are responsible for transporting cobalt and nickel ions within the cell. Nickel and cobalt ions play important roles in cellular metabolism and survival, activating and catalyzing numerous enzymes. Therefore, cobalt/nickel transport proteins contribute to maintaining the homeostasis of these metal ions inside the cell, ensuring normal biochemical processes.

Additionally, there are 2 Co^{2+}/Ni^{2+} transport permease proteins in the genome

of *V. gazogenes*, forming channels on the cell membrane for the transportation of cobalt and nickel ions. This process is crucial for the uptake and efflux of cobalt and nickel ions by the cell, contributing to the maintenance of metal ion balance and ensuring normal cellular functions.

Table 5 Prediction of Ni^{2+} resistance and secretion systems

Accession number	**Prediction**
SHE49819.1 peptide/nickel transport system substrate-binding protein	SP
SHE59948.1 cobalt/nickel transport system permease protein	OTHER
SHE59989.1 cobalt/nickel transport protein	SP
SHE60021.1 cobalt/nickel transport system permease protein	OTHER
SHE60055.1 cobalt/nickel transport system ATP-binding protein	OTHER
SHE60510.1 peptide/nickel transport system ATP-binding protein	OTHER
SHE60554.1 peptide/nickel transport system permease protein	OTHER
SHE60600.1 peptide/nickel transport system permease protein	OTHER
SHF49653.1 cobalt/nickel transport protein	SP
SHF70382.1 peptide/nickel transport system permease protein	OTHER
SHF70414.1 peptide/nickel transport system permease protein	OTHER
SHF70450.1 peptide/nickel transport system ATP-binding protein	OTHER
SHF70550.1 peptide/nickel transport system substrate-binding protein	SP

SHF96391.1	peptide/nickel transport system substrate-binding protein	OTHER	
SHF96417.1	peptide/nickel transport system permease protein	OTHER	
SHF96442.1	peptide/nickel transport system permease protein	OTHER	
SHF96465.1	peptide/nickel transport system ATP-binding protein	OTHER	
SHG03657.1	peptide/nickel transport system ATP-binding protein	OTHER	
SHG03688.1	peptide/nickel transport system substrate-binding protein	SP	
SHG03714.1	peptide/nickel transport system permease protein	OTHER	
SHG03746.1	peptide/nickel transport system permease protein	OTHER	

The conceptel model of Ni^{2+} permease transporter system was constructed in Figure 18. Ni^{2+} permease protein locate at outer membrane and transport Ni^{2+} relying on ATP, especially efflux Ni^{2+} to outer cell. While Ni^{2+} transporters are found in both the outer and inner membranes, the active efflux of Ni^{2+} against its concentration gradient is mediated by the inner membrane protein and outer membrane protein, driven by ATP hydrolysis.

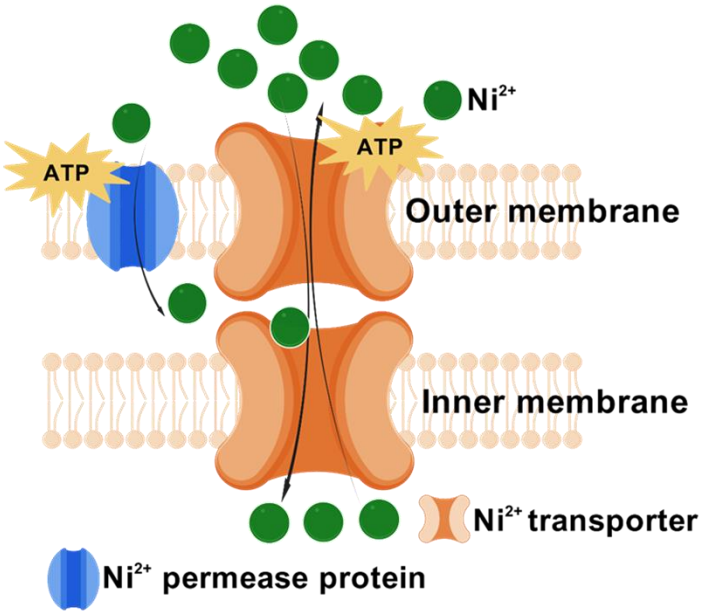

Figure 18: Prediction of Ni transporter system in *V. gazogenes*. The uptake of Ni^{2+} into the cell is mediated by a Ni^{2+}-permease and requires ATP. Additional Ni^{2+} transporters are localized to both the outer and inner membranes. Among these, certain inner membrane transporters facilitate the ATP-dependent efflux of Ni^{2+} from the cell

Phylogenetic analysis of the Ni^{2+}/peptide transport proteins revealed significant similarity (>70%) with proteins from 4 genera, showing high sequence conservation across different species (Figure 19). The most similar protein to that in *V. gazogenes* is found in *Vibrio spartinae* with a similarity of 96.3%, while the least similar protein originates from *Marinomonas piezotolerans* with 85.7% similarity. Similarities exceeding 90% were also observed with proteins from *Celerinatantimonas diazotrophica*, *Oceanospirillaceae* bacterium, and *Marinomonas* genus.

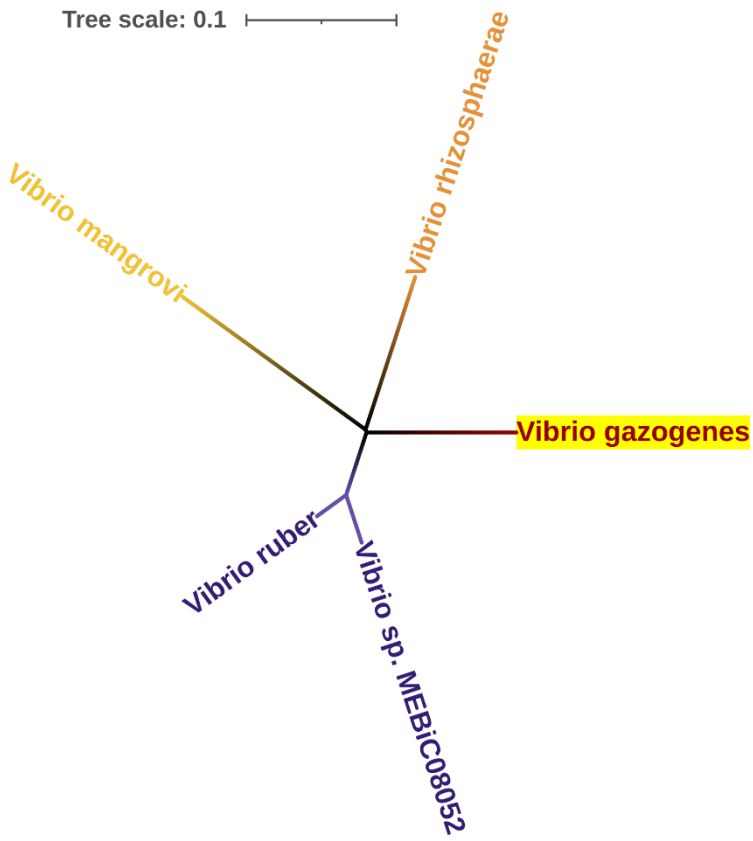

Figure 19: Phylogenetic tree of SHF49653.1 cobalt/nickel transport protein; *Vibrio gazogenes* (WP_072955317.1)，*Vibrio ruber* (WP_077337134.1)，*Vibrio sp.* MEBiC08052 (WP_059121919.1)， *Vibrio rhizosphaerae* (WP_051680216.1)， *Vibrio mangrove* (WP_087482597.1)

The predicted metal-binding sites for SHF49653.1 are shown in Figure20, with amino acid residues His22 and His47 identified. MetalNET assigned a high confidence score of 95.5%. The AlphaFold 3 prediction yields ipTM=0.89 and pTM=0.89, indicating highly reliable results. The metal-binding sites predicted by both models are fully aligned, confirming that Ni^{2+} binds via His22 and His47 and undergoes transport.

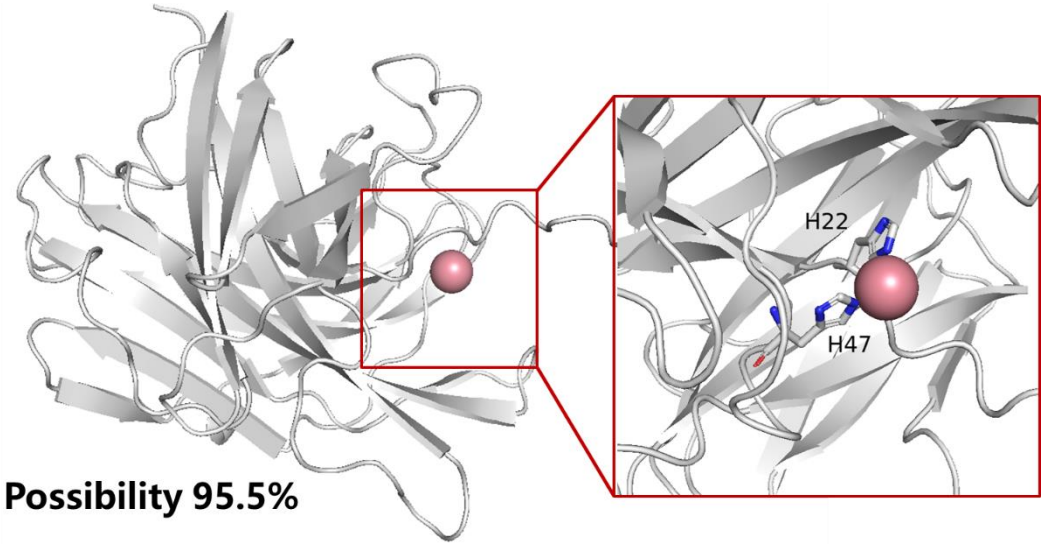

Figure 20: SHF49653.1 Co/Ni transporter protein binding site；Red spheres, metal ions; H, histidine

4.1.2 The effect of Ni^{2+} on *V. gazogenes* growth

Cell numbers in the medium decreased with elevated Ni^{2+} treatment. The optical density was similar between 100 mg/L Ni^{2+} and the control, while it decreased by up to 2-fold-change when the concentration of Ni^{2+} reached or exceeded 2.55 mM Ni^{2+} (Figure 21). It indicated that *V. gazogenes* growth was inhibited with 150 mg/L Ni^{2+}. Higher concentrations of Ni^{2+} inhibited bacterial growth which coincides with the findings of most studies (Guo et al., 2010; Xie et al., 2021). Bacteria can maintain normal metabolic activities at lower concentrations of heavy metals, but higher concentrations can damage cell membranes, reduce viability, and disrupt proteins (Syed et al., 2021).

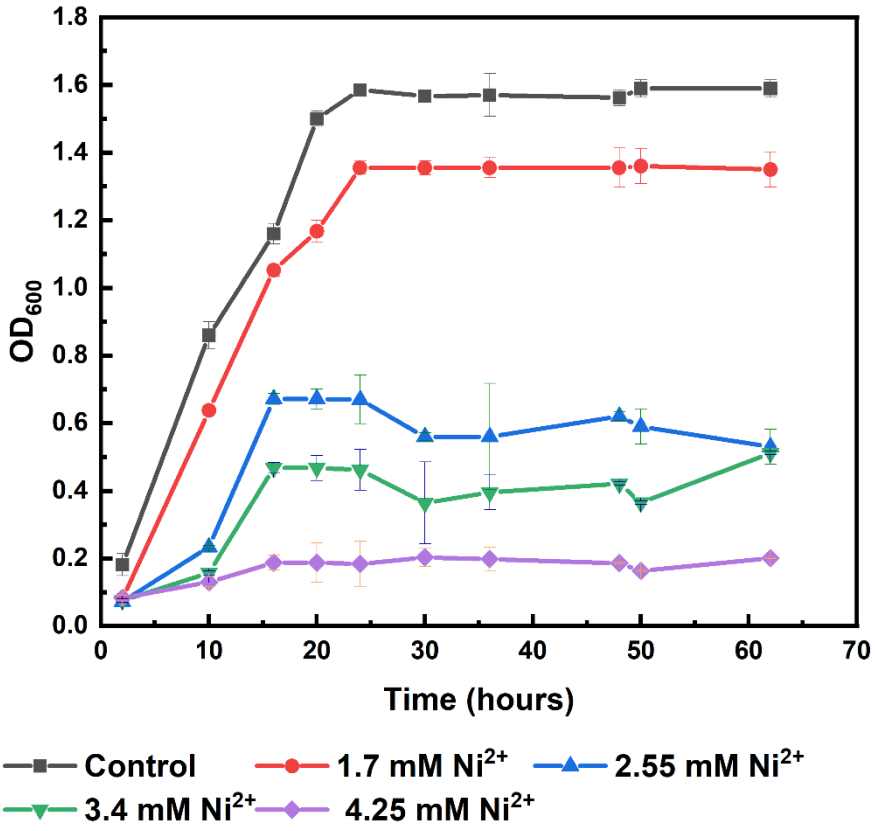

Figure 21 Growth curve of *V. gazogenes* under Ni^{2+} stimulation. *V. gazogenes* was cultivated in artificial seawater medium at 28 °C under aerobic conditions with concentration of 1.7 mM Ni^{2+}, 2.55 mM Ni^{2+}, 3.4 mM Ni^{2+} and 4.25 mM Ni^{2+} treatments. bars indicate standard deviation and data are mean values of three independent measurements

4.1.3 Extracellular polymeric substance quantification and e-PN characterisation

For a visual understanding of the changes in EPS with Ni^{2+} treatment in bacteria, we determined the content of various components of EPS and characterized the fluorescent substances of EPS using 3D-EEM. E-PN was the major contributor under Ni^{2+} stimulation, as shown in Figure 22. This indicates that e-PN plays a vital role in Ni^{2+} resistance and detoxification. In addition, the

content of e-PN was 4,5-fold higher under Ni^{2+} stimulation with 100 mg/L Ni^{2+} than the control. At a concentration of 150 mg/L Ni^{2+}, the e-PN content decreases again but is still twice as high as that of the control (Figure 22). This could be attributed to the fact that high concentrations of heavy metals cause protein misfolding and aggregation (Tamás et al., 2014). Moreover, high protein content can enhance the large adsorption capacities of HMs due to a large number of active adsorption sites.

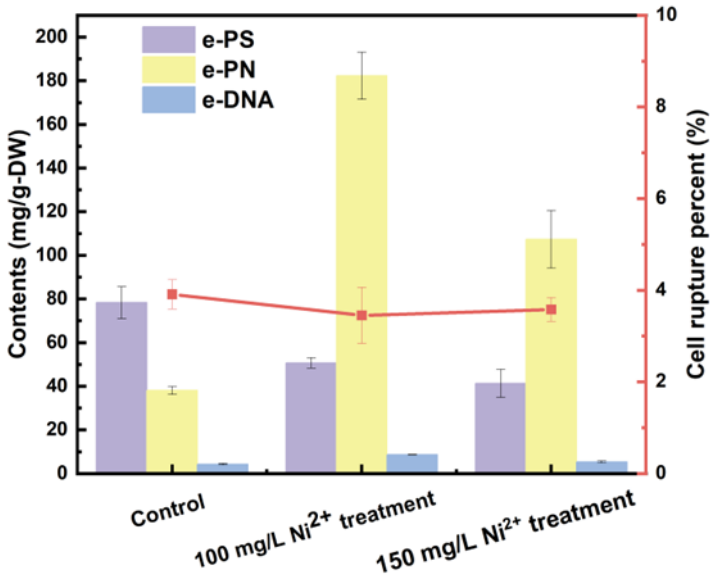

Figure 22 The contents of major extracellular polymeric substance components and cell rupture percent. The concentration of e-PS was determined by the phenol sulphuric acid method with glucose as the standard. Protein contents were measured using the Bradford protein assay kit with bovine serum albumin as the standard. DNA content was determined using a NanoDrop ND-1000 spectrophotometer (NanoDrop Technologies, Wilmington, USA). Bars indicate standard deviation and data are mean values of three independent measurements. Cells rupture rate (the red line) was calculated by G6PDH. To evaluate the extent of cell lysis, the activity of G6PDH in the EPS extract was measured using a G6PDH kit (Beijing Solarbio Technologies Ltd,

Beijing, China) in accordance with the product's instructions

The 3D-EEM results revealed many peaks and substances in *V. gazogenes* in Figures 23 a-c. Peaks A and B, which respectively represent aromatic proteins I and II (Chen et al.), increased with the concentration of heavy metals. This finding differs from the typical HM resistant bacteria in which the fluorescence intensity of aromatic protein-like substances in regions A and B usually either decreased or did not follow the changes in HMs concentrations as they increased (Linlin et al., 2021; Wang et al., 2024; Zeng et al., 2019). However, it has also been shown that fluorescence intensity can either be raised or diminished based on the interactions between the fluorophore (EPS) and the quencher (HMs) (Wei et al., 2016). In addition, aromatic proteins were found to induce self-aggregation in *Chlorophyta sp.* (Zhou et al., 2017). *V. gazogenes* were also found to form aggregation in this study as shown in Figure 24. Region C represents tryptophan, which increased under Ni^{2+} stress, but decreased when the concentration of the heavy metal was above 100 mg/L. These results are similar to previous studies (Luo et al., 2022; Wang et al., 2024). Tryptophan can bind with HMs, which leads to a decrease in the fluorescence of the e-PNs. Furthermore, tryptophan protein-like molecules oxidize into aromatic ring compounds in the presence of a strong oxidant, forming a protective barrier to respond to HM stress (Luo et al., 2022). The fluorescence intensity of the humic acid-like substance (region D) increases as the concentration of Ni^{2+} increases (below 100 mg/L Ni^{2+}) but decreases at

higher Ni^{2+} concentrations. The significant fluorescence quenching of region D by Ni^{2+} indicated that humic acid has an excellent adsorption capacity. It has been reported that humic acid binds with Ni^{2+} through complexation (Liangliang et al., 2019). Furthermore, humic acid is negative which is attractive for metal ions. Region E, a fulvic acid-like substance, increased with the concentration of Ni^{2+}. This suggests that more fulvic acid is present on the surface of cells to prevent heavy metals from entering the cells' interiors (Li et al., 2023). Fulvic acid facilitated Cr removal by *C. vulgaris* by enhancing the secretion of EPS and providing more adsorption sites (Li et al., 2023).

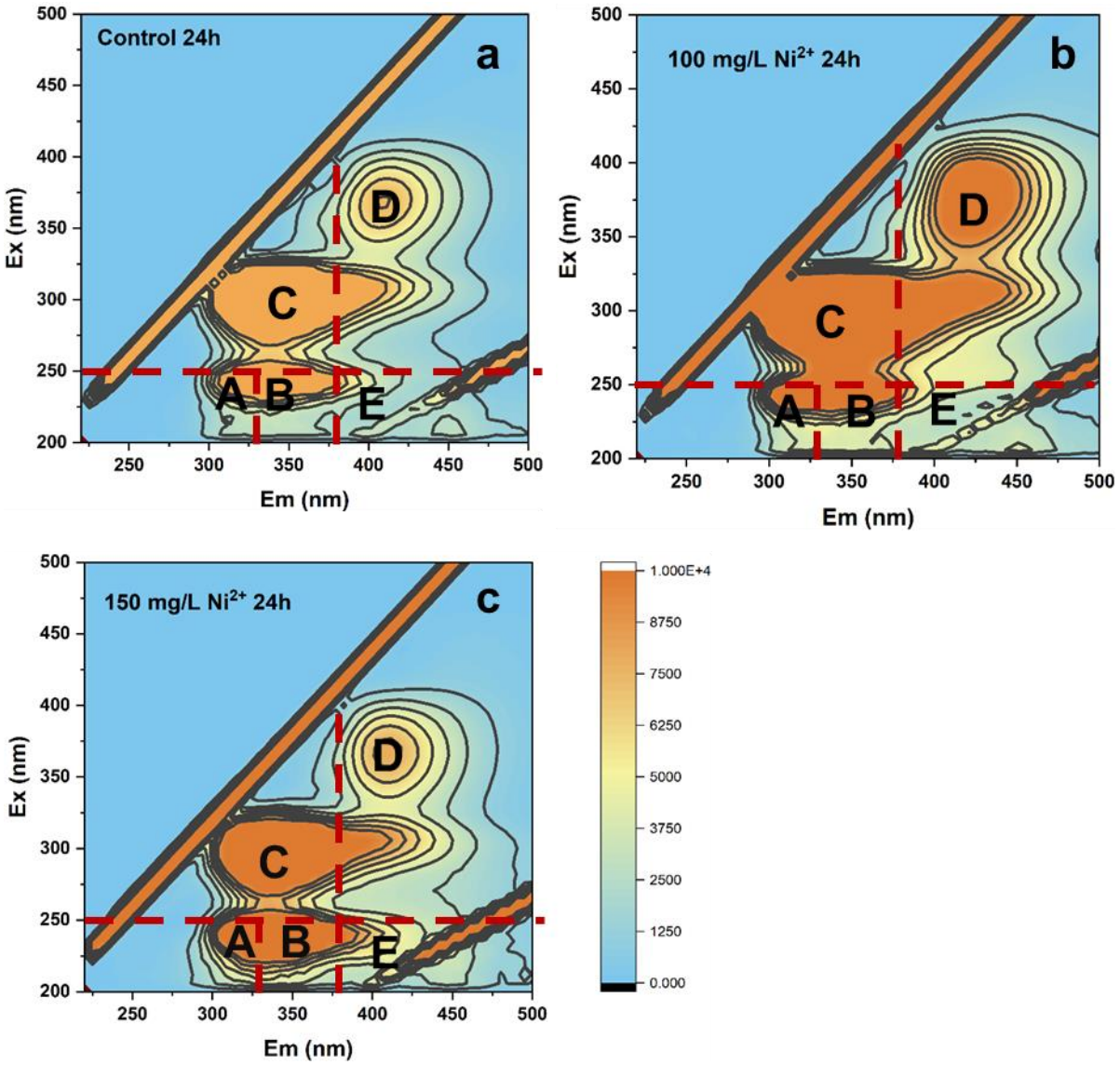

Figure 23: 3D-EEM fluorescence spectra of EPS at 24 h culture extracts from *V. gazogenes* under Ni^{2+} stimulation and control. Region A and B are aromatic protein-like substances region C is tryptophan protein-like substance, region D is a humic acid-like substance, and region E is a fulvic acid-like substance

4.1.4 Extracellular polymeric substance visualization

To visually observe the developments of EPS, CLSM was used in this study. As shown in Figure 24 (b2-b3, d2-d3), e-PN, green fluorescence, took

up a larger ratio than extracellular polysaccharides (e-PS) in EPS under Ni^{2+} stimulation, especially after four hours. It may illustrate that Ni^{2+} enhanced EPS secretion, particularly e-PN. It's reported that microbes secrete more EPS as the primary barrier to protect cells from toxicity (Sihui et al., 2021). In addition, the EPS also contributed to the adsorption of heavy metals due to the electrons and functional groups of the adsorption site. Moreover, similar to the typical HM-resistant bacteria (Wang et al., 2024), bacteria form aggregates that help cells resist Ni^{2+} and facilitate the binding with metal ions (Syed et al., 2023). However, the aggregates decreased with the increased concentration of Ni^{2+}. As shown in Figure 22, EPS contents, including humic acid and e-PS, decreased with the increased concentration of Ni^{2+}. It suggested that EPS promoted biofilm formation, especially humic acid and e-PNs (Syed et al., 2023).

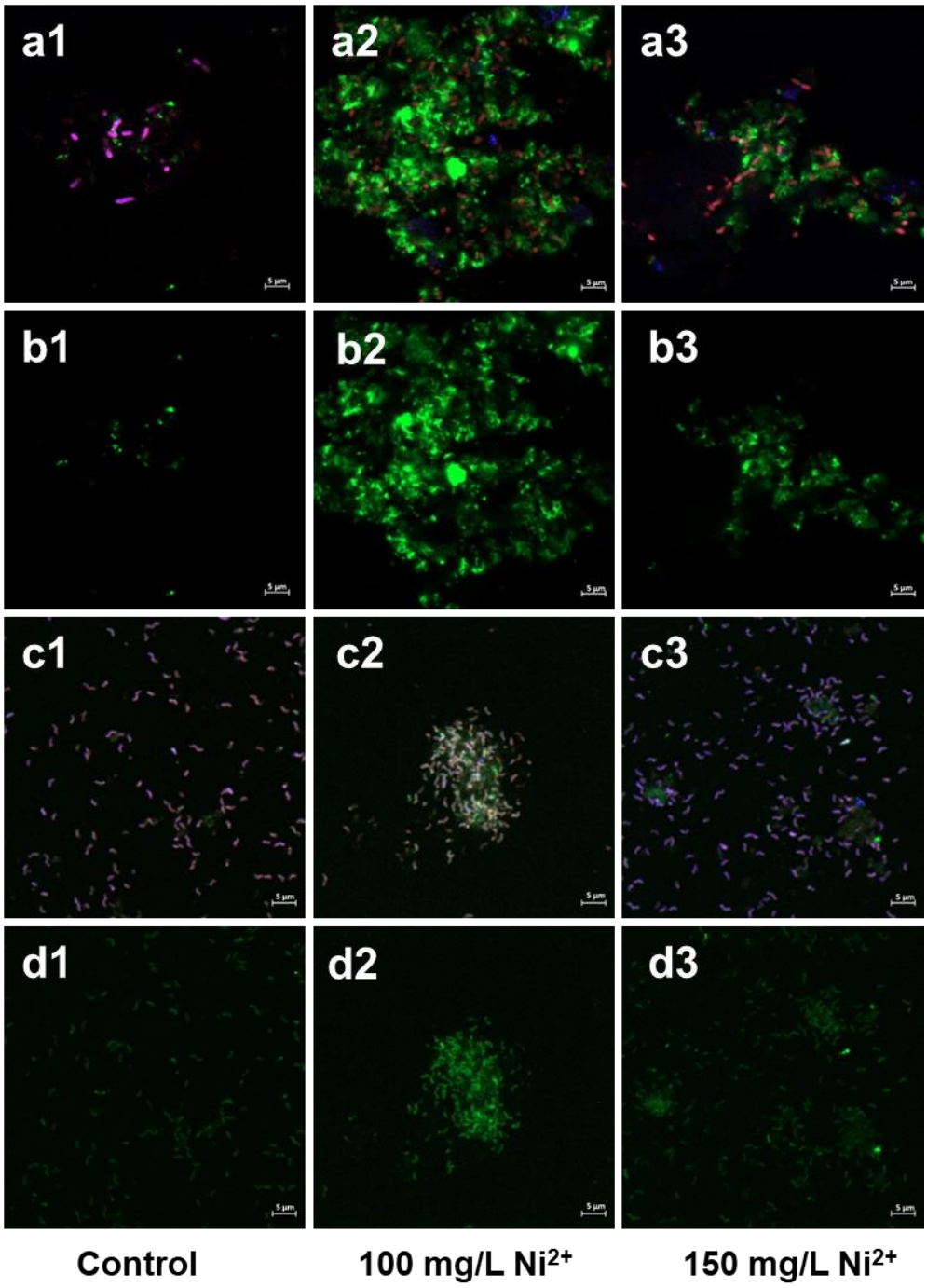

Figure 24: EPS staining of *V. gazogenes* cells after 4 (a1-b3) and 24 hours (c1-d3) with/without Ni^{2+} treatment. The scale bar is 5 µm. (b1-b3, d1-d3), e-PN is green stained using fluorescein isothiocyanate (FITC). (a1-a3, c1-c3), e-PS was stained with concanavalin A (for α-D-glucopyranose polysaccharides, red) and calcofluor white (for β-D-glucopyranose polysaccharides, blue). Purple-stained cells result from different ratios of α- and β-D-glucopyranose

polysaccharides stained; red-stained cells show higher levels of α-D-glucopyranose polysaccharides

4.1.5 Volcano plot visualization of the t-testing results

To extend the potential functions of e-PNs on Ni^{2+} resistance, LC-MS/MS-based proteomics was conducted.

2307 peptides and 220 proteins were identified when searched against a *V. gazogenes* secretomic database. The proteins are identified based on aligning the identified and measured peptide sequence to the protein sequence. Among these, 52 proteins were found to be significantly differentially abundant between the Ni^{2+} treatment and the control. There were 25 proteins with a significant increase in abundance, showing over a 2-fold change, and 26 proteins with a significant decrease in abundance, also over 2-fold, after the treatment (Figure 25). The significant regulation of e-PNs is listed in Table 6.

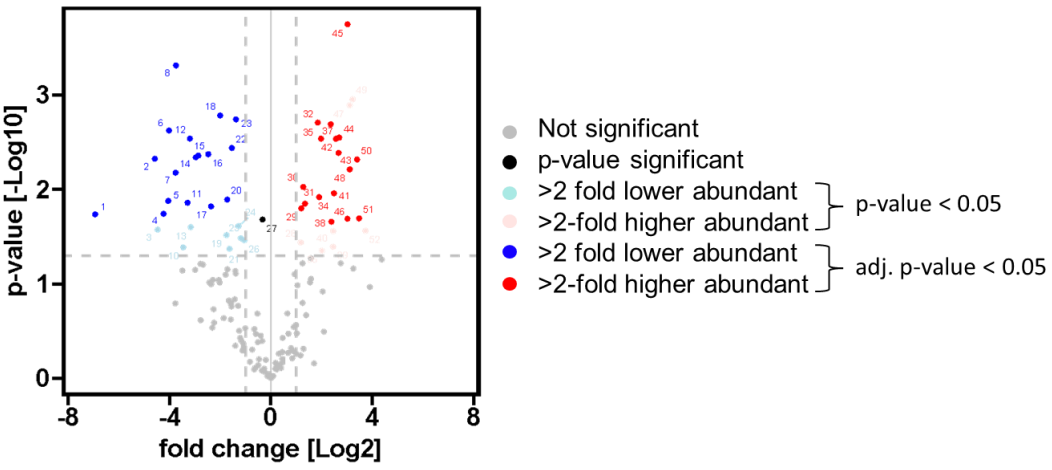

Figure 25: Volcano plot visualization of the t-testing results between the phenotypes and using proteome analysis of EPS extracts. Proteins were considered significantly differentially abundant if they exceeded a p-value cutoff

<0.05 and> 2-fold difference. Red and blue dots represent significantly up-regulated and down-regulated proteins over 2-fold, respectively. Black dots mean significant changes <2-fold difference. Grey dots indicate no significant changes. SHF26201.1 is the highest upregulated protein, which related to oxidative stress defense. SHG04300.1, porin, is the highest down-regulated proteins

Table 6 List of significantly regulated proteins

Gene	Accession number	Log2 transformed-fold change	Protein
1	SHG04300.1	-6.93757	porin
2	SHF69183.1	-4.58099	C4-dicarboxylate-binding protein DctP
3	SHG15411.1	-4.47513	Lipoprotein
4	SHE61141.1	-4.23491	Carboxypeptidase regulatory-like domain-containing protein
5	SHF15748.1	-4.05485	Outer membrane protein beta-barrel domain-containing protein (porin)
6	SHG08351.1	-4.02363	TPR repeat
7	SHF83423.1	-3.76146	outer membrane lipoprotein
8	SHE99057.1	-3.74689	nucleoside-specific channel-forming protein
10	SHF15357.1	-3.46084	CARDB protein
11	SHF24636.1	-3.29172	LPS-assembly protein
12	SHF19437.1	-3.19811	amino acid ABC transporter substrate-binding protein, PAAT family (TC 3.A.1.3.-)
13	SHE60405.1	-3.1647	Vibriolysin. Metallopeptidase. MEROPS family M04
14	SHF54695.1	-2.9666	tripartite ATP-independent transporter solute receptor, DctP family
15	SHF56176.1	-2.86578	outer membrane protein (porin)
16	SHF70550.1	-2.47242	peptide/nickel transport system substrate-binding protein

17	SHE29444.1	-2.36236	Carbohydrate-binding domain-containing protein
18	SHG10870.1	-2.0078	FKBP-type peptidyl-prolyl cis-trans isomerase FkpA
19	SHE93214.1	-1.75644	5'-nucleotidase / UDP-sugar diphosphatase
20	SHF66407.1	-1.72683	Lipoprotein
21	SHE30003.1	-1.63342	para-nitrobenzyl esterase
22	SHF18886.1	-1.54194	Protein of unknown function
23	SHE79163.1	-1.38179	Uncharacterized protein
24	SHF24197.1	-1.27642	TRAP transporter solute receptor, TAXI family
25	SHF82986.1	-1.19057	Alpha-2-macroglobulin
26	SHE86070.1	-1.05024	peptidyl-prolyl cis-trans isomerase A (cyclophilin A)
27	SHE33655.1	-0.327619	glycine betaine/proline transport system substrate-binding protein
28	SHF04378.1	1.17478	V8-like Glu-specific endopeptidase
29	SHF64710.1	1.19638	TRAP transporter solute receptor, TAXI family
30	SHG03806.1	1.26742	ABC-type Fe^{3+}-hydroxamate transport system, substrate-binding protein
31	SHF50725.1	1.34291	microcin C transport system substrate-binding protein
32	SHE93612.1	1.84784	Beta-barrel assembly machine subunit BamC
34	SHE31329.1	1.89929	cytochrome bo_3 quinol oxidase subunit 2
35	SHF40915.1	1.97288	CARDB protein
36	SHE30764.1	2.0121	PEGA domain-containing protein
37	SHF39236.1	2.35732	2',3'-cyclic-nucleotide 2'-phosphodiesterase / 3'-nucleotidase
38	SHF52054.1	2.3835	manganese/iron transport system substrate-binding protein, PsaA
39	SHF49059.1	2.44936	ATPase
40	SHF66028.1	2.45299	Tetratricopeptide repeat-containing protein
41	SHE88885.1	2.48321	Flagellar assembly protein T, N-terminal

			domain
42	SHE35162.1	2.5619	asparaginase
43	SHE60645.1	2.66764	The ABC-type transport system, substrate-binding protein
44	SHF86965.1	2.69168	lipoprotein
45	SHF84805.1	3.01613	beta-glucosidase
46	SHF91168.1	3.01658	Uncharacterized protein
47	SHG03771.1	3.10402	Sporulation related domain-containing protein
48	SHG06085.1	3.11194	putative amino-acid transport system substrate-binding protein
49	SHE40059.1	3.22343	phosphate transport system substrate-binding protein
50	SHF66735.1	3.39949	LPS-assembly lipoprotein, LptE
51	SHF26201.1	3.47804	Oxidative stress defense protein
52	SHE30797.1	3.72642	Formylglycine-generating enzyme, required for sulfatase activity, contains SUMF1/FGE domain

4.1.6 Analysis of potential functional proteins

To extend the potential functions of e-PNs on Ni^{2+} resistance, we performed LC-MS/MS-based proteomics. The e-PNs located at the cell membrane, secreted into the periplasm and involved in cell adhesion, oxidative stress defense, electron transfer, flagellar assembly, ABC transporters, cell membrane assembly, and response to Ni^{2+} were significantly up-regulated (Table 6).

The proteins in the blue box in Figure 26 that participated in cell membrane assembly were up-regulated over a 2-fold change. *Bam*C (SHE93612.1) was the outer membrane protein assembly factor. *Bam* complex participated in

protein folding and inserting of nascent outer membrane proteins into the outer membrane in bacteria (Lin et al., 2018). It suggested that the upregulation of *Bam*C contributed to the outer membrane permeability barrier function for the improvement of Ni^{2+} resistance in bacteria (Lin et al., 2018). The ORF SHF86965.1 was a lipoprotein up-regulated 2,7-fold-change, which is the main component of the membrane and probably functions in removing Ni^{2+} from the periplasmic compartment. In addition, ROS generated by high concentrations of Ni^{2+} causes oxidation of low-density lipoproteins, therefore may also induce the high expression of lipoproteins (Analia et al., 2017). SHF66735.1 is a lipoprotein involved in LPS assembly that is up-regulated by 3,4-fold-change. The up-regulation of lipoprotein-associated with the peptidoglycan or induced extracellular lipopolysaccharide (LPS) synthesis (lptE) maintained outer membrane integrity or produced more outer membrane to enhance the detoxification mechanism of HMs (Manara et al., 2012). LPS is related to membrane stability, the interactions of the bacteria with the environment, and the binding of different heavy metals (Pereira et al., 2006). Bacteria produce more LPS to adsorb heavy metals for detoxification, which is a mechanism reported by many researchers (Liping & Gianluca Li, 2022; Pereira et al., 2006; Wang et al., 2024). The proteins related to cell adhesion showed an upregulation of over 2-fold change as well. SHF40915.1 is a CARDB protein that enhances cell adhesion and promotes the formation of cell aggregates. *Psa*A (SHF52054.1), a manganese/iron transport system substrate-binding

lipoprotein, was observed to promote cell adhesion. Previous research has indicated the significance of *Psa*A in Mn^{2+} transmembrane transport. However, it has also been discovered that *Psa*A binds with Other divalent transition metal ions and prevents their release. This occurs not solely due to *Psa*A's specificity in binding with Mn^{2+}, but rather through the concerted action of protein-metal ion coordination chemistry and structural rearrangements (Begg et al., 2015). Additionally, in response to Ni^{2+} stress, cells must enhance iron uptake and induce proteins with stronger iron binding affinity (Macomber & Hausinger, 2011). This process may be facilitated by *Psa*A to transport iron in bacteria. Therefore, *Psa*A may bind with Ni^{2+} to prevent its entry into the inner cells and facilitate cell adhesion, thereby detoxifying excessive Ni^{2+}.

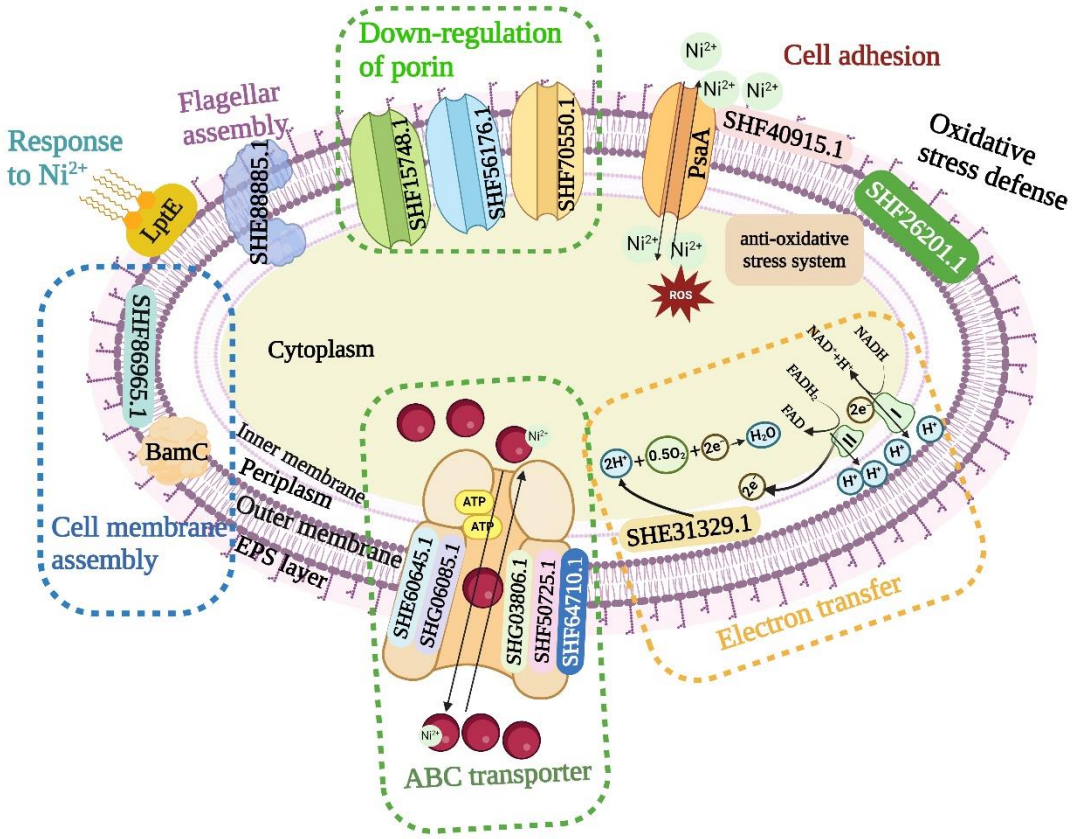

Figure 26 Conceptual model of key proteins involved in Ni^{2+} resistance and adsorption of *V. gazogenes*. The proteins were divided into 8 types including downregulation of porin in red box, protein related to electron transfer chain in orange box, ABC transporter in green box, proteins involved in cell membrane assembly in blue box, LPS assembly protein, flagellar assembly protein, Ni^{2+} transporter and ROS defense protein

Similar to HM-resistant bacteria (Wang et al., 2024), the protein related to oxidative stress defense up-regulated. SHF26201.1, an oxidative stress defense protein, is involved in detoxifying ROS. It is up-regulated by 3.5-fold and ranks as the second most up-regulated protein. As is commonly known, ROS in bacteria was significantly generated by HM. SHG15411.1 is a

lipoprotein down-regulated by 4,5-fold. Moreover, it's reported that the lipid peroxidation reactions in the membrane can also be stimulated by heavy metals to produce ROS (Rabbul Ibne & Mayashree, 2021). Therefore, we measured ROS induced by Ni^{2+}. ROS levels slightly increased with Ni^{2+} treatment compared with the control, and escalated in tandem with the rising concentration of Ni^{2+} (Figure 27 a). The ORF designated SHF26201.1 may enhance repairing the damage of ROS overproduction and coping with heavy metal-induced oxidative stress. Similarly, the number of oxidative stress defense proteins increased significantly in *Burkholderia vietanamiensis* and *Pseudomonas putida* due to Ni^{2+} toxicity (Pal et al., 2022). There are numerous cases indicating that ROS levels increase upon induction by HMs (Hillol et al., 2022; Wang et al., 2024). In contrast, the CAT and GSH activities decreased with increasing Ni^{2+} concentration, indicating that they are more sensitive to Ni^{2+}, and may be inactivated by high concentrations of Ni^{2+}. When ROS levels are excessively high, intracellular ROS levels rise due to the action of SOD, but CAT and GSH are unable to promptly convert H_2O_2, thereby impairing normal cellular growth and metabolism.

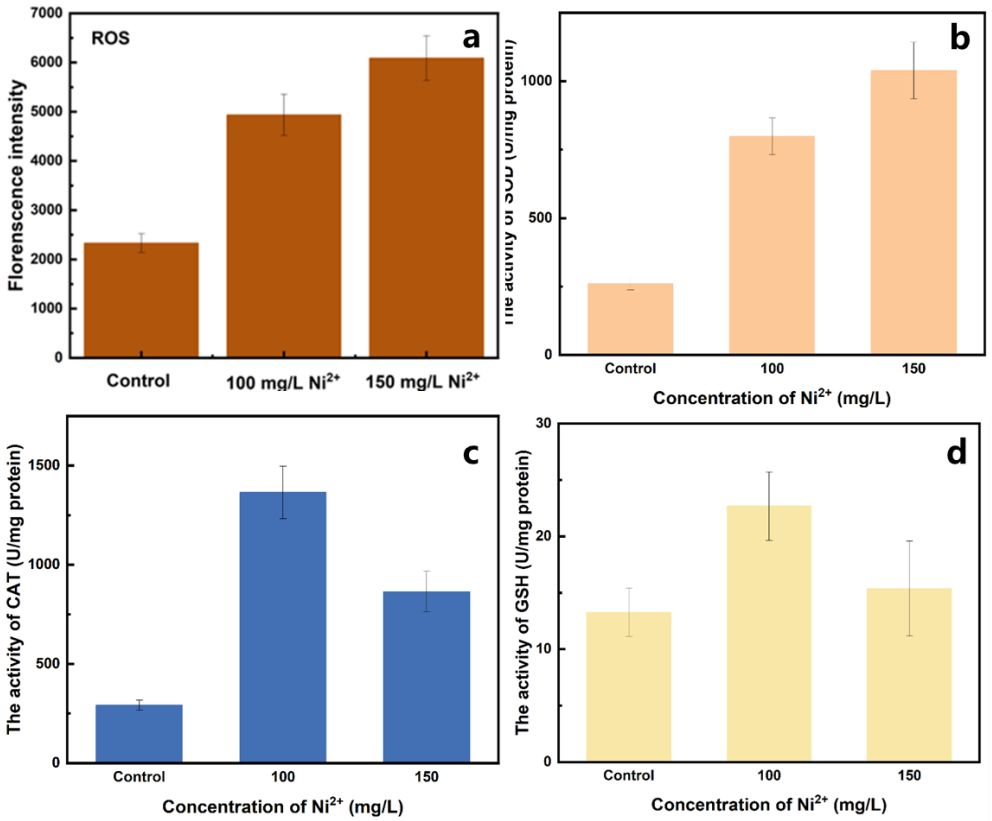

Figure 27: The ROS levels (a), and the activity of CAT (b), SOD (c) and GSH (d) with Ni^{2+} treatment. (a), ROS levels detection under Ni^{2+} stimulation. (b,c,d) CAT, SOD and GSH were detected by kits under Ni^{2+} stimulation. All of the experiments preformed three times and bars mean standard deviation

In addition, the proteins associated with electron transfer up-regulated over 2-fold change. ORF SHE31329.1, a cytochrome bo3 quinol oxidase subunit 2, belongs to the respiratory chain. Cytochrome bo3 quinol oxidase plays a crucial role in energy generation at the membrane and maintains its biological functions. Bacteria require a significant amount of energy to produce and secrete EPS. In addition, proteins related to ABC transporters were up-regulated over a 2-fold change. Bacteria consumed more ATP to maintain the transport under the Ni^{2+} stress conditions. Therefore, cytochrome bo3 quinol

oxidase was up-regulated over 2-fold. ABC transporter proteins are involved in the uptake of iron, ions, amino acids, peptides, and Other essential nutrients. SHG03806.1 and SHF50725.1 are two proteins located in the cell membrane that participate in iron or iron complex transport. It seems that ABC transporters that are associated with heavy metal resistance are widespread in microbes. Ferrous iron uptake systems are essential for bacteria survival, especially under HM stress. The Other ABC transporters are involved in amino acids (SHG06085.1) or other substrate (SHG03806.1 and SHE60645.1) transport. Moreover, ABC transporters are also responsible for transporting the HM complexes from the inner cell to the extracellular space to achieve steady-state regulation of metal ions in microbes treated with Cd^{2+} (Wang et al., 2022). SHF6470.1 is TRAP transporter substrate-binding protein, and was found for recognition of two aromatic compounds (Mulligan et al., 2011). As shown in Figure 23 (a-c), the aromatic compounds including aromatic proteins, humic acid and fulvic acid increased with Ni^{2+} treatment.

SHE88885.1, a protein associated with flagellar assembly, is up-regulated over 2-fold change. Likewise, the flagellum is verified to be an essential factor in biofilm formation. Knockout of the flagellar hook-associated protein (FlgK) led to a decrease in biofilm formation, while HM resistance was affected (Chih-Ching et al., 2013). This demonstrated that the flagellum is critical in bacterial HM detoxification. Bacteria sense toxic chemicals in the environment and swim

away from them using flagella. Conversely, they swim toward new nutrients in the medium if they sense them (Annapurna et al., 2022).

Furthermore, the porin proteins (SHG04300.1, SHF15748.1, SHF56176.1) were down-regulated 6,9-fold-change, 4-fold-change, and 2,9-fold-change, separately, especially SHG04300.1 (the highest down-regulation protein). Down-regulated porins were also identified in complex communities under HM stimulation (Gillan, 2016). This implied that reduced porins may prevent the excessive HMs from entering the inner cells (Gillan, 2016; Hillol et al., 2022). The porins in *Klebsiella pneumoniae* were down-regulated under As(III) stress, resulting in increased As(III) resistance (Vandana et al., 2012). It seems that these kinds of resistance mechanisms are bacteria responses to environmental stress. Moreover, the gene for the porin (ompC) in *E. coli* exhibited both up-regulation and down-regulation simultaneously, demonstrating a finely tuned response to environmental stress (Yuan et al., 2021). Up-regulation of porin contributes to the acquisition of nutrients for survival under stressful conditions, whereas down-regulation of porin may minimize oxidative stress-induced damage by limiting the entry of ROS into cells (van der Heijden et al., 2016). Additionally, the secretome data of *V. gazogenes* reveals that it possesses 21 specific proteins for the transport of Ni^{2+} (Table 5). However, these proteins were not observed to be expressed in the proteomics data, contrary to the previous results (Zhang et al., 2023). Zhang et al. performed proteomic analysis

with *Vibrio cholerae* under 50 mg/L Ni^{2+} stimulation and found efflux pump RND transporters were induced (Zhang et al., 2023).

4.1.7 q-RTPCR verify the regulation of Ni^{2+} transporters

To determine whether the Ni^{2+} transporters were expressed, we performed q-RTPCR. As shown in Figure 28, the Ni^{2+} transporters were up-regulated during the first 2 to 3 hours. This indicates that Ni^{2+} transporters were one of the bacterial resistance strategies. Once cells adapt to the Ni^{2+}, negative feedback mechanisms may occur, leading to the proteins' expression to basal levels or below. It is reported that cells detoxify Cd^{2+} toxicity through down-regulation of Cd^{2+} transporter (Aiba et al., 2008). Nevertheless, maintaining transport activities required more energy, while the cell metabolism was inhibited due to the high concentration of Ni^{2+} and there was not enough energy available. A similar study also demonstrated that efflux pumps were active during the first several hours, suggesting that they may constitute an immediate response to HMs (Dario Rangel & Jenny, 2018). Additionally, efflux pumps may also be inhibited by high concentrations of HMs. But for *Psa*A, it kept up-regulated until 24h. As we mentioned above, *Psa*A is an Mn^{2+}/Fe^{2+} transporter, which maybe not only participated in Fe^{2+}, Zn^{2+} and Cd^{2+} etc.. In addition, it may also respond to Ni^{2+} through detoxification superoxide and biofilm formation.

Therefore, it may also be involved in preventing Ni^{2+} from entering inner cells. This result is consistent with the LC-MS/MS data.

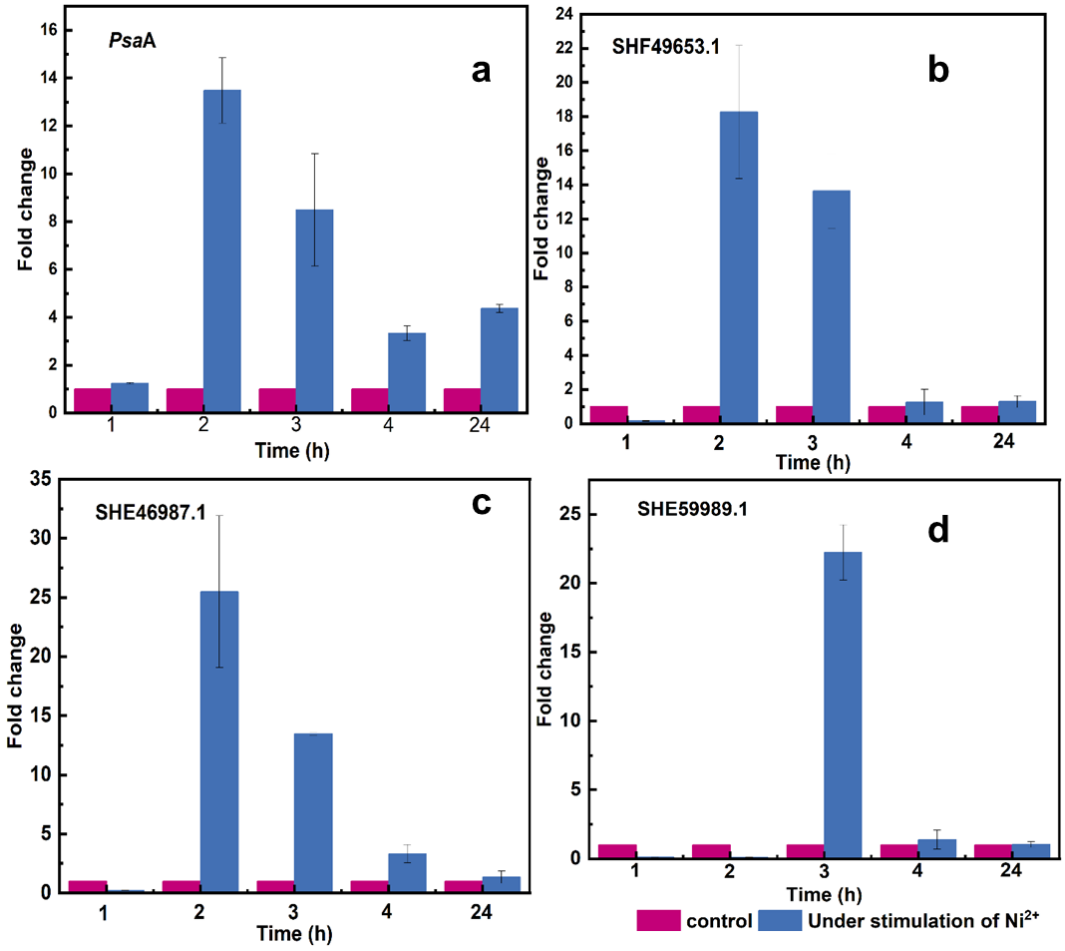

Figure 28: (a,b,c,d) Gene expression levels of selected ORFs linked to Ni resistance at different time points. *V. gazogenes* was incubated until the OD600 values were 0.2. Data are results of three independent measurements and cultures. Error bars indicate the standard deviations. Data were normalized against the 16S rRNA gene. (a), PsaA is a protein involved in manganese/iron transport system substrate-binding protein. (b), SHE46987.1, peptide/nickel transport system substrate-binding protein;(c), SHF49653.1, cobalt/nickel transport protein; (d), SHE59989.1, cobalt/nickel transport protein.

4.1.8 Sequence-based searches against NCBI's non-redundant database

(1) Phylogenetic tree of *PsaA* protein

Blasting *PsaA* (SHF52054.1) in NCBI revealed homologs of *PsaA* belonging to different lineages as shown in Figure 29. We selected the proteins that Query cover > 90%, and percent identity > 70%. Proteins were annotated as manganese/iron transport system substrate-binding protein, metal ABC transporter substrate-binding protein, and putative periplasmic iron-binding protein. The proteins were mostly from vibrio species, but also some of them were from *Winslowiella*, *Shinella*, *Roseateles*, and *Haemophilus* species. The closest proteins were from *Vibrio spartinae* except *Vibrio gazogenes.*

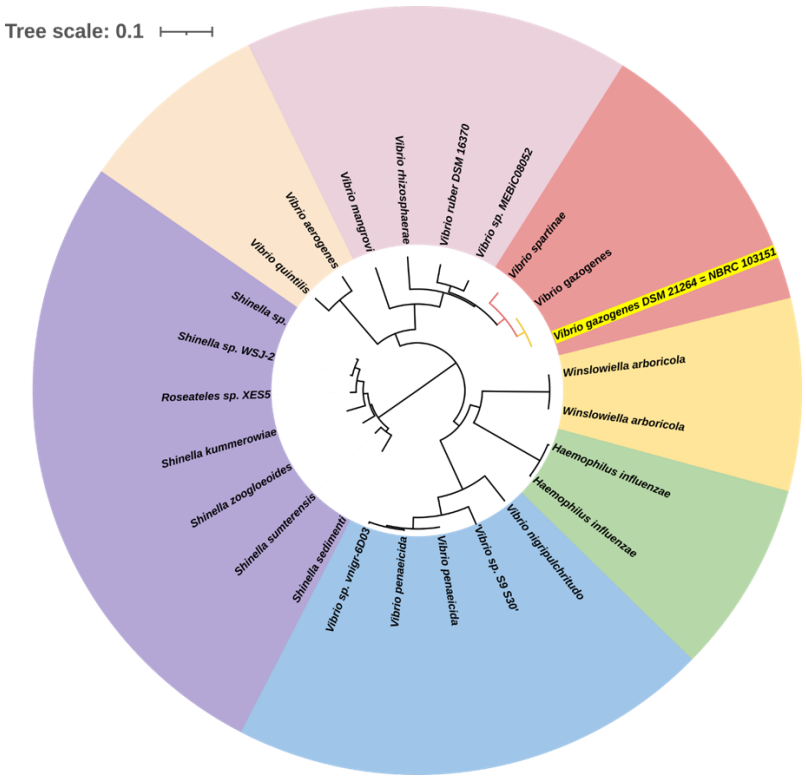

Figure 29: Phylogenetic tree of *PsaA* protein; *Shinella sp.* (MBO9628501.1), *Shinella sp.* WSJ-2 (RFZ87171.1), *Roseateles sp.* XES5 (WP_226917797.1), *Shinella kummerowiae* (WP_261005029.1), *Shinella zoogloeoides* (WP_306032480.1), *Shinella sumterensis* (WP_306037508.1), *Shinella*

sedimenti (WP_241601724.1), *Vibrio sp.* S9_S30 (WP_190335836.1), *Vibrio sp. vnigr*-6D03 (WP_101111868.1), *Vibrio penaeicida* (RTZ22740.1), *Vibrio penaeicida* (WP_224055951.1), *Vibrio nigripulchritudo* (WP_022560555.1), *Haemophilus influenzae* (WP_239494817.1), *Haemophilus influenzae* (WP_223364826.1), *Winslowiella arboricola* (WP_323372732.1), *Winslowiella arboricola* (MCU5774037.1), *Vibrio aerogenes* (WP_073605040.1), *Vibrio quintilis* (WP_073584191.1), *Vibrio mangrovi* (SMS02078.1), *Vibrio rhizosphaerae* (WP_038180962.1), *Vibrio sp.* MEBiC08052 (WP_059122531.1), *Vibrio ruber* DSM 16370 (SJN53784.1), *Vibrio spartinae* (SI096499.1), *Vibrio gazogenes* DSM 21264 (SHF52054.1), *Vibrio gazogenes* (WP_235862446.1)

(2) Sequence comparision between PsaA and its nine closest homologs

Compared PsaA with its nine closest homologs reveals that high amino acid conservation within vibrio species (Figure 30). the sequences were nearly identical in all homologues, with only *Shinella zoogloeoides* (WP_160785153.1), *Vibrio penaeicida* (WP_237324139.1) and *Vibrio mangrovi* (WP_ 200807773.1) have partial deletions at sequence start sites 1-22, suggesting that their common ancestor exchanged genetic information between species during evolution. In addition, they are functionally similar, involved in the transport of metal ions, and have been subjected to strong selective pressure to maintain their function unchanged during evolution.

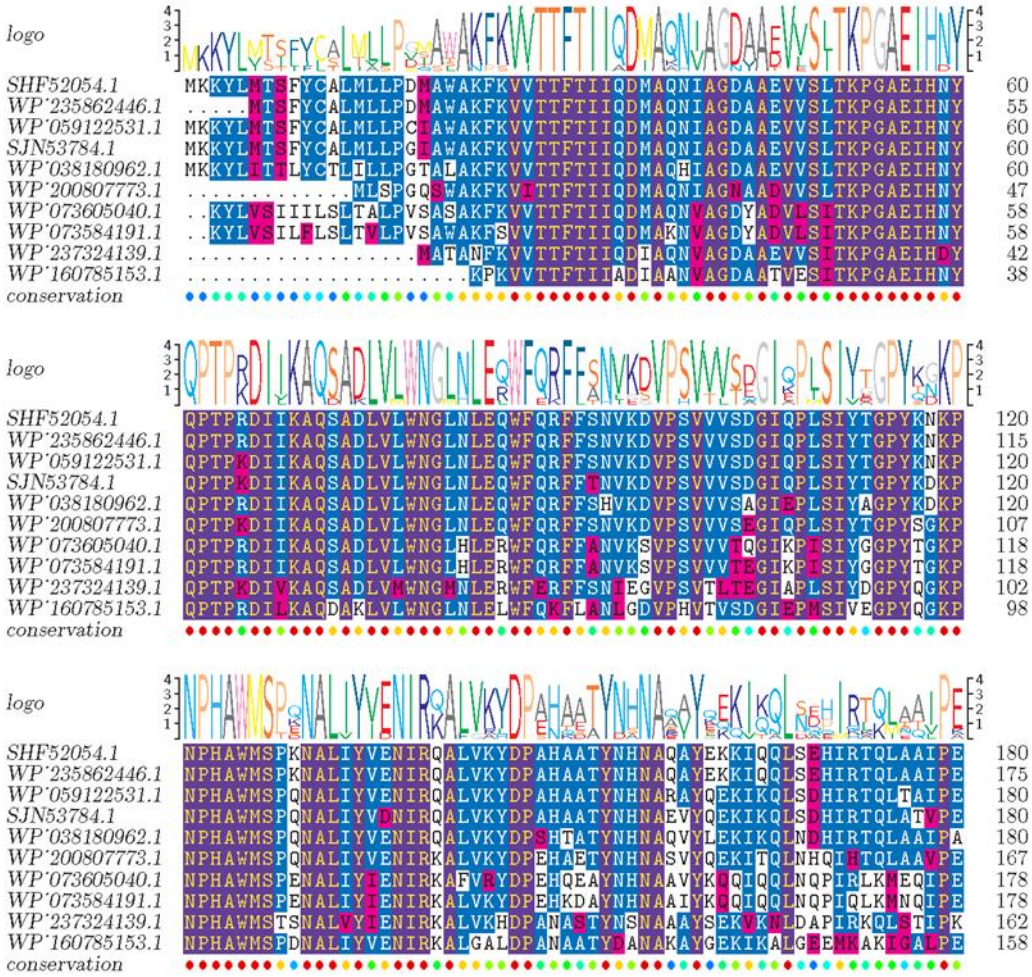

Figure 30: Sequence comparision between PsaA and its homologs; *Shinella zoogloeoides* (WP_160785153.1), *Vibrio penaeicida* (WP_237324139.1), *Vibrio aerogenes* (WP_073605040.1), *Vibrio quintilis* (WP_073584191.1), *Vibrio mangrovi* (WP_200807773.1), *Vibrio rhizosphaerae* (WP_038180962.1), *Vibrio sp.* MEBiC08052 (WP_059122531.1), *Vibrio ruber* DSM 16370 (SJN53784.1), *Vibrio gazogenes* DSM 21264 (SHF52054.1), *Vibrio gazogenes* (WP_235862446.1)

Metal binding sites were predicted by Metal 3D as shown in Figure 31. Predicting amino acid residues at the 100% probability metal-binding sites reveals that His123, Asp264, Glu189, and His58 collectively form a metal-binding site capable of binding multiple ions, including Cu^{2+}, Ni^{2+}, Mn^{2+}, Zn^{2+}, Fe^{2+}, and Fe^{3+}.

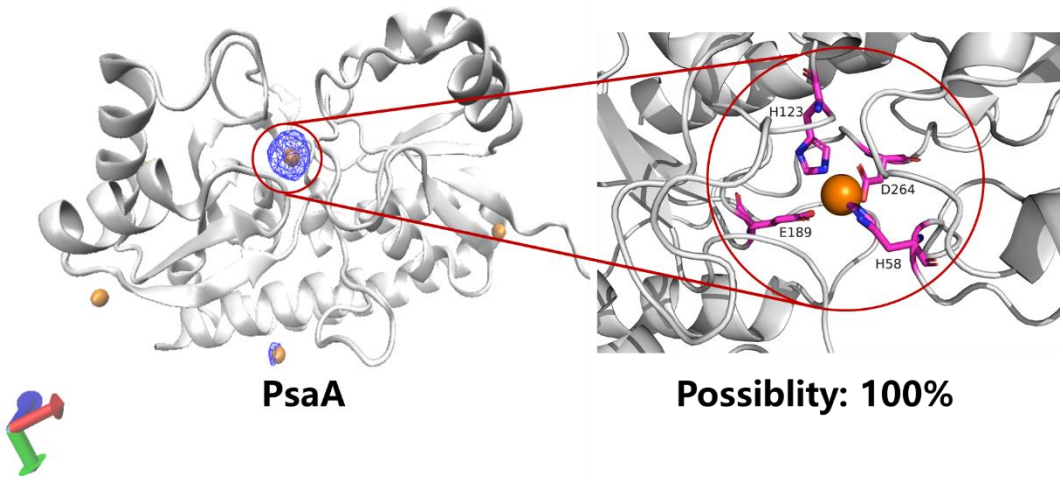

Figure 31: Metal binding sites predicted based on Metal 3D; orange ball represent metal ions, and the blue mesh represents the probability percentage for Cu^{2+}, Ni^{2+}, Mn^{2+}, Zn^{2+}, Fe^{2+}, and Fe^{3+}; H: His, D: Asp, E: Glu

Metal binding sites predicted by MetalNet and AlphaFold 3 are shown in Figure 32. The metal binding sites predicted by AlphaFold 3 for Mn^{2+}, Cu^{2+}, Mn^{2+}, Zn^{2+}, and Co^{2+} are entirely consistent. The amino acid residues align with those predicted by MetalNet and are consistent with the most probable metal binding sites predicted by Metal 3D. In the AlphaFold 3 Protein-Glycan-Ion model, ipTM serves as an indicator of prediction accuracy for subunit relative positions within complexes. Results with ipTM values between 0.6 and 0.8 cannot be guaranteed as correct, while values below 0.6 indicate errors. Values above 0.8 signify high-quality and reliable predictions. *PsaA*'s AlphaFold 3 prediction yielded an ipTM of 0.98, indicating highly accurate and reliable results; Furthermore, the predicted amino acid residues align with MetalNet predictions

In summary, the simulation results from the three models are consistent, indicating that the predicted metal-binding site is highly reliable. *PsaA* may be a protein capable of binding multiple metal ions simultaneously, with the binding site amino acid residues identified as His123, Asp264, Glu189, and His58.

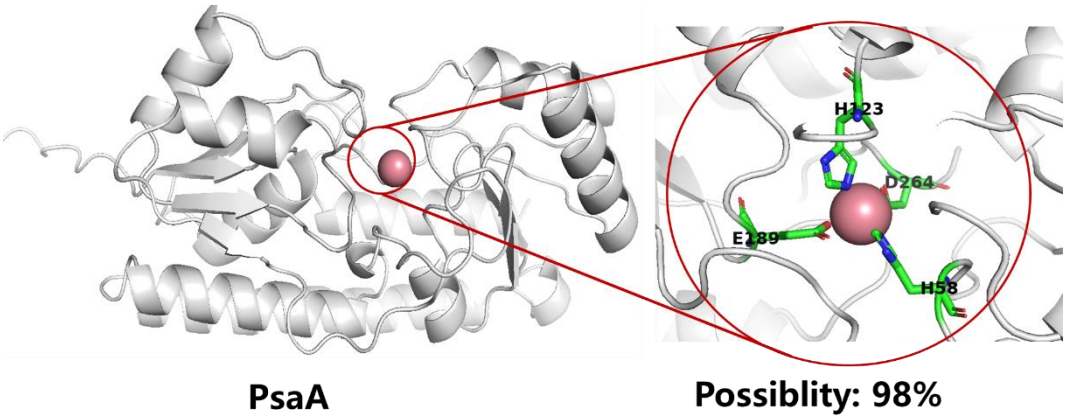

Figure 32 Metal binding sites predicted based on AlphaFold 3 and Metal Net; red ball represents metal ions, and the blue mesh represents the probability percentage for Cu^{2+}, Ni^{2+}, Mn^{2+}, Zn^{2+}, Fe^{2+}, and Fe^{3+}; H: His, D: Asp, E: Glu

4.2 Discussion

4.2.1 Function of extracellular proteins on heavy metal resistance

Tryptophan protein-like substances were important to resist heavy metals. With heavy metal treatment, the content of tryptophan protein-like substances increased. However, the peak of tryptophan protein-like substances was gradually quenched with the increasing metal concentrations due to the tryptophan binding with metal ions (Joshi et al., 2023). It's proved that tryptophan and tyrosine from cellular components and EPS are the main participants in lead (Pb^{2+}), Cu^{2+} and Other metal ions adsorption or fixation (Sihui et al., 2021; Xianxin et al., 2022; Xiaobo et al., 2023; Zedong et al., 2019). In addition, tryptophan participated in protein-ligand interactions and the formation of hydrophobic cores which is the major driving force of cell adhesion (Ge et al., 2024). Therefore, compared tryptophan in *C. pauculus* with the one in *V. gazogenes*, tryptophan is important in Ni^{2+} adsorption and resistance.

From the results of liquid chromatography-tandem mass spectrometry (LC-MS/MS), we can see the proteins involved in lipopolysaccharide (LPS) synthesis protein up-regulated over two-fold change in two strains. It indicates that LPS is a common mechanism of resistance. It belongs to extracellular barrier and also can enhance cell adhesion (Liping & Gianluca Li, 2022). LPS is an integral membrane component in the cell envelope of gram-negative bacteria (Coughlin et al., 1983; Pereira et al., 2006b). The protein involved in LPS synthesis increased seems to be significant for not only Ni^{2+} resistance but Other heavy metals, since bacteria such as *Psedomonas aeruginosa* and *Acidthiobacillus ferrooxidans* can adsorb heavy metals on the cell surface through electrostatic interactions with LPS (Javiera et al., 2019; S. Langley, 1998). Therefore, it is the primary barrier for detoxification metals. In addition, it's proved that LPS bind cations unspecifically and sequestrate cations to prevent metals from entering to inner cell (Pereira et al., 2006b).

Proteins related to efflux pump also significantly participated in heavy metal resistance. Bacteria detoxify heavy metals through efflux of the overdose of heavy metals from inner cells or periplasm. During the different growth periods, the expression of Ni^{2+} efflux pumps showed different. It is also a common phenomenon in two strains. There are specific nickel efflux pumps in *C. pauculus* and *V. gazogenes*. However, after 24 hours incubation, there are almost no efflux pumps up-regulated in both stains. In *C. pauculus*, the specific nickel efflux pumps were active at the first 4 hours while the multidrug efflux pump up-regulated over two-fold change after 24-hours incubation. Differently, in *V. gazogenes*, nickel transport system substrate-binding protein was down-regulated while the proteins related to manganese/iron transport system substrate-binding protein was up-regulated over 2-fold change. It indicates that nickel efflux pumps and multidrug efflux increased in Ni^{2+} resistance. It well known that manganese/iron substrate binding protein is high-affinity to Mn^{2+} and Fe^{3+}. Nevertheless, MntA, the typical Mn^{2+} binding proteins, can binds not

only Mn^{2+} or $Fe^{2/3+}$, but Zn^{2+}, Ni^{2+}, Co^{2+}, Cd^{2+} and Other metals (Elena et al., 2015). In addition, Cd^{2+} was found to be transported by the manganese transport system in *Staphylococcus* (Nies & Silver, 1995). Therefore, we guess that Ni^{2+} can be transported through manganese systems, too. Moreover, the expression of efflux pumps depends on the environmental conditions. Cells need to produce energy to synthesize and support activity of efflux pumps, such as high affinity metal transport system, cation diffusion facilitator proteins (CDF), ATP-binding cassette transporters, P-type ATPase utilizes ATP to transport heavy metals from cytoplasm to periplasm (Pal et al., 2022; Shaw & Dussan, 2015). It suggests that other detoxification pathways are more effective or spend less energy, cells can active the efficiency pathway to detoxify the heavy metals rather than expressing efflux pumps. In addition, it's also reported that bacterial genomes may be mutant due to the stress of heavy metals, resulting in non-expression of those efflux pumps (Sincak et al., 2023). Moreover, some efflux pumps can only resist low-level concentration of heavy metals, such as CDF family. Interestingly, multidrug efflux pump in *C. pauculus*, was up-regulated over 2-fold change after 24 hours incubation. It's reported that multidrug efflux can expel a wide range of toxic compounds from bacteria (Yang & Zhang, 2020a). Increasing evidence indicates that the co-selection of heavy metal resistance and antibiotic resistance occurs through shared resistance mechanisms (Nguyen et al., 2023a; Sincak et al., 2023). And numerous research suggests that heavy metal generate the spread of antibiotic-resistance in the environment (Xiangyang et al., 2019). The low concentration of heavy metals can induce bacterial antibiotic resistance through co-selection (Xiangyang et al., 2019). Multidrug efflux pumps expression maybe can demonstrate the reason. Moreover, heavy metals generated genes in bacteria involved in multidrug efflux pump and outer membrane porin permeability (Sumei et al., 2022).

Interestingly, there are some porin proteins were down-regulated over 2-

fold change. the lack of porin proteins disrupts the cell wall integrity and leads to increased sensitivity to solvents (Pal et al., 2022). Consequently, adaptation to solvents strengthens resistance against heavy metals and antibiotics (Juan et al., 1997). For instance, knocking down porin proteins in E. coli hinder the entry of Ag^{+} into the cells at higher concentrations (Li et al., 1997). Up-regulated multidrug efflux pump and down-regulated outer membrane porin promoted antibiotic resistance with heavy metal exposure (Yan et al., 2022).

4.2.2 The Common Features of Extracellular Protein-Mediated Resistance Mechanisms in *C. pauculus* and *V. gazogenes*

(1) Upregulation of Extracellular Lipopolysaccharide (LPS) Assembly and Expression for Ni^{2+} Adsorption and Sequestration

Extracellular lipopolysaccharide (LPS)-mediated heavy metal tolerance represents a prevalent resistance mechanism among microbial populations. This constitutes a broad-spectrum resistance strategy against various environmental stressors, including heavy metals, antibiotics, and organic pollutants, likely serving as a universal stress response mechanism in bacteria.

Figure 33 illustrates the proposed mechanistic model of LPS under Ni^{2+} stress. Both *C. pauculus* and *V. gazogenes* exhibited upregulated expression of LPS assembly proteins upon Ni^{2+} exposure, suggesting LPS serves as the primary defense line against heavy metal stress. This phenomenon parallels observations in Pseudomonas aeruginosa under Cd^{2+} stress, where spectroscopic changes occurred in the O-specific region and the core oligosaccharide-lipid A linkage zone - critical sites for heavy metal adsorption.

Furthermore, Gram-negative bacteria adapt to environmental stress through outer membrane modifications, primarily mediated by structural remodeling of the lipid A moiety in LPS. To maintain membrane stability under stress conditions, bacteria incorporate cationic substituents (e.g., arabinose

and phosphoethanolamine [PEtN]) at lipid A phosphate groups (Nowicki et al., 2015). However, LPS-mediated defense alone proves insufficient, requiring synergistic action with Other bacterial resistance mechanisms (Pereira et al., 2006a).

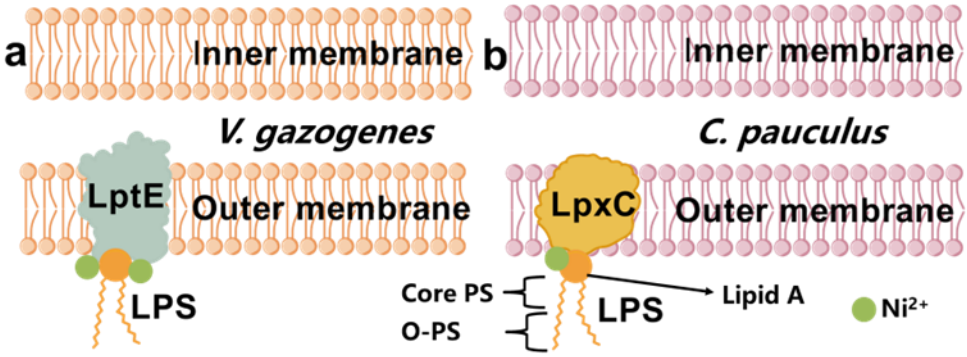

Figure 33: Ni^{2+} resistance mechanism model based on LPS; (a) LPS resistance mechanism in *V. gazogenes*, LptE is a protein involved in LPS assembly; (b) LPS resistance mechanism in *C. pauculus*, LpxC is a protein related to LPS assembly. LPS has three regions, including O-PS, core-PS and lipid A. Core-PS is linked with lipid A

(2) Mechanisms of Oxidative Damage and ROS Defense

Intracellular Ni^{2+} induces oxidative stress, triggering antioxidant responses mediated by ROS-scavenging proteins as shown in Figure 34. This defense mechanism represents a universal stress response to environmental challenges, not exclusively to heavy metal exposure. The primary enzymes involved in ROS detoxification include superoxide dismutase (SOD), catalase (CAT), and glutathione (GSH), with this system being evolutionarily conserved across multiple species.

The membrane-bound oxidative defense proteins in both species predominantly contain iron-sulfur (Fe-S) clusters, which have been identified as redox switches critical for combating oxidative stress (Jennifer et al., 2023). Notably, intracellular H_2O_2 readily undergoes Fenton reactions, causing

damage to essential cellular components including proteins and DNA.

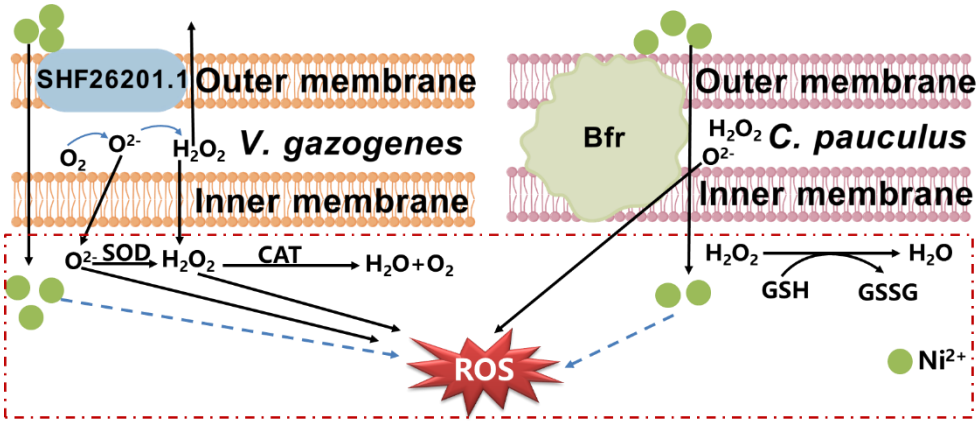

Figure 34: Mechanism of ROS production and detoxification; SHF26201.1 in *V. gaozgenes* and Bfr in *C. pauculus*, located in membrane, are proteins participating in oxidative stress defense. Due to respiration, O_2 is converted into superoxide (O^{2-}), which subsequently forms hydrogen peroxide (H_2O_2) in the presence of protons. The O^{2-} and H_2O_2 generated in the periplasm then cross the inner membrane into the cytoplasm, leading to the production of ROS. Meanwhile, the entry of Ni^{2+} can also induce ROS production. O^{2-} is converted into H_2O_2 by SOD, which is subsequently transformed into H_2O and O_2 by CAT, thereby detoxifying ROS. Additionally, H_2O_2 generated can be converted to H_2O through GSH, further reducing ROS levels

(3) Dual Regulatory Effects of Ni^{2+} on Extracellular Protein Secretion and EPS Structure

Ni^{2+} promotes extracellular protein secretion and cell aggregation, protecting cells from toxicity and altering the structure of EPS (Figure 35). However, high Ni^{2+} concentrations inhibit extracellular protein secretion. Bacterial aggregation, caused by spatiotemporary stress, is divided into self-aggregation (stronger due to prior communication of bacterial physicochemical properties and surface hydrophobicity) and co-aggregation (weaker and multi-species). Cell aggregation is an initial step in biofilm formation, which can

enhance tolerance to metals and antibiotics by up to 1,000 times. Even dead cells in biofilms can protect live cells by precipitating or isolating metal ions, as they remain chemically reactive and contain biosorption sites. Biofilms alter bacterial physiological properties, enabling resistance to metal species and activating stress response mechanisms during maturation to counteract metal toxicity. Many studies also show that different Ni^{2+} concentrations and Other heavy metal ions can promote bacterial biofilm formation.

Under Ni^{2+} stimulation, the secretion of extracellular proteins by *C. pauculus* and *V. gazogenes* increases, and bacterial aggregation occurs. Extracellular proteins in bacteria play a key role in regulating cellular Ni^{2+} homeostasis and adsorption. For instance, under cobalt and nickel stimulation, proteins involved in enzymatic reactions and metal binding, such as periplasmic [NiFeSe] hydrogenase, significantly increase. Additionally, studies have shown that in the EPS of eight pure strains isolated from activated sludge, the protein content is much higher than that of polysaccharides, and the complexation ability for Ni^{2+} is significantly higher than that for Cd^{2+} (Gilles et al., 2005).

Moreover, researchers analyzed the adsorption and distribution of Ni^{2+} in bacterial microcolonies using CLSM, SEM, and X-ray microprobes and found that nickel adsorption occurs on negatively charged residues in the extracellular polymeric matrix and is not directly associated with cells. The extracellular polymers of biofilms largely protect cells from heavy metal toxicity. Researchers observed the same phenomenon in *H. salinaru* (Lawrence et al., 2019). Under Ni^{2+} stimulation, extracellular proteins, relative to extracellular polysaccharides, are the main components of EPS, and in the formed biofilm, the content of extracellular proteins increased 2.7 times under Ni^{2+} stimulation. This finding indicates that multifunctional groups of proteins in the EPS of *H. salinarum* are involved in metal ion binding (Völkel et al., 2020). Furthermore, researchers conducted comparative secretomics and proteomics analyses of three strains

of V. cholerae under Ni^{2+} stimulation and found that sublethal concentrations of Ni^{2+} (50 mg/L) increased cell membrane fluidity and enhanced the secretion of extracellular proteins under Ni^{2+} stimulation (Zhang et al., 2023). It has also been reported that as the concentration of Ni^{2+} increases, the content of extracellular proteins in methanogenic mixed cultures decreases. When the metal concentration is increased to 1840 mg/L, the content of extracellular proteins in EPS decreases by 64.7% (Margaryan et al., 2021). Therefore, the secretion of extracellular proteins is regulated by different concentrations of Ni^{2+}. At low concentrations, the secretion of extracellular proteins increases with the increase of Ni^{2+}, but when the concentration of Ni^{2+} is high enough to be lethal or higher than the semi - lethal concentration, the secretion decreases.

In addition, the structure of extracellular polysaccharides (PS) has changed, and the ratio of α-extracellular polysaccharides (α-PS) and β-extracellular polysaccharides (β-PS) has changed. As shown in Figure 35, in *C. pauculus*, under the stimulation of 200 mg/L Ni^{2+}, the structure of PS in the first 4 hours and 24 hours is completely different. It changed from bright purple to blue - purple, and the content of β-PS increased. The same phenomenon was found in *V. gazogenes*. At 4 hours, there was almost only α-PS, but at 24 hours, the content of β-PS increased. α-Polysaccharides, due to their helical structure, are suitable for energy storage; β - polysaccharides, due to their linear structure, are suitable for providing structural support. β-PS has been proven to be the main framework structure of EPS. By embedding extracellular proteins and α-PS, it maintains the stability of EPS (Adav et al., 2008). Their combined action promotes bacterial aggregation and biofilm formation.

In summary, under Ni^{2+} stimulation, the extracellular proteins of some bacteria show an increasing trend in secretion, indicating that they play an important role in Ni^{2+} resistance mechanisms and are a broad-spectrum mechanism for bacteria to resist Ni^{2+}. However, in some bacteria, extracellular proteins are inhibited by high concentrations of Ni^{2+}. As the concentration of

Ni^{2+} increases, the content of extracellular proteins decreases. The reason for this phenomenon is that cellular metabolic activities are seriously inhibited, and the expression of proteins responsible for protein folding and Other secreted proteins is down - regulated. The structure of EPS has also changed, with an increase in the content of β-PS, which plays a supporting role in maintaining the stability of EPS. Therefore, during the stationary phase or late growth phase, α-PS can be broken down to provide energy for cells, while β-PS, as the EPS framework, maintains the stability of the EPS structure.

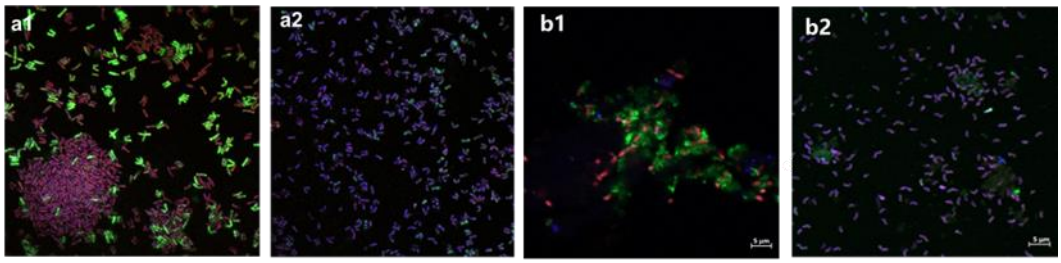

Figure 35: EPS of *C. pauculus* (a1-a2) and *V. gazogenes* (b1-b2) under the stimulation of high concentrations of Ni^{2+}; (a1, a2), the EPS of *C. pauculus* under 200 mg/L Ni^{2+} stimulation at 4 h and 24 h, respectively; (b1, b2) the EPS of *V. gazogenes* under 150 mg/L Ni^{2+} stimulation at 4 h and 24 h, respectively. Green fluorescence: extracellular proteins, red fluorescence: α-exopolysaccharides (α-PS), blue fluorescence: β-exopolysaccharides (β-PS), purple fluorescence: caused by different ratios of α-PS to β-PS

(4) The upregulation of flagella expression and assembly proteins

The upregulation of flagella expression allows bacteria to swim away from toxic substances, a common mechanism in microbial heavy metal resistance. When exposed to Pb^{2+}, B. coagulans significantly regulates genes related to flagellar formation and chemotaxis, forming flagella and chemotaxis systems to escape Pb^{2+} rather than expelling it. Thus, upregulated flagellar protein expression helps bacteria quickly avoid toxic substances.

4.2.3 The differences between the extracellular protein-mediated resistance mechanisms of *C. pauculus* and *V. gazogenes*

In *C. pauculus*, 43 proteins were significantly upregulated by over 2 times, with only 1 protein downregulated by more than 2 times. Notably, ParC, a cell division related protein, was upregulated by over 2 times, while ABC transporters showed little change. In *V. gazogenes*, 25 proteins were upregulated by over 2 times, and 26 proteins were downregulated by more than 2 times. Among the top 5 upregulated proteins, many were ABC transporters. In contrast, the top 5 downregulated proteins were mostly linked to cell membrane channels and lipoproteins, with downregulation as high as 6.9 times.

（1）The special nickel resistance mechanism in *V. gazogenes*

In *V. gazogenes*, porin proteins are downregulated (Figure 36). The outer membrane is the first barrier for metal entry into the cell. Porins play a role in membrane permeability and are important for transporting metal ions into the cell. In *V. gazogenes*, porin proteins, including those in the cell membrane and Ni^{2+} transporters, are downregulated. This phenomenon is not observed in the extracellular proteome of *C. pauculus*. Studies have shown that knocking out porin genes in E. coli alters the structure and composition of membrane lipids and proteins, increasing the levels of fatty acids, phospholipids, and polysaccharides. The absence of some membrane proteins can enhance Cu^{2+} resistance. A similar phenomenon is observed in the iron - oxidizing bacterium *A. ferrooxidans*, where major outer membrane porins and some ion transporters are downregulated under Cu^{2+} stress. This suggests a reduced influx of metals and other cations into the cell, potentially enhancing Cu^{2+} resistance. As shown in Figure 36, intracellular Ni^{2+} binding to its sensor enzyme inhibits porin expression, reducing Ni^{2+} uptake. However, there are few reports of downregulated membrane porin expression under Ni^{2+} stimulation, with most

reports focusing on other heavy metals. In summary, bacteria commonly maintain intracellular heavy metal homeostasis and enhance resistance by downregulating membrane porin and ion channel proteins.

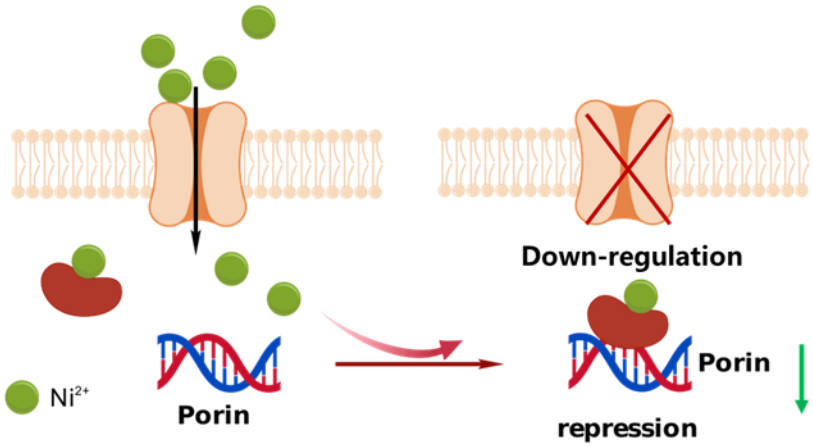

Figure 36: Conceptual model of down-regulation of porin under Ni^{2+} stress; The Ni^{2+}-sensing factor binds to Ni^{2+} and reduces Ni^{2+} uptake by downregulating the expression of Ni^{2+} porin on the cell membrane

(2) *C. pauculus* combats Ni^{2+} toxicity by increasing cell density through upregulated *ParC*, a cell division - related protein as show in Figure 37. Generally, bacterial density decreases with rising heavy metal concentrations, and *V. gazogenes* shows this trend under Ni^{2+} stress. However, under 200 mg/L Ni^{2+}, *C. pauculus* shows higher cell density than the control group. *ParC* is crucial for cell division and survival in high concentrations of pollutants like Ni^{2+}. This mechanism, aiding in bacterial adaptive evolution, enhances Ni^{2+} resistance by increasing cell division and providing more extracellular metal binding sites to block its intracellular entry. This finding deepens our understanding of microbial Ni^{2+} tolerance mechanisms.

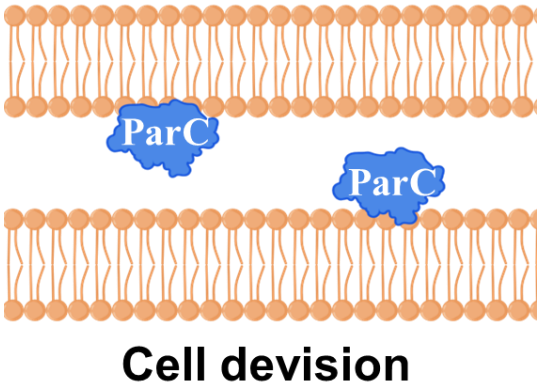

Figure 37: Specific resistance mechanism in *C. pauculus*

(3) Ni^{2+} transport - related proteins are not involved In the upregulated extracellular proteins of *C. pauculus* and *V. gazogenes*, there are no Ni^{2+} - efflux or transport proteins. The well - documented Ni^{2+} efflux mechanism doesn't work. Instead, metal transporters not related to Ni^{2+} transport are significantly upregulated. *C. pauculus* and *V. gazogenes* were isolated from non - heavy - metal - contaminated areas. *C. pauculus* was from bottled mineral water, and *V. gazogenes* from marine sediments. V. cholerae, from goldfish and white - carp, also from a non-heavy-metal-contaminated area, shows upregulated ABC transporters under 50 mg/L Ni^{2+} (sublethal). But in this study, under 100 mg/L Ni^{2+}, *V. gazogenes* downregulates peptide/ Ni^{2+} - transport - system substrate - binding proteins. The reason might be different Ni^{2+} concentrations. At low concentrations, Ni^{2+} transporters maintain intracellular Ni^{2+} homeostasis by transporting Ni^{2+} in and out. At high concentrations, they and membrane channels are downregulated to reduce Ni^{2+} uptake and combat stress. The common Ni^{2+} - resistance mechanism is through the cnrYHXCBAT gene system, which expresses CnrCBA efflux proteins to expel Ni^{2+}. Other systems like CzcCBA, CnrCBA, and NccCBA are also reported. Although *C. pauculus* has the complete cnrYHXCBAT - CnrCBA system, these genes aren't expressed under Ni^{2+} stress. Instead, the multidrug efflux pump WP_460 is upregulated. In *V. gazogenes*, multiple membrane channel proteins are downregulated,

especially Ni^{2+}/peptide transporters. But other metal transporters not related to Ni^{2+} transport, like iron-manganese transporter *PsaA*, are upregulated. This doesn't match the reported Ni^{2+}-resistance mechanisms. Metal-binding-site prediction shows *PsaA* can adsorb various metal ions, including Ni^{2+}, with high accuracy. However, WP_460 has no predicted metal-binding sites with over 60% probability, and its Ni^{2+}-transport mechanism is unknown. Yet, WP_460 is highly similar to *czrB*, a divalent-cation transporter, which also has no metal-binding-site predictions with over 60% probability. Moreover, WP_460 is a multidrug efflux protein induced by heavy metals, potentially enhancing antibiotic resistance and posing a serious health risk. *C. pauculus* is often found in water, such as contaminated hospital water systems and sink pipes. If it upregulates multidrug efflux protein expression due to metal ions like Cu^{2+} and Ni^{2+}, leading to increased antibiotic resistance, the consequences would be severe. Future research on this protein, especially its metal-binding sites and relationship with antibiotic-molecule docking sites, could provide theoretical support for understanding the co-resistance between heavy metals and antibiotics. When bacteria are from non-heavy-metal-contaminated sources and their heavy-metal-resistance systems aren't activated, they may upregulate proteins to transport Ni^{2+} and maintain intracellular homeostasis, even using transporters related to growth and metabolism. These transporters can be induced by various toxic substances. In contrast, bacteria from heavy metal contaminated sources mainly use the reported Ni^{2+}-efflux mechanisms. Under environmental stress, some drug-resistant bacteria may increase heavy metal tolerance without activating adaptive mechanisms, while others use adaptive strategies to adjust to environmental changes.

5 Conclusions and outlook

Microorganisms secrete a large number of extracellular polymers, especially extracellular proteins (e-PN), during the removal of heavy metals from wastewater. E-PN plays essential roles in heavy metal detoxification. However, there are still some knowledge gaps about e-PN in the mechanism of heavy metal resistance, such as the interactions of e-PN, the connection between membrane proteins and periplasmic space proteins. etc. We took the typical heavy metal-resistant bacterium *C. pauculus* and the atypical heavy metal-resistant bacterium *V. gazogenes* as the research objects, firstly, we mined the Ni^{2+} resistance genes in whole genome, predicted the location of extracellular proteins through secretomics and analyzed the function of extracellular proteins; then, we constructed a conceptual model of the mechanism of Ni^{2+} resistance with the help of the qualitative and quantitative analysis of extracellular proteomics. Finally, we summarized the similarities and differences between the Ni^{2+} resistance mechanisms based on e-PN in typical and atypical heavy metal resistant bacteria. The main findings are summarized below:

First, there are 10 gene associated with Ni^{2+}/Co^{2+}, 12 RND super family genes and P-type ABC heavy metal resistant gene in *C. pauculus* whole genome. To investigate the reasons for the difference of Ni^{2+} tolerance, the extracellular proteins of *C. pauculus* were characterized under Ni^{2+} stimulation. The functional groups N-H, C=O and NH_2-R in the extracellular proteins play important roles in adsorption and tolerance of Ni^{2+}. Forty-three proteins were significantly up-regulated and nine proteins were significantly down-regulated in response to Ni^{2+} stimulation, of which 27 proteins were up-regulated by more than two-fold and only one protein was down-regulated by more than two-fold. The mechanism of *C. pauculus* responding to Ni^{2+} resistance was mainly through the establishment of extracellular barriers, metal-ion efflux, and

extracellular chelation to achieve Ni^{2+} detoxification, in which the multidrug efflux proteins were the major contributors to the efflux of Ni^{2+}. At the same time, Ni^{2+} induces an increase in reactive oxygen species (ROS) and regulates electron transport, and proteins related to detoxification of ROS and electron transport play an important role in responding to Ni^{2+} aspects and maintaining bacterial growth and metabolism.

The heavy metal tolerance of *V. gazogenes* was much weaker than that of *C. pauculus*. There are 21 Co^{2+}/Ni^{2+}-related transporter proteins in the whole genome of *V. gazogenes*, 6 genes related to Arsenate resistance, and 4 genes related to Cu^{2+}, Zn^{2+} and Fe^{2+} resistance. The metal-binding sites of Ni^{2+} transporter proteins were mostly composed of His, Glu and Asp. In order to investigate the reasons for the poor tolerance compared to typical heavy metal tolerant bacteria, extracellular proteins were qualitatively and quantitatively analysed in response to Ni^{2+} stimulation, and in contrast to typical heavy metal tolerant bacteria, *V. gazogenes* lacked specific Ni^{2+} RND, CDF and MFS efflux pumps. Due to the lack of these specific Ni^{2+} efflux pumps, most porins were down-regulated to prevent Ni^{2+} entry into the cell, especially Ni^{2+} transporter proteins PsaA. Proteins involved in promoting protein folding and assembly were also significantly downregulated, affecting bacterial metabolism. To counteract Ni^{2+} toxicity, bacteria aggregated and formed biofilms by secreting more e-PNs, which include proteins associated with flagellar synthesis and cell adhesion. In addition, proteins associated with ABC transporter proteins, cell membrane lipoproteins, lipopolysaccharide synthesis, electron transport and oxidative stress defense also play important roles in bacterial response to Ni^{2+} stress. The present study enhances the understanding of extracellular proteins in the mechanism of *V. gazogenes* Ni^{2+} resistance and elucidates the factors that contribute to the sensitivity of *V. gazogenes* to high concentrations of heavy metals compared to typical heavy metal tolerant bacteria.

Microbiological treatment of heavy metal wastewater has a broad

application prospect due to its advantages such as green and low price, and has the potential to become a mainstream treatment method, but the lack of microbial tolerance, low removal efficiency, re-release of heavy metals and the lack of specific and efficient adsorption strains limit the industrial application of microbial treatment of influent wastewater, and the research carried out in the future can be carried out in the following aspects: Travelling to more extreme environments for sampling, screening strains with high tolerance and removal ability, and enriching the microbial strain resource base; Establishing a real-time detection system to track heavy metal concentration and microbial activity in real time using microbial sensors and data analysis techniques, in order to adjust the treatment process in a timely manner and improve the treatment efficiency. Use macro-proteomics technology and Other modern molecular technology to screen efficient heavy metal resistance and multiple adsorption site proteins, and construct a functional protein database to provide guidance for the development of green, efficient and specific heavy metal treatment technology. To modify key extracellular proteins by genetic engineering and synthetic biology techniques, and to develop new carrier materials in combination with immobilization techniques to achieve efficient adsorption of metals, providing new ideas for industrial applications. (5) *C. pauculus* can be used for the treatment of multiple metal pollution or heavy metal-organic pollutants in combination, in view of its high bacterial concentration under Ni^{2+} stimulation at low concentration compared with the control group and its ability to degrade a variety of organic compounds.

6 References

Adav, S.S., Lee, D.-J., Tay, J.-H. 2008. Extracellular polymeric substances and structural stability of aerobic granule. *Water Research*, **42**(6-7), 1644-1650.

Agarwal, S., Khan, S. 2020. Heavy metal phytotoxicity: DNA Damage. *Cellular and molecular phytotoxicity of heavy metals*, 157-177.

Aleksandra Duda-Chodak, U.B. 2008. The impact of nickle on human health. *J. Elementol*, **13**(4).

Amit, A.K., Kumar, V., Thakur, M., Bakshi, P., Koul, A., Javaid, A., Radziemska, M., Pandey, V.C. 2023. Comprehensive review of nickel biogeochemistry, bioavailability, and health risks in the environment. *Land Degradation & Development*, **34**, 4141 - 4156.

Amit, K., Dharmendra, K.J., Amit, K., Gangavarapu, S., Raju, M., Aftab, A.S., Cabral-Pinto, M.M.S., Sandeep, K.M., Ashish, K.C., Dipak Kumar, G., Ram Kishor, F., Shakeel, A.K., Arti, B. 2021. Nickel in terrestrial biota: Comprehensive review on contamination, toxicity, tolerance and its remediation approaches. *Chemosphere*, **275**, 129996.

Antoine, P.M., Eric, G., Widade, Z., Isabelle, P.-H., Richard, K., Jacques, C. 2014. The Crystal Structure of the Anti-σ Factor CnrY in Complex with the σ Factor CnrH Shows a New Structural Class of Anti-σ Factors Targeting Extracytoplasmic Function σ Factors. *Journal of Molecular Biology*, **426**(12), 2313-2327.

Bellmaine, S., Schnellbaecher, A., Zimmer, A. 2020. Reactivity and degradation products of tryptophan in solution and proteins. *Free Radical Biology and Medicine*, **160**, 696-718.

Berges, J.A., Franklin, D.J., Harrison, P.J. 2001. Evolution of an artificial seawater medium: improvements in enriched seawater, artificial water over the last two decades. *Journal of phycology*, **37**(6), 1138-1145.

Calzadilla, A., Rehdanz, K., Tol, R.S. 2011. Water scarcity and the impact of improved irrigation management: a computable general equilibrium analysis. *Agricultural Economics*, **42**(3), 305-323.

Catherine Ratcliffe, R.L.S., Ludmila Tittel, and R. W. O Brien. amylase and porteease secretion by the marine bacterium Vibiro gazogenes. *Austalian Journal of Biological Sciences*, **35**(4), 457-467.

Chaintreuil, C., Rigault, F., Moulin, L., Jaffré, T., Fardoux, J., Giraud, E., Dreyfus, B., Bailly, X. 2007. Nickel resistance determinants in bradyrhizobium strains from nodules of the endemic New Caledonia legume Serianthes calycina. *Appl Environ Microbiol*, **73**(24), 8018-22.

Chang-Ho, K., YuJin, S., HongSik, Y., SuKyung, K., Jae-Seong, S. 2018. Antibiotic and heavy-metal resistance of Vibrio parahaemolyticus isolated from oysters in Korea. *Marine Pollution Bulletin*, **135**, 69-74.

Chen, S., Li, X., Sun, G., Zhang, Y., Su, J., Ye, J. 2015. Heavy Metal Induced Antibiotic Resistance in Bacterium LSJC7. *Int J Mol Sci*, **16**(10), 23390-404.

Chen, Y., Chao, Y., Li, Y., Lin, Q., Bai, J., Tang, L., Wang, S., Ying, R., Qiu, R. 2016. Survival Strategies of the Plant-Associated Bacterium Enterobacter sp. Strain EG16 under Cadmium Stress. *Applied and Environmental Microbiology*, **82**(6), 1734-1744.

Cheng, L., Li, X., Jiang, R., Wang, C., Yin, H.B. 2011. Effects of Cr(VI) on the performance and kinetics

of the activated sludge process. *Bioresour Technol*, **102**(2), 797-804.

Coughlin, R.T., Tonsager, S., McGroarty, E.J. 1983. Quantitation of metal cations bound to membranes and extracted lipopolysaccharide of Escherichia coli. *Biochemistry*, **22**(8), 2002-2007.

Craig, B.-A., Meredith, S.W., Ramunas, S., McArthur, J.V. 2006. Co-selection of antibiotic and metal resistance. *Trends in Microbiology*, **14**(4), 176-182.

Cubillas, C., Vinuesa, P., Tabche, M.L., García-de los Santos, A. 2013. Phylogenomic analysis of Cation Diffusion Facilitator proteins uncovers Ni^{2+}/Co^{2+} transporters. *Metallomics*, **5**(12), 1634-43.

Das, K.K., Reddy, R.C., Bagoji, I.B., Das, S., Bagali, S., Mullur, L., Khodnapur, J.P., Biradar, M.S. 2019. Primary concept of nickel toxicity – an overview. *Journal of Basic and Clinical Physiology and Pharmacology*, **30**(2), 141-152.

Dickinson, A.W., Power, A., Hansen, M.G., Brandt, K.K., Piliposian, G., Appleby, P., Neill, P.A.O., Jones, R.T., Sierocinski, P., Koskella, B., Vos, M. 2019. Heavy metal pollution and co-selection for antibiotic resistance: A microbial palaeontology approach. *Environment International*, **132**, 105117.

Efaq, N., Adel, A.-G., Radin, M., Mohamed, A.-S., Md Sohrab, H., Dai-Viet, N.V., Naushad, M. 2022. Sustainable approaches for nickel removal from wastewater using bacterial biomass and nanocomposite adsorbents: A review. *Chemosphere*, **291**, 132862.

Elena, Vigonsky, Inbar, Fish, Nurit, Livnat-Levanon, Ovcharenko, Nir, Ben-Tal, Oded. 2015. Metal binding spectrum and model structure of the Bacillus anthracis virulence determinant MntA. *Metallomics : integrated biometal science*.

Fashola, M., Anagun, O., Babalola, O.O. 2023. Heavy metal pollution: Toxic effects on bacterial cells.

Ferreira dos Santos, A., Amancio Frutuoso, F.K., de Amorim de Carvalho, C., Sousa Aguiar Lira, V.N., Mendes Barros, A.R., Bezerra dos Santos, A. 2022. Carbon source affects the resource recovery in aerobic granular sludge systems treating wastewater. *Bioresource Technology*, **357**, 127355.

Figueiredo, M.C.O., Lobo, S.A.L., Carita, J.N., Nobre, L.S., Saraiva, L.M. 2012. Bacterioferritin protects the anaerobe Desulfovibrio vulgaris Hildenborough against oxygen. *Anaerobe*, **18**(4), 454-458.

Ge, S., Shunan, Z., Jiaqi, W., Kai, Z., Jing, Z., He, L., Ruiping, L., Yu-You, L., Chengzhi, H., Jiuhui, Q. 2024. Enzyme-enhanced acidogenic fermentation of waste activated sludge: Insights from sludge structure, interfaces, and functional microflora. *Water Research*, **249**, 120889.

Geets, J., Vanbroekhoven, K., Borremans, B., Vangronsveld, J., Diels, L., van der Lelie, D. 2006. Column experiments to assess the effects of electron donors on the efficiency of in situ precipitation of Zn, Cd, Co and Ni in contaminated groundwater applying the biological sulfate removal technology. *Environmental Science and Pollution Research*, **13**(6), 362-378.

Genchi, G., Carocci, A., Lauria, G., Sinicropi, M.S., Catalano, A. 2020. Nickel: Human Health and Environmental Toxicology. *International Journal of Environmental Research and Public Health*, **17**(3), 679.

Gilles, G., Sophie, C., François, B., Sèverine, D., Michel, B. 2005. Comparison of the complexation potential of extracellular polymeric substances (EPS), extracted from activated sludges and produced by pure bacteria strains, for cadmium, lead and nickel. *Chemosphere*, **59**(5),

629-638.

Große, C., Kohl, T.A., Niemann, S., Herzberg, M., Nies, D.H. 2022. Loss of Mobile Genomic Islands in Metal-Resistant, Hydrogen-Oxidizing Cupriavidus metallidurans. *Applied and Environmental Microbiology*, **88**(4), e02048-21.

Guo, H., Luo, S., Chen, L., Xiao, X., Xi, Q., Wei, W., Zeng, G., Liu, C., Wan, Y., Chen, J., He, Y. 2010. Bioremediation of heavy metals by growing hyperaccumulaor endophytic bacterium Bacillus sp. L14. *Bioresour Technol*, **101**(22), 8599-605.

Haritha, A., Sagar, K.P., Tiwari, A., Kiranmayi, P., Rodrigue, A., Mohan, P.M., Singh, S.S. 2009. MrdH, a Novel Metal Resistance Determinant of Pseudomonas putida KT2440, Is Flanked by Metal-Inducible Mobile Genetic Elements. *Journal of Bacteriology*, **191**(19), 5976-5987.

Harlow, E., Lane, D. 2006. Bradford assay. *Cold Spring Harbor Protocols*, **2006**(6), pdb. prot4644.

Hausinger, L.M.a.R.P. 2016. Nickel Toxicity, Regulation, and Resistance in Bacteria. in: *Stress and Environmental regulation of Gene Expression and Adaptation in Bacteria*, (Ed.) F.J.d. Bruijn, John Wiley & Sons, Inc, pp. 1133-1144.

Hausinger, R.P. 2022. Microbial metabolism of nickel. in: *Microbial metabolism of metals and metalloids*, Springer, pp. 417-502.

Hayashi, S., Abe, M., Kimoto, M., Furukawa, S., Nakazawa, T. 2000. The dsbA-dsbB disulfide bond formation system of Burkholderia cepacia is involved in the production of protease and alkaline phosphatase, motility, metal resistance, and multi-drug resistance. *Microbiol Immunol*, **44**(1), 41-50.

He, Y., Guo, J., Song, Y., Chen, Z., Lu, C., Han, Y., Li, H., Hou, Y., Zhao, R. 2021. Acceleration mechanism of bioavailable Fe(Ⅲ) on Te(IV) bioreduction of *Shewanella oneidensis* MR-1: Promotion of electron generation, electron transfer and energy level. *J Hazard Mater*, **403**, 123728.

Hønneland, G. 2003. Industrial pollution discourse in the European Arctic. *Acta Borealia*, **20**(1), 49-73.

Hu, H.-W., Wang, J.-T., Li, J., Shi, X.-Z., Ma, Y.-B., Chen, D., He, J.-Z. 2017. Long-Term Nickel Contamination Increases the Occurrence of Antibiotic Resistance Genes in Agricultural Soils. *Environmental Science & Technology*, **51**(2), 790-800.

Huang, L., Puma, G.L. 2022. Physiological response of electroactive bacteria via secretion of extracellular polymeric substances in microbial electrochemical processes: a review. *Current Opinion in Electrochemistry*, 101168.

Hussain, S., Khan, M., Sheikh, T.M.M., Mumtaz, M.Z., Chohan, T.A., Shamim, S., Liu, Y. 2022. Zinc essentiality, toxicity, and its bacterial bioremediation: A comprehensive insight. *Frontiers in Microbiology*, **13**, 900740.

Javiera, R.-Z., Sebastián, G., Cristóbal, M.-B., Rodrigo, N., Claudio, A.N., Alberto, P., Carlos, A.J. 2019. Response of the biomining Acidithiobacillus ferrooxidans to high cadmium concentrations. *Journal of Proteomics*, **198**, 132-144.

Jennifer, B.G., Claire, E.E., Loren Dean, W. 2023. Something old, something new, something borrowed, something blue: the anaerobic microbial ancestry of aerobic respiration. *Trends in Microbiology*, **31**(2), 135-141.

Joshi, S., Gangola, S., Bhandari, G., Bhandari, N.S., Nainwal, D., Rani, A., Malik, S., Slama, P. 2023. Rhizospheric bacteria: the key to sustainable heavy metal detoxification strategies. *Front Microbiol*, **14**, 1229828.

Juan, L.R., Estrella, D., José-Juan, R.-H., Patricia, G., Ali, H., Fernando, R., Alejandro, F.-B. 1997. Mechanisms for Solvent Tolerance in Bacteria*. *Journal of Biological Chemistry*, **272**(7), 3887-3890.

Kumar, A., Balouch, A., Pathan, A.A., Abdullah, Jagirani, M.S., Mahar, A.M., Zubair, M., Laghari, B. 2019. Remediation of Nickel ion from wastewater by applying various techniques: a review. *Acta Chemica Malaysia*, **3**, 1 - 15.

Kumar, A., Kumar, V., Thakur, M., Bakshi, P., Koul, A., Javaid, A., Radziemska, M., Pandey, V.C. 2023. Comprehensive review of nickel biogeochemistry, bioavailability, and health risks in the environment. *Land Degradation & Development*, **34**(14), 4141-4156.

Kumar, S., Vinella, D., De Reuse, H. 2022. Nickel, an essential virulence determinant of Helicobacter pylori: transport and trafficking pathways and their targeting by bismuth. *Advances in Microbial Physiology*, **80**, 1-33.

Lawrence, J.R., Swerhone, G.D.W., Neu, T.R. 2019. Visualization of the Sorption of Nickel within Exopolymer Microdomains of Bacterial Microcolonies Using Confocal and Scanning Electron Microscopy. *Microbes and Environments*, **34**(1), 76-82.

Li, C., Xiaochen, L., Ruixue, J., Chao, W., Hua-bin, Y. 2011. Effects of Cr(VI) on the performance and kinetics of the activated sludge process. *Bioresource Technology*, **102**(2), 797-804.

Li, X., Ren, Z., Crabbe, M.J.C., Wang, L., Ma, W. 2021. Genetic modifications of metallothionein enhance the tolerance and bioaccumulation of heavy metals in Escherichia coli. *Ecotoxicology and Environmental Safety*, **222**, 112512.

Li, X.Z., Nikaido, H., Williams, K.E. 1997. Silver-resistant mutants of *Escherichia coli* display active efflux of Ag+ and are deficient in porins. *Journal of bacteriology*, **179**(19), 6127-6132.

Liancheng, F., Hao, Z., Yuehan, G., Genrong, Z., Houpu, Z., Taozhong, S., Xiangwei, W., Qing, X.L., Rimao, H. 2022. Resistance properties and adaptation mechanism of cadmium in an enriched strain, Cupriavidus nantongensis X1T. *Journal of Hazardous Materials*, **434**, 128935.

Liping, H., Gianluca Li, P. 2022. Physiological response of electroactive bacteria via secretion of extracellular polymeric substances in microbial electrochemical processes: A review. *Current Opinion in Electrochemistry*, **36**, 101168.

Lu, S., Li, X., Xi, Y., Liu, H., Zhang, Z., Huang, Y., Xie, T., Liu, Y., Quan, B., Zhang, C. 2021. Insight the roles of loosely-bound and tightly-bound extracellular polymeric substances on Cu^{2+}, Zn^{2+} and Pb^{2+} biosorption process with *Desulfovibrio vulgaris*. *Journal of Colloid and Interface Science*, **596**, 408-419.

Luo, X., Zhou, X., Peng, C., Shao, P., Wei, F., Li, S., Liu, T., Yang, L., Ding, L., Luo, X. 2022. Bioreduction performance of Cr (VI) by microbial extracellular polymeric substances (EPS) and the overlooked role of tryptophan. *Journal of Hazardous Materials*, **433**, 128822.

Makkar, N., Casida Jr, L. 1987. *Cupriavidus necator* gen. nov., sp. nov.; a nonobligate bacterial predator of bacteria in soil. *International journal of systematic bacteriology*, **37**(4), 323-326.

Margaryan, A., Panosyan, H., Birkeland, N.-K. 2021. Heavy Metal Resistance in Prokaryotes: Mechanism and Application. in: *Microbial Communities and their Interactions in the Extreme Environment*, (Eds.) D. Egamberdieva, N.-K. Birkeland, W.-J. Li, H. Panosyan, Springer Singapore. Singapore, pp. 273-313.

Masuko, T., Minami, A., Iwasaki, N., Majima, T., Nishimura, S.-I., Lee, Y.C. 2005. Carbohydrate

analysis by a phenol–sulfuric acid method in microplate format. *Analytical biochemistry*, **339**(1), 69-72.

Mata, M.T., Baquero, F., Pérez-Díaz, J.C. 2000. A multidrug efflux transporter in Listeria monocytogenes. *FEMS Microbiology Letters*, **187**(2), 185-188.

McLean, R.J., Beauchemin, D., Clapham, L., Beveridge, T.J. 1990. Metal-Binding Characteristics of the Gamma-Glutamyl Capsular Polymer of Bacillus licheniformis ATCC 9945. *Appl Environ Microbiol*, **56**(12), 3671-7.

Mo Lu, Y.J., Shu Wang, Hua jin, Rongguang Zhang, Mariejoelle Virolle, Yuxing Chen, Congzhao Zhou. 2014. Streptomyces coelicolor SCO4226 Is a Nickel Binding Protein. *Plos one*, **9**(10), e10966.

Muhammad, A., Shah, A.u.H.A., Bilal, S. 2020. Effective Adsorption of Hexavalent Chromium and Divalent Nickel Ions from Water through Polyaniline, Iron Oxide, and Their Composites. *Applied Sciences*, **10**(8), 2882.

Munkelt, D., Grass, G., Nies, D.H. 2004. The chromosomally encoded cation diffusion facilitator proteins DmeF and FieF from Wautersia metallidurans CH34 are transporters of broad metal specificity. *J Bacteriol*, **186**(23), 8036-43.

Musiani, F., Zambelli, B., Bazzani, M., Mazzei, L., Ciurli, S. 2015. Nickel-responsive transcriptional regulators. *Metallomics*, **7**(9), 1305-1318.

Nada, H., Ashok, J.T., Cecilia. 2023. Antibiotic concentrations and antibiotic resistance in aquatic environments of the WHO Western Pacific and South-East Asia regions: a systematic review and probabilistic environmental hazard assessment. *The Lancet Planetary Health*, **7**(1), e45-e54.

Nakajima, H., Kobayashi, K., Kobayashi, M., Asako, H., Aono, R. 1995. Overexpression of the robA gene increases organic solvent tolerance and multiple antibiotic and heavy metal ion resistance in Escherichia coli. *Appl Environ Microbiol*, **61**(6), 2302-7.

Nasution, M.J., Bakri, S., Setiawan, A., Wulandari, C., Wahono, E.P. 2024. The Impact of Increasing Nickel Production on Forest and Environment in Indonesia: A Review. *Jurnal Sylva Lestari*, **12**(3), 549-579.

Nguyen, T.H.T., Nguyen, H.D., Le, M.H., Nguyen, T.T.H., Nguyen, T.D., Nguyen, D.L., Nguyen, Q.H., Nguyen, T.K.O., Michalet, S., Dijoux-Franca, M.-G., Pham, H.N. 2023a. Efflux Pump Inhibitors in Controlling Antibiotic Resistance: Outlook under a Heavy Metal Contamination Context. *Molecules*, **28**(7), 2912.

Nguyen, T.H.T., Nguyen, H.D., Le, M.H., Nguyen, T.T.H., Nguyen, T.D., Nguyen, D.L., Nguyen, Q.H., Nguyen, T.K.O., Michalet, S., Dijoux-Franca, M.G., Pham, H.N. 2023b. Efflux Pump Inhibitors in Controlling Antibiotic Resistance: Outlook under a Heavy Metal Contamination Context. *Molecules*, **28**(7).

Nies, D.H., Silver, S. 1995. Ion efflux systems involved in bacterial metal resistances. *J Ind Microbiol*, **14**(2), 186-99.

Nowicki, E.M., O'Brien, J.P., Brodbelt, J.S., Trent, M.S. 2015. Extracellular zinc induces phosphoethanolamine addition to *P seudomonas* aeruginosa lipid A via the ColRS two-component system. *Molecular microbiology*, **97**(1), 166-178.

Olga, K.-R., David, R., Kevin, A.H., Pembroke, J.T., Tewfik, S. 2015. Cation Diffusion Facilitator family: Structure and function. *FEBS Letters*, **589**(12), 1283-1295.

Pal, A., Bhattacharjee, S., Saha, J., Sarkar, M., Mandal, P. 2022. Bacterial survival strategies and

responses under heavy metal stress: a comprehensive overview. *Critical Reviews in Microbiology*, **48**(3), 327-355.

Pal, A., Paul, A.K. 2010. Nickel uptake and intracellular localization in *Cupriavidus pauculus* KPS 201, native to ultramafic ecosystem. *Advances in Bioscience & Biotechnology*, **1**(4), 276-280.

Pal, C., Asiani, K., Arya, S., Rensing, C., Hobman, J.L. 2017a. Metal resistance and its association with antibiotic resistance. *Advances in Microbial Physiology*, **70**, 261-313.

Pal, C., Asiani, K., Arya, S., Rensing, C., Stekel, D.J., Larsson, D.G.J., Hobman, J.L. 2017b. Chapter Seven - Metal Resistance and Its Association With Antibiotic Resistance. in: *Advances in Microbial Physiology*, (Ed.) R.K. Poole, Vol. 70, Academic Press, pp. 261-313.

Pal, C., Bengtsson-Palme, J., Kristiansson, E., Larsson, D.G.J. 2015. Co-occurrence of resistance genes to antibiotics, biocides and metals reveals novel insights into their co-selection potential. *BMC Genomics*, **16**(1), 964.

Panagopoulos, I., Karayannis, A., Kollias, K., Xenidis, A., Papassiopi, N. 2015. Investigation of potential soil contamination with Cr and Ni in four metal finishing facilities at Asopos industrial area. *Journal of Hazardous Materials*, **281**, 20-26.

Pearce, D.A., Sherman, F. 1999. Toxicity of Copper, Cobalt, and Nickel Salts Is Dependent on Histidine Metabolism in the YeastSaccharomyces cerevisiae. *Journal of Bacteriology*, **181**, 4774 - 4779.

Pereira, S.I., Lima, A.I., Figueira, E.M. 2006a. Screening possible mechanisms mediating cadmium resistance in Rhizobium leguminosarum bv. viciae isolated from contaminated Portuguese soils. *Microb Ecol*, **52**(2), 176-86.

Pereira, S.I.A., Lima, A.I.G., Figueira, E.M.d.A.P. 2006b. Screening Possible Mechanisms Mediating Cadmium Resistance in *Rhizobium leguminosarum* bv. viciae Isolated from Contaminated Portuguese Soils. *Microbial Ecology*, **52**(2), 176-186.

Perron, K., Caille, O., Rossier, C., Van Delden, C., Dumas, J.L., Köhler, T. 2004. CzcR-CzcS, a two-component system involved in heavy metal and carbapenem resistance in Pseudomonas aeruginosa. *J Biol Chem*, **279**(10), 8761-8.

Poonkothai, M., Vijayavathi, B.S. 2012. Nickel as an essential element and a toxicant. *International Journal of Environmental Sciences*, **1**(4), 285-288.

Qi, S., Li, X., Luo, J., Han, R., Chen, Q., Shen, D., Shentu, J. 2022. Soil heterogeneity influence on the distribution of heavy metals in soil during acid rain infiltration: Experimental and numerical modeling. *Journal of Environmental Management*, **322**, 116144.

Robert, H. 2022. Microbial Metabolism of Nickel. in: *microbial metabolism of metals and metalloids*, (Ed.) C.J. Hurst, Vol. advances in Environmental Microbiology, Springer International Publishing. USA, pp. 417-502.

S. Langley, T.J.B. 1998. Effect of o side-chain-lipopolysaccharide chemistry on metal binding. *Applied & Environmental Microbiology*, **65**(2), 489-498.

Sar, P., Kazy, S.K., Singh, S.P. 2001. Intracellular nickel accumulation by Pseudomonas aeruginosa and its chemical nature. *Lett Appl Microbiol*, **32**(4), 257-61.

Shah, S.B. 2021. Heavy metals in the marine environment—an overview. *Heavy Metals in Scleractinian Corals*, 1-26.

Shahzad, B., Tanveer, M., Rehman, A., Cheema, S.A., Fahad, S., Rehman, S., Sharma, A. 2018. Nickel; whether toxic or essential for plants and environment - A review. *Plant Physiol Biochem*,

132, 641-651.

Shaw, D.R., Dussan, J. 2015. Mathematical Modelling of Toxic Metal Uptake and Efflux Pump in Metal-Resistant Bacterium Bacillus cereus Isolated From Heavy Crude Oil. *Water Air & Soil Pollution*, **226**(4), 112.

Shen, L., Li, Z., Wang, J., Liu, A., Li, Z., Yu, R., Wu, X., Liu, Y., Li, J., Zeng, W. 2018. Characterization of extracellular polysaccharide/protein contents during the adsorption of Cd(II) by Synechocystis sp. PCC6803. *Environmental ence and Pollution Research*.

Shengzhi, Y., Wenwen, D., Shuliang, L., Xiumei, Y., Ghulam Raza, M., Shujuan, C., Li, H., Xiaolin, A., Yong, Y., Kang, Z., Bei, L., Xinfeng, H., Xuebin, X., Likou, Z. 2020. Presence of heavy metal resistance genes in Escherichia coli and Salmonella isolates and analysis of resistance gene structure in E. coli E308. *Journal of Global Antimicrobial Resistance*, **21**, 420-426.

Shevchenko, A., Tomas, H., Havlis, J., Olsen, J.V., Mann, M. 2006. In-gel digestion for mass spectrometric characterization of proteins and proteomes. *Nat Protoc*, **1**(6), 2856-60.

Sihui, L., Xin, L., Yanni, X., Huinian, L., Zhuang, Z., Yicai, H., Tanghuan, X., Yanfen, L., Bangyu, Q., Chang, Z., Weihua, X. 2021. Insight the roles of loosely-bound and tightly-bound extracellular polymeric substances on Cu2+, Zn2+ and Pb2+ biosorption process with Desulfovibrio vulgaris. *Journal of Colloid and Interface Science*, **596**, 408-419.

Sincak, M., Šoltisová, K., Luptakova, A., Sedlakova-Kadukova, J. 2023. Overproduction of Efflux Pumps as a Mechanism of Metal and Antibiotic Cross-Resistance in the Natural Environment. *Sustainability*, **15**(11), 8767.

Singh, A., Pal, D.B., Mohammad, A., Alhazmi, A., Haque, S., Yoon, T., Srivastava, N., Gupta, V.K. 2022. Biological remediation technologies for dyes and heavy metals in wastewater treatment: New insight. *Bioresource Technology*, **343**, 126154.

Soares, E.V., Hebbelinck, K., Soares, H.M. 2003. Toxic effects caused by heavy metals in the yeast Saccharomyces cerevisiae: a comparative study. *Can J Microbiol*, **49**(5), 336-43.

Sonia, G., David, W.G., Sreekrishnan, T.R., Shaikh Ziauddin, A. 2023. Heavy metal and antibiotic resistance in four Indian and UK rivers with different levels and types of water pollution. *Science of The Total Environment*, **857**, 159059.

Sumei, Y., Yingnan, W., Fan, S., Hua, F., Yunlong, Y. 2022. Copper-based fungicide copper hydroxide accelerates the evolution of antibiotic resistance via gene mutations in *Escherichia coli*. *Science of The Total Environment*, **815**, 152885.

Tang, B., Yang, H., Jia, X., Feng, Y. 2021. Coexistence and characterization of Tet(X5) and NDM-3 in the MDR-Acinetobacter indicus of duck origin. *Microb Pathog*, **150**, 104697.

Teufel, F., Almagro Armenteros, J.J., Johansen, A.R., Gíslason, M.H., Pihl, S.I., Tsirigos, K.D., Winther, O., Brunak, S., von Heijne, G., Nielsen, H. 2022. SignalP 6.0 predicts all five types of signal peptides using protein language models. *Nat Biotechnol*, **40**(7), 1023-1025.

Thai, T.D., Lim, W., Na, D. 2023. Synthetic bacteria for the detection and bioremediation of heavy metals. *Frontiers in Bioengineering and Biotechnology*, **11**(1), 21.

Vischetti, C., Marini, E., Casucci, C., De Bernardi, A. 2022. Nickel in the environment: Bioremediation techniques for soils with low or moderate contamination in European Union. *Environments*, **9**(10), 133.

Völkel, S., Hein, S., Benker, N., Pfeifer, F., Lenz, C., Losensky, G. 2020. How to cope with heavy metal ions: cellular and proteome-level stress response to divalent copper and nickel in *Halobacterium salinarum* R1 planktonic and biofilm cells. *Frontiers in Microbiology*, **10**,

3056.

Wang, M., Vollstedt, C., Siebels, B., Yu, H., Wu, X., Shen, L., Li, J., Liu, Y., Yu, R., Streit, W.R., Zeng, W. 2024. Extracellular proteins enhance *Cupriavidus pauculus* nickel tolerance and cell aggregate formation. *Bioresource Technology*, **393**, 130133.

Wang, W., Liu, J., Guo, S., Liu, L., Yuan, Q., Guo, L., Pan, S. 2020. Identification of *Vibrio parahaemolyticus* and *Vibrio* spp. Specific Outer Membrane Proteins by Reverse Vaccinology and Surface Proteome. *Front Microbiol*, **11**, 625315.

Wang, Z., Luo, P., Zha, X., Xu, C., Kang, S., Zhou, M., Nover, D., Wang, Y. 2022. Overview assessment of risk evaluation and treatment technologies for heavy metal pollution of water and soil. *Journal of Cleaner Production*, **379**, 134043.

Xia, M., Bao, P., Zhang, S., Liu, A., Shen, L., Yu, R., Liu, Y., Chen, M., Li, J., Wu, X. 2019. Extraction and characterization of extracellular polymeric substances from a mixed fungal culture during the adaptation process with waste printed circuit boards. *Environmental Science and Pollution Research*.

Xiangyang, L., April, Z.G., Ye, Z., Bin, X., Dan, L., Jianmin, C. 2019. Sub-lethal concentrations of heavy metals induce antibiotic resistance via mutagenesis. *Journal of Hazardous Materials*, **369**, 9-16.

Xianxin, L., Xiaoyu, Z., Chengyi, P., Penghui, S., Feng, W., Shujing, L., Ting, L., Liming, Y., Lin, D., Xubiao, L. 2022. Bioreduction performance of Cr(VI) by microbial extracellular polymeric substances (EPS) and the overlooked role of tryptophan. *Journal of Hazardous Materials*, **433**, 128822.

Xiaobo, Z., Wenhui, G., Wang, L., Chuanxiang, Z. 2023. Fixating lead in coal gangue with phosphate using phosphate-dissolving bacteria: Phosphorus dissolving characteristics of bacteria and adsorption mechanism of extracellular polymer. *Journal of Hazardous Materials*, **458**, 131923.

Xu, Y., Tan, L., Li, Q., Zheng, X., Liu, W. 2022. Sublethal concentrations of heavy metals Cu^{2+} and Zn^{2+} can induce the emergence of bacterial multidrug resistance. *Environmental Technology & Innovation*, **27**, 102379.

Yan, X., Lu, T., Qian, L., Xiangqun, Z., Wei, L. 2022. Sublethal concentrations of heavy metals Cu2+ and Zn2+ can induce the emergence of bacterial multidrug resistance. *Environmental Technology & Innovation*, **27**, 102379.

Yang, K., Zhang, Y. 2020a. Reversal of heavy metal-induced antibiotic resistance by dandelion root extracts and taraxasterol. *Journal of Medical Microbiology*, **69**(8).

Yang, K., Zhang, Y. 2020b. Reversal of heavy metal-induced antibiotic resistance by dandelion root extracts and taraxasterol. *Journal of Medical Microbiology*, **69**(8), 1049-1061.

Yu, H., Yan, X., Weng, W., Xu, S., Xu, G., Gu, T., Guan, X., Liu, S., Chen, P., Wu, Y. 2022a. Extracellular proteins of Desulfovibrio vulgaris as adsorbents and redox shuttles promote biomineralization of antimony. *Journal of Hazardous Materials*, **426**, 127795.

Yu, S., Wang, Y., Shen, F., Fang, H., Yu, Y. 2022b. Copper-based fungicide copper hydroxide accelerates the evolution of antibiotic resistance via gene mutations in *Escherichia coli*. *Science of The Total Environment*, **815**, 152885.

Zedong, T., Wen, S., Keyao, Z., Yaoqiang, H., Jing, Z., Min, L. 2019. Pb biosorption by Leclercia adecarboxylata: Protective and immobilized mechanisms of extracellular polymeric substances. *Chemical Engineering Journal*, **375**, 122113.

Zeng, W., Li, F., Wu, C., Yu, R., Wu, X., Shen, L., Liu, Y., Qiu, G., Li, J. 2020a. Role of extracellular polymeric substance (EPS) in toxicity response of soil bacteria Bacillus sp. S3 to multiple heavy metals. *Bioprocess and Biosystems Engineering*, **43**(1), 153-167.

Zeng, W., Zhang, S., Xia, M., Wu, X., Qiu, G., Shen, L. 2020b. Insights into the production of extracellular polymeric substances of Cupriavidus pauculus 1490 under the stimulation of heavy metal ions. *RSC Advances*, **10**.

Zhang, B., Xu, J., Xie, L., Chen, L. 2023. Comparative secretomic and proteomic analysis reveal multiple defensive strategies developed by *Vibrio cholerae* against the heavy metal (Cd^{2+}, Ni^{2+}, Pb^{2+}, and Zn^{2+}) stresses. *Frontiers in Microbiology*, **14**, 1294177.

Zhang, Y.-T., Wei, W., Huang, Q.-S., Wang, C., Wang, Y., Ni, B.-J. 2020. Insights into the microbial response of anaerobic granular sludge during long-term exposure to polyethylene terephthalate microplastics. *Water research*, **179**, 115898.

Zhou, L., Li, S., Li, F. 2022. Damage and elimination of soil and water antibiotic and heavy metal pollution caused by livestock husbandry. *Environ Res*, **215**(Pt 2), 114188.

Zhu L, Q.H., Kong Y, et al. 2012. Component analysis of extracellular polymeric substances (EPS) during aerobic sludge granulation using FTIR and 3D-EEM technologies. *Bioresource Technology*, **124**, 455-459.

7 Acknowledgements

I am very grateful to my supervisor, Prof Wolfgang Streit, host me in his group, bringing me to develop an international perspective, and enabling me to look at the problem from a different perspective when encountering difficulties and frustrations. I am thankful for his kindness, patience, and tolerance. I believe the time I spent in his office, meticulously correcting my manuscript word by word, will be forever etched in my memory.

I would like to thank Christel Vollstedt, for her timely presence, helping me to rebuild my confidence, and giving me encouragement when I needed it the most. Whenever I encountered problems in my experiments, she was always able to identify the problems and provide solutions, and the smooth running of the molecular experiments was all due to her guidance.

I would like to express my deepest gratitude to all the members of our group for their support. In particular, I am immensely grateful to Yuchen Han, Hongli Zhang, Ly Trinh, Sasipa Wongwattanarat, Golo Fire Bolt, Myllena Pereira Silverio, Inka Sivers Helling, Angela Jordan, and Nurcan Taskin for their invaluable help in the experiments, as well as their care, companionship, and encouragement throughout my journey.

With deepest gratitude, I thank my beloved family. My parents have always shown me love in the most selfless and genuine way, supporting every decision I've made without hesitation. A special thanks to my younger brOther, who has been so understanding and thoughtful—sharing joy with me in happy times, offering patient comfort in difficult moments, and taking care of our parents while I pursued my studies abroad, allowing me to focus without worry.

I am truly grateful to my friends—Sun Yanna, Li Mengke, Liang Yuting, Nan Meihua, Liu Sha, Wang Xiaoxue, Hu Bingyan, Wei Yuanjie, Tian Lingyu, Niu Tianyu, and Jia Xiao. The challenging journey of studying in both China and Germany was made bearable—and even meaningful—because of your companionship, encouragement, and support. Together, we persevered to graduation. My dear friends, may we continue to walk the path of flowers in the future!

Finally, I want to thank myself who never gave up. Though I often wavered and thought of quitting, disappointment, confusion, but pain did not defeat me. "The light boat has passed countless mountains"—and I've grown to love who I am today. If everyone's flowers blooms in their own time, then I will keep going until my flowers unfold.

Words often feel inadequate compared with emotion. So, with the sincerest heart, I thank all those not mentioned here—teachers, classmates, and loved ones—who have cared for and supported me. Thank you for your encouragement, kindness, and companionship. May all those I love, and those who love me, walk a path of happiness, peace, and boundless blessings in the

years to come!